IEKP-KA/2011-22

PRESENT AND FUTURE CONSTRAINTS ON SUPERSYMMETRY FROM COSMOLOGICAL AND ELECTROWEAK DATA

EVA ZIEBARTH

Zur Erlangung des akademischen Grades eines
DOKTORS DER NATURWISSENSCHAFTEN
von der Fakultät für Physik am
Karlsruher Institut für Technologie (KIT)

genehmigte

Dissertation

von

Dipl.-Phys. Eva Barbara Ziebarth
aus Speyer

Tag der mündlichen Prüfung: Freitag der 10. Juni 2011
Referent: Prof. Dr. W. de Boer, Institut für Experimentelle Kernphysik
Korreferent: Prof. Dr. Th. Müller, Institut für Experimentelle Kernphysik

Contents

List of Figures

List of Tables

CHAPTER 1

Introduction

The Standard Model of particle physics (SM) [2–12] was developed in the 1970s. Tested in many collider and cosmological experiments it stays accepted until today. In the Glashow-Weinberg-Salam theory (GWS) [13–15] a unification of the electromagnetic and the weak force could be obtained. A unification of all SM forces (the electromagnetic, the weak and the strong force) would complete the SM. However, a unification of this kind cannot be obtained in the standalone SM. Therefore it needs an extension.
In the 1930s Fritz Zwicky postulated the existence of non-illuminating matter, Dark Matter (DM), to be responsible for the effect that the outer galaxies of the Coma galaxy cluster orbiting faster around the centre than can be expected from visible matter alone [16]. Today this theory is established and the DM content of the Universe is measured to be 23% [17]. If DM consists of thermal relics from the early Universe the constituents of DM have to be weakly interacting, massive and stable. The SM does not provide a particle like this [18].
These two aspects mentioned above imply the need for an extension of the SM. An ansatz of such an extension is the introduction of a new symmetry between matter and interaction particles, so-called Supersymmetry (SUSY). In this case the SM does not have to be replaced but it gets extended. This extension causes the introduction of an additional SUSY partner to each SM particle, the so-called SUSY particles [19–24].
SUSY theories introduce more than 100 free parameters. Thus the properties of the lightest supersymmetric particle (LSP) which provides a perfect DM candidate, are not exactly known, yet. From this the question arises if data taken by new colliders like the Large Hadron Collider (LHC) can be used to determine the properties of the LSP. The knowledge about the LSP could then be used to determine the DM Relic Density provided by these SUSY particles. This would answer the question if DM consists completely of SUSY particles because it could also be a mixture between different candidates.
The Relic Density can be used to constrain the large number of possible SUSY scenarios. If its value, provided by these models, is too large these models can be excluded due to cosmological measurements.
SUSY particles could also influence known SM processes. In the last few years many precision measurements have taken place, some of them with surprising results. This could be caused by SUSY particles. Hence the results of these measurements can be used to constrain SUSY models.
The combination of these different constraints can be thought of as a multi-dimensional optimisation process. Such optimisations in a multidimensional parameter space have to be done numerically. There are diverse analyses existing applying different statistical methods to do this optimisation process [1, 25, 26] all getting different results. In the current analysis a so-called Markov Chain Monte Carlo (MCMC) [27], a wisely chosen random walk through parameter space, is applied [28]. This optimisation method is implemented in an own framework, where the minimiser MINUIT [29] was integrated, too. The result of the current analysis seems to include the results of all other analyses.
The LHC now runs for about one year with a centre of mass energy of 7 TeV. SUSY has

not been discovered yet. Thus an exclusion limit could be determined from the data. This has been added to the present study to investigate the influence of this new exclusion curve on the hitherto excluded region.
The thesis is arranged as follows: The second chapter introduces both the theoretical framework of SUSY, based on the theory of the SM, and the framework of DM as thermal relic. The third chapter gives an introduction into the implementation of the software framework and the tools integrated into it. Finally, chapter four is divided into two main parts. The first part answers the question “Can one measure the Relic Density at the LHC?“. In the second part cosmological and electroweak data are combined to constrain the SUSY parameter space.

CHAPTER 2

Theoretical Framework

”Willst du dich am Ganzen erquicken, so musst du das Ganze im Kleinsten erblicken.” J.W. von Goethe

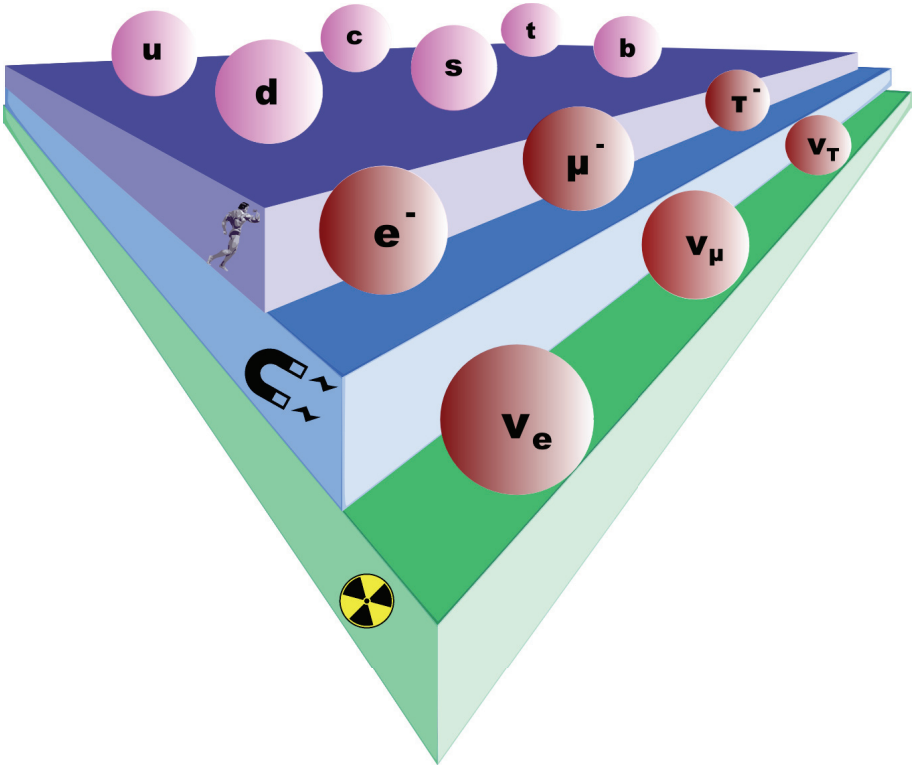

Figure 2.1: SM fermions: Neutrinos underlie the weak force. Charged leptons underlie additionally the electromagnetic force. Quarks underlie all forces.

2.1 The Standard Model of Particle Physics

The Standard Model (SM) of particle physics was developed in the seventies. It includes matter particles, so-called fermions, as well as particles transmitting the interactions, the so-called bosons. Nearly all these particles have already been discovered in particle physics experiments. All experiments are well described by the SM, thus the SM seems to be well proven [30].
The only particle not discovered yet is the so-called Higgs boson. Through the Higgs Mechanism [31–36] it gives mass to the heavy gauge bosons of the weak interaction.
Nevertheless there are some aspects, which make the SM not looking like the complete description of nature. Thus one should think about extensions. An example for such an extension will be discussed in Sect. .

2.1.1 Fermions

Matter is made of so-called fermions which are particles with half-integer spin. Fermions can be divided into two groups: leptons and quarks. Leptons come as charged particles and as neutrinos which are the lightest particles in the Standard Model [30].
Leptons are grouped into three families each unifying one electrically charged lepton with

its neutral neutrino partner.

$$\begin{pmatrix} \nu_e \\ e \end{pmatrix} \begin{pmatrix} \nu_\mu \\ \mu \end{pmatrix} \begin{pmatrix} \nu_\tau \\ \tau \end{pmatrix} \tag{2.1}$$

Here e is the electron, which is the lightest charged lepton. Muons (μ) are about 200 times heavier than the electrons (their weight is 105.6 MeV/c^2). They are produced abundantly by cosmic rays. The heaviest lepton (1777 MeV/c^2) is the τ-lepton which has only be discovered in collider experiments [30].
The neutrino can be noticed in β-decays as missing energy:

$$n \rightarrow p + e^- + \bar{\nu}_e \tag{2.2}$$

It is hard to detect neutrinos directly, because they are just weakly interacting and very light. Thus they hardly interact with material. In the SM they are assumed to be massless, but through flavour oscillations they are proven to be massive. There are many Ansätze how to extend the SM accordingly to this fact, which won't be further discussed here, but can be looked out in literature (for example [37]).
Quarks can also be arranged in three families:

$$\begin{pmatrix} u \\ d \end{pmatrix} \begin{pmatrix} c \\ s \end{pmatrix} \begin{pmatrix} t \\ b \end{pmatrix} \tag{2.3}$$

Additionally to weak and electromagnetic force they underlie the strong force. The charge of the strong force is called colour [38–40]. The quarks can be grouped into $SU(3)$ multiplets:

$$\begin{pmatrix} q_b \\ q_g \\ q_r \end{pmatrix}, \tag{2.4}$$

where the indices assign their colour charge: blue (b), green (g) and red (r) [30].
Their electromagnetic charge is $-1/3e$ for down- (d), strange- (s) and bottom-quarks (b) and $+2/3e$ for up- (u), charm- (c) and top-quarks (t). Up- and down-quarks are the lightest quarks and they are constituents of the atomic nucleus. The strange quark is a constituent of strange particles (kaons), for instance, which can be found in cosmic rays.
The charm quark was discovered in the J/ψ resonance and the bottom quark in the Υ resonance. The weight of the bottom quark is 4.2 GeV/c^2 [41]. It is 43 times lighter than its partner, the top quark (172 GeV/c^2) [41]. This one was the last quark, which was discovered only 15 years ago [30].
The energy of a fermion can be expressed by the relativistic energy mass equation:

$$E^2 = m^2c^4 + \vec{p}^2c^2 \tag{2.5}$$

This equation has two solutions:

$$E = +\sqrt{\vec{p}^2c^2 + m^2c^4} \qquad E = -\sqrt{\vec{p}^2c^2 + m^2c^4} \tag{2.6}$$

The first (positive) solution is associated with the already mentioned fermions. The negative solution is associated with another kind of particles, the so-called antiparticles. There exists an antiparticle partner to each particle. It can be obtained by inverting the charge

conjugation of the particle (the so-called C-parity) and its parity (P).
The dynamics of a fermion can be expressed by the so-called Dirac-Lagrangian [42]:

$$\mathcal{L} = i\left(\hbar c\right)\bar{\psi}\gamma^{\mu}\partial_{\mu}\psi - \left(mc^{2}\right)\bar{\psi}\psi, \tag{2.7}$$

where ψ is the so-called Dirac field which describes fermions, ∂_{μ} the space time derivative and m its mass. $\bar{\psi}$ is connected to the adjoined of the field by:

$$\bar{\psi} = \psi^{\dagger}\gamma^{0} \tag{2.8}$$

The Dirac matrices have to to fulfil the condition:

$$\{\gamma^{\mu}, \gamma^{\nu}\} = 2g^{\mu\nu} \times \mathbf{1}, \tag{2.9}$$

where $g^{\mu\nu}$ is the Cartesian metric tensor. So a 4×4 representation can be chosen as:

$$\gamma^{0} \equiv \begin{pmatrix} 1 & 0 \\ 0 & 1 \end{pmatrix}, \qquad \gamma^{i} \equiv \begin{pmatrix} 0 & \sigma^{i} \\ -\sigma^{i} & 0 \end{pmatrix}, \tag{2.10}$$

where σ^{i} are the Pauli matrices. This is the so-called Dirac representation [42].
It can be easily seen, that this representation is block diagonal and so reducible. Due to this fact a two-dimensional representation can be formed by considering each block separately:

$$\psi = \begin{pmatrix} \psi_{L} \\ \psi_{R} \end{pmatrix}. \tag{2.11}$$

The two occurring components are called left- and right-handed Weyl spinors. They have a slightly different behaviour under Lorentz transformations:

$$\begin{aligned} \psi_{L} &\rightarrow \left(1 - i\theta \cdot \frac{\sigma}{2} - \beta\frac{\sigma}{2}\right)\psi_{L} \\ \psi_{R} &\rightarrow \left(1 - i\theta \cdot \frac{\sigma}{2} + \beta\frac{\sigma}{2}\right)\psi_{L}, \end{aligned} \tag{2.12}$$

where θ describes a rotation and β describes a Lorentz boost [42].
The Dirac field can be quantised by writing it as:

$$\begin{aligned} \psi\left(\mathbf{x}\right) &= \int \frac{d^{3}p}{\left(2\pi\right)^{3}} \frac{1}{\sqrt{2E_{\mathbf{p}}}} \sum_{s} \left(a^{s}_{\mathbf{p}} u^{s}(p) e^{-i\mathbf{p}\cdot\mathbf{x}} + b^{s\dagger}_{\mathbf{p}} v^{s}(p) e^{i\mathbf{p}\cdot\mathbf{x}}\right) \\ \bar{\psi}\left(\mathbf{x}\right) &= \int \frac{d^{3}p}{\left(2\pi\right)^{3}} \frac{1}{\sqrt{2E_{\mathbf{p}}}} \sum_{s} \left(b^{s}_{\mathbf{p}} \bar{v}^{s}(p) e^{-i\mathbf{p}\cdot\mathbf{x}} + a^{s\dagger}_{\mathbf{p}} \bar{u}^{s}(p) e^{i\mathbf{p}\cdot\mathbf{x}}\right), \end{aligned} \tag{2.13}$$

where S assigns the two free solutions for p^{2}, u and v are spinors corresponding to particle and antiparticle and $E_{\mathbf{p}}$ is the energy solution corresponding to the momentum state $\mathbf{p}$. The creators and the annihilators obey the anti-commutation rules [42]:

$$\{a^{s}_{\mathbf{p}}, a^{s\dagger}_{\mathbf{q}}\} = \{b^{s}_{\mathbf{p}}, b^{s\dagger}_{\mathbf{q}}\} = \left(2\pi\right)^{3}\delta^{3}\left(\mathbf{p} - \mathbf{q}\right)\delta_{ab}. \tag{2.14}$$

In the framework of fermions one needs two different types of operators, because there are particles and antiparticles (fermions are no so-called Majorana particles[1]). For both of them one needs one creator and one annihilator. The vacuum state is the same for both particles types [42]:

$$a^{s}_{\mathbf{p}}\left|0\right\rangle = b^{s}_{\mathbf{p}}\left|0\right\rangle = 0. \tag{2.15}$$

[1] It is identical with its antiparticle.

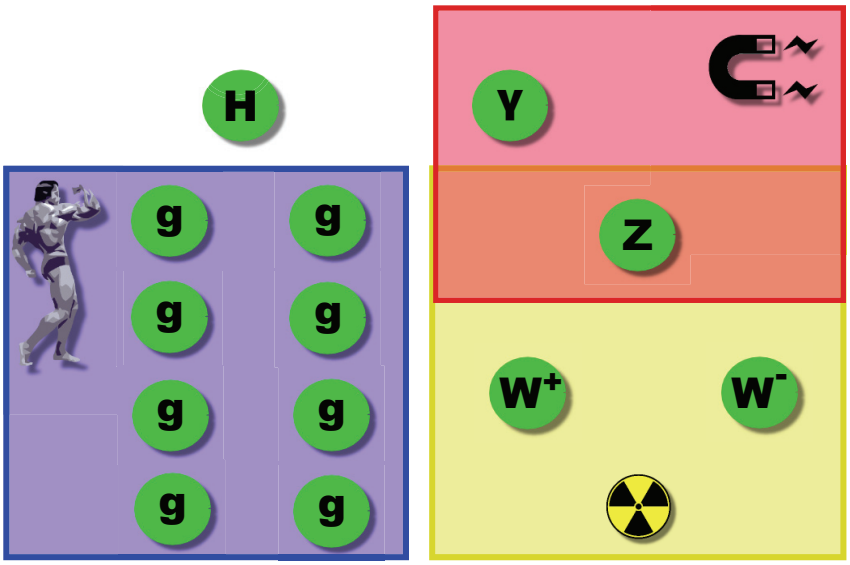

Figure 2.2: SM bosons: The strong interaction is carried by eight gluons. γ is the neutral carrier of the electromagnetic interaction. The weak interaction has three carriers, the electrically neutral Z-boson and the two electrically charged W-bosons.

2.1.2 Gauge Bosons

Additional to the matter particles there are particles carrying forces, the so-called gauge bosons. Bosons are particles with integer spin (vector particles). The carrier of the electromagnetic force is the photon (γ). The photon is also known as the light quantum. This quantisation was first proven in 1905 by the photo effect. The photon is electromagnetically neutral, thus it is not able to self-interact. The electromagnetic interaction can be described by a $U(1)$ gauge theory[30].
The carriers of the weak interaction are the W- ($W^{\pm}$) and Z-bosons (Z^0). The weak isospin of the Z- and W-bosons is non-zero. Therefore they are self-interacting. The weak gauge bosons are massive, which cannot be easily described in the SM. All possible mass terms would be non-renormalisable. Due to this fact the Higgs mechanism has been introduced, which will be further described in Sect. 2.1.3 [30].
The strong force underlies a $SU(3)$ symmetry group. For $SU(N)$ groups the number of generators is $N^2 - 1$ the so-called gluons. These particles are able to interact with themselves due to the non-Abalian structure of the $SU(3)$. The gluon even carries two colour

charges. This is how the different gluon eigenstates can be built:

$$\begin{array}{ll} \frac{\left|r\bar{b}\right\rangle + \left|\bar{r}b\right\rangle}{\sqrt{2}} & -i\frac{\left|r\bar{b}\right\rangle - \left|\bar{r}b\right\rangle}{\sqrt{2}} \\ \frac{\left|r\bar{g}\right\rangle + \left|\bar{r}g\right\rangle}{\sqrt{2}} & -i\frac{\left|r\bar{g}\right\rangle - \left|\bar{r}g\right\rangle}{\sqrt{2}} \\ \frac{\left|r\bar{b}\right\rangle + \left|\bar{r}b\right\rangle}{\sqrt{2}} & -i\frac{\left|r\bar{b}\right\rangle - \left|\bar{r}b\right\rangle}{\sqrt{2}} \\ \frac{\left|r\bar{r}\right\rangle - \left|\bar{b}b\right\rangle}{\sqrt{2}} & \frac{\left|r\bar{r}\right\rangle + \left|\bar{b}b\right\rangle - 2\left|g\bar{g}\right\rangle}{\sqrt{6}} \end{array} \tag{2.16}$$

Gauge bosons can be described by Maxwell fields:

$$\mathcal{L} = -\frac{1}{16\pi} F_{\mu\nu} F^{\mu\nu}, \tag{2.17}$$

where $F_{\mu\nu}$ is the so-called field tensor and can for photons be written as

$$F_{\mu\nu} = \partial_\mu A_\nu - \partial_\nu A_\mu,$$

where A^μ is the four vector of the vector potential. It is invariant under $U(1)$ gauge transformations [42]. For non-Abelian theories another term is coming into the game, which takes the self-interactions of the gauge bosons into account:

$$F^a_{\mu\nu} = \partial_\mu A^a_\nu - \partial_\nu A^a_\mu + g f^{abc} A^b_\mu A^c_\nu, \tag{2.18}$$

where g is the coupling, f^{abc} the structure constant of the gauge group defined by:

$$[t_a, t_b] = f^{abc} t_c. \tag{2.19}$$

a, b, c run over $\{1, ..., N^2 - 1\}$.
The vector fields come into play, if one assumes local gauge invariance of the fermion Lagrangian under the gauge groups of the fundamental forces. If one assumes a gauge transformation $\psi \to e^{i\theta(x)}\psi$, where θ is the transformation parameter, the Lagrangian of a Dirac field transforms as:

$$\mathcal{L} \to \mathcal{L} - \hbar c \left(\partial_\mu \theta\right) \psi \gamma_\mu \psi. \tag{2.20}$$

To make the Lagrangian invariant under local gauge transformations, interactions to a gauge field have to be introduced:

$$\mathcal{L} = \left(i\hbar c \bar{\psi}\gamma^\mu \partial_\mu \psi - mc^2 \bar{\psi}\psi\right) - q\bar{\psi}\gamma^\mu \psi A_\mu, \tag{2.21}$$

where q is the charge of the involved particle. If one assumes freedom of gauge $A_\mu \to A_\mu + \partial_\mu \lambda$ and chooses λ to be defined by:

$$\lambda\left(x\right) \equiv -\frac{\hbar c}{q}\theta\left(x\right). \tag{2.22}$$

the Lagrangian is invariant under gauge transformations again [42]. Additional to the interaction term the kinetic term of the vector field has to be introduced to describe the kinematics of the vector field. The final is then given by [43–50]:

$$\mathcal{L} = \left(i\hbar c \bar{\psi}\gamma^\mu D_\mu \psi - mc^2 \bar{\psi}\psi\right) + \left(-\frac{1}{16\pi} F_{\mu\nu} F^{\mu\nu}\right), \tag{2.23}$$

where $D_\mu = \partial_\mu + i\frac{q}{\hbar c}A_\mu$. This Lagrangian describes electromagnetic processes. The theory is called quantum-electrodynamics (QED). It describes a photon interacting with electrically charged fermions (positrons and electrons).
In case of the strong interaction, the ψ field gets a colour multiplet and the field tensor gets an additional term like in equation 2.18. Thus the gauge transformation U can be divided into two parts:

$$U = e^{i\theta}e^{i\lambda\cdot\tau}. \tag{2.24}$$

The first part looks the same like in QED case. In the second part τ^a are the generators of the gauge group and λ^a are the additional transformation parameters. Now again the covariant derivative has to be introduced:

$$D_\mu = \partial_\mu + i\frac{q}{\hbar c}\lambda\cdot\mathbf{A}_\mu. \tag{2.25}$$

Here the $\mathbf{A}_\mu$ are eight gauge fields. The resulting Lagrangian of quantum chromodynamics (QCD) is [8–12, 40]:

$$\mathcal{L} = \left(i\hbar c\bar{\psi}\gamma^\mu\partial_\mu\psi - mc^2\bar{\psi}\psi\right) - \frac{1}{16\pi}F^{\mu\nu}F_{\mu\nu} - \left(q\bar{\psi}\gamma^\mu\lambda\psi\right)\cdot\mathbf{A}_\mu \tag{2.26}$$

2.1.3 Electroweak Unification and the Higgs Mechanism

Up to this point only massless gauge fields have been considered. To consider also massive gauge fields as observed in the weak interaction a new formalism has to be introduced, the spontaneous symmetry breaking (SSB) [31–36, 51]. Just introducing new mass terms would not be possible in the SM, because they would not be renormalisable.
One can picture SSB by imaging a hungry donkey standing on top of a hill surrounded by grass (figure 2.3). At this moment it does not matter to the donkey on which point it goes down the hill to eat the grass growing there. For the donkey there are several ”vacua” (best states) given. The problem of the donkey to satisfy his appetite is invariant under change of xy-direction. As soon as the donkey starts to run down the hill this symmetry is spontaneously broken, because the donkey decided for one ”vacuum” and thus chooses one direction of preference [52].
It is the same with the Lagrangian of a scalar field:

$$\mathcal{L} = \underbrace{\left(\partial_\mu\phi\right)\left(\partial^\mu\phi\right)}_{T} + \underbrace{\frac{1}{2}\mu^2\phi^2 - \frac{\lambda^2}{4}\phi^4}_{U}. \tag{2.27}$$

Here ϕ is the scalar field, μ and λ are free parameters. T is the kinetic energy and U the potential. The ground state of this potential is $\phi = \pm\frac{\mu}{\lambda}$ [30].
If one introduces:

$$\eta = \phi \pm \frac{\mu}{\lambda} \tag{2.28}$$

as new field variable, the Lagrangian can be expanded as:

$$\mathcal{L} = \frac{1}{2}\left(\partial_\mu\eta\right)\left(\partial^\mu\eta\right) - \mu^2\eta^2 \pm \mu\lambda\eta^3 - \frac{1}{4}\lambda^2\eta^4 + \frac{1}{4}\frac{\mu^4}{\lambda^2}. \tag{2.29}$$

Now the second term can be interpreted as a mass term and the mass can be read out to be:

$$m = \sqrt{2}\frac{\mu\hbar}{c}. \tag{2.30}$$

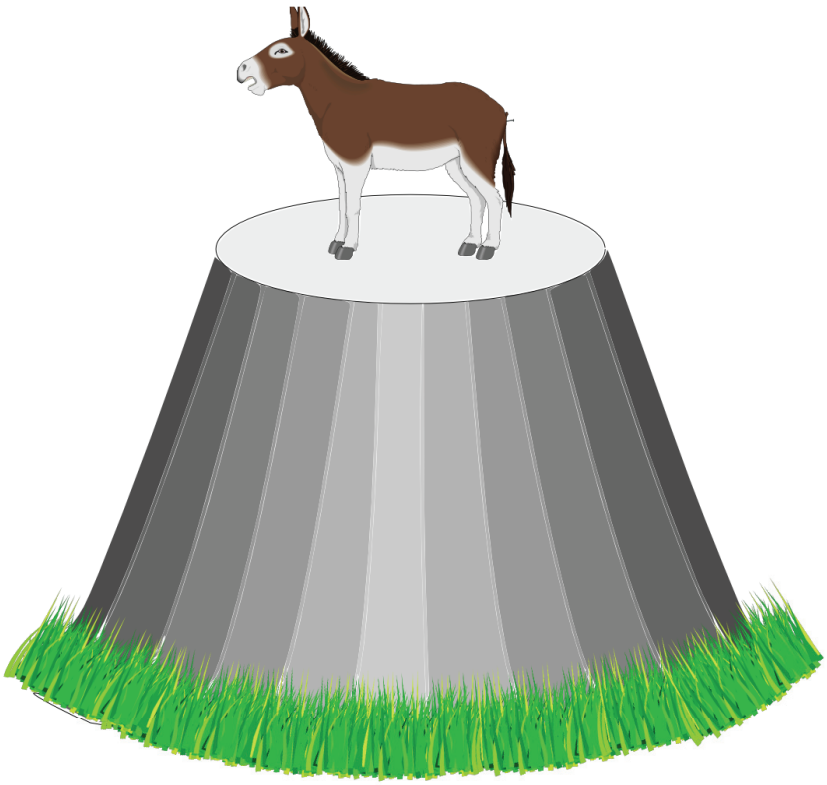

Figure 2.3: Spontaneous Symmetry Breaking: As long as the donkey is standing on top of the hill the problem to satisfy his appetite is invariant under rotation in the xy-plane. As soon as the donkey runs down the hill one direction is preferred and the symmetry given before is spontaneously broken.

The Lagrangian given in is invariant under $\phi \to -\phi$ transformation while the ground state is either $+\frac{\mu}{\lambda}$ or $-\frac{\mu}{\lambda}$ and is not invariant under the change of sign. This indicates a spontaneous breaking of this symmetry [30].

The GWS theory and the Higgs Mechanism

The GWS (Glashow Weinberg Salam) theory was developed in the 1960s and it unifies the electromagnetic with the weak force to an electroweak force [4, 14, 15]. The resulting Lagrangian has to be invariant under symmetry transformations of $SU(2) \bigotimes U(1)$. That means the Lagrangian has to be invariant under a transformation like:

$$\phi \to \exp\left(i\alpha_a \tau^a\right) \exp\left(i\frac{\beta}{2}\right) \phi, \tag{2.31}$$

where $\tau^a = \frac{\sigma^a}{2}$ (σ^a are the three Pauli matrices in case of $SU(2)$) and α^a and β parametrise the transformation [42].
The scalar field can be parametrised as:

$$\phi = \exp\left(-i\frac{\vec{\psi}\vec{\sigma}}{2}\right) \begin{pmatrix} 0 \\ \frac{v+h(x)}{\sqrt{2}} \end{pmatrix}. \tag{2.32}$$

Therefore ϕ acquires the vacuum expectation value

$$\langle\phi\rangle = \frac{1}{\sqrt{2}} \begin{pmatrix} 0 \\ v \end{pmatrix}.$$

The Lagrangian of the scalar field (2.27) is required to be invariant under a $SU(2) \bigotimes U(1)$ gauge transformation, the covariant derivative has to be chosen as [42]:

$$\mathcal{D}_\mu = \partial_\mu - igA^a_\mu \tau^a - i\frac{g'}{2}. \tag{2.33}$$

If the resulting Lagrangian is evaluated at the vacuum expectation value, three massive gauge bosons can be identified:

$$\begin{aligned} W^\pm_\mu &= \frac{1}{\sqrt{2}} \left(A^1_\mu \mp iA^2_\mu\right) \\ Z^0_\mu &= \frac{1}{\sqrt{g^2+g'^2}} \left(gA^3_\mu - g'B_\mu\right). \end{aligned} \tag{2.34}$$

The fourth gauge boson A_μ appears to be massless:

$$A_\mu = \frac{1}{\sqrt{g^2+g'^2}} \left(g'A^3_\mu + gB_\mu\right). \tag{2.35}$$

To change between mass and interaction eigenstates of the neutral bosons a rotation can be introduced:

$$\begin{pmatrix} Z^0 \\ A \end{pmatrix} = \begin{pmatrix} \cos\theta_W & -\sin\theta_W \\ \sin\theta_W & \cos\theta_W \end{pmatrix} \begin{pmatrix} A^3 \\ B \end{pmatrix},$$

where θ_W is the so-called Weinberg angle [42]. It can be expressed by

$$\cos\theta_W = \frac{g}{\sqrt{g^2+g'^2}}, \qquad \sin\theta_W = \frac{g'}{\sqrt{g^2+g'^2}}.$$

The masses of the gauge bosons can be extracted from the quadratic term of the potential:

$$\begin{aligned} m_W &= g\frac{v}{2} \\ m_Z &= \sqrt{g^2+g'^2}\frac{v}{2}. \end{aligned} \tag{2.36}$$

By additionally introducing

$$\tau^{\pm} = \tau^1 \pm \tau^2,$$

the covariant derivative can be written in the mass basis (and therefore also the Lagrangian):

$$\begin{aligned} \mathcal{D}_\mu =& \partial_\mu - i\frac{g}{\sqrt{2}}\left(W_\mu^+\tau^+ + W_\mu^-\tau^-\right) \\ & - i\frac{g}{\cos\theta_W}Z_\mu\left(\tau^3 - \sin^2\theta_W Q\right) - ig'\sin\theta_W A_\mu Q, \end{aligned}$$

where $Q = I_3 + \frac{Y}{2}$ is the electromagnetic charge [42].

2.1.4 Limits of the Standard Model

Despite the Standard Model describes many phenomena precisely, there are some phenomena, which cannot be explained. In this section some limitations of the Standard Model will be given.

Unification of the coupling constants

Actually the Standard Model coupling constants are not constant, but they are changing with the energy. The reason for this change is that the electromagnetic potential and the colour potential change for different energy scales Q^2. Due to the self-coupling of the gluon the vacuum polarisation obtains more terms than the one of the electromagnetic.
In renormalisable theories ultraviolet divergences ($Q^2 \to \infty$) are absorbed by the coupling constants. Other divergences get cancelled by adding appropriate amplitudes. For that reason the couplings become dependent on the energy scale. For the electromagnetic force after renormalisation the coupling is given by:

$$\alpha\left(Q^2\right) = \frac{\alpha}{1 - \frac{\alpha}{3\pi}\ln\left(\frac{Q^2}{m_e^2}\right)},$$

where m_e is the mass of the electron. The strong coupling can be calculated to be

$$\alpha_S\left(Q^2\right) = \frac{a\pi}{\left(11 - \frac{2N_f}{3}\right)\cdot\ln\left(\frac{Q^2}{\Lambda^2}\right)},$$

where N_f is the number of generations and Λ is the confinement scale. From precise measurements and the extrapolation to higher energies one can exclude that they unify in one point (see figure 2.4) [53].

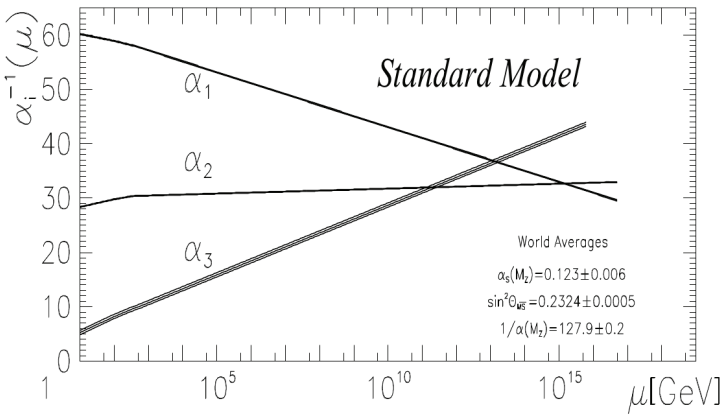

Figure 2.4: Dependence of SM gauge couplings on the energy scale. α_1 is the electromagnetic, α_2 the weak and α_3 the strong coupling. μ is the energy scale. One can easily see, that they don't meet all together in one single point. Taken from [53].

The Hierarchy Problem

There are two very different energy scales in the Standard Model: the energy scale of the weak interaction M_W and the Planck scale M_{Planck}. Their relation is

$$\frac{M_W}{M_{\text{Planck}}} = 10^{-17}.$$

This number is small and the question is: How to get such a small number in a natural way?
The same problem is given for the Higgs boson compared to the Planck scale. Even if this number is introduced radiative corrections like shown in figure 2.5 would destroy it. These corrections have quadratic divergences $\Delta M_H \approx \mathcal{O}(M_{\text{Planck}})$. Thus to keep the Higgs mass at the order of the electroweak scale would cause an incredible fine-tuning [53].

2.2 Supersymmetry

The SM describes many phenomena of nature precisely. However, it leaves many open questions. Therefore one should introduce theories embedding the Standard Model. One of these theories is supersymmetry (SUSY), which is a symmetry between bosons and fermions (Fig. 2.6). A SUSY generator Q can be defined by [54]:

$$\begin{aligned} Q\,|\text{boson}\rangle &= |\text{fermion}\rangle \\ Q\,|\text{fermion}\rangle &= |\text{boson}\rangle \end{aligned} \tag{2.37}$$

The difficulty of a theory like SUSY is the connection of a commuting (bosonic) with an anti-commuting (fermionic) algebra. For this reason the SUSY algebra has to be a generalisation of the Poincare group. It links together various representations with different

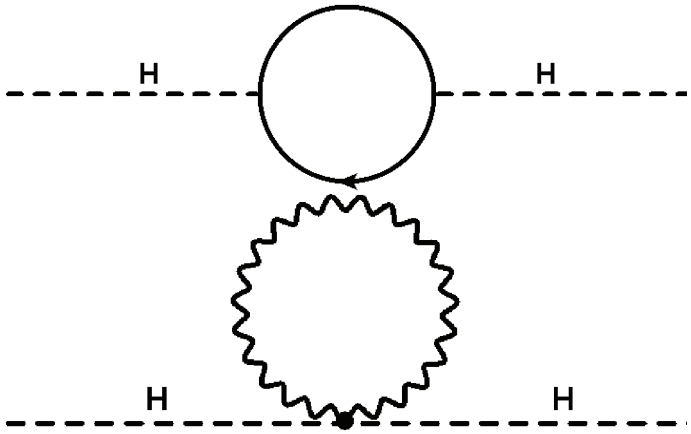

Figure 2.5: Corrections to the Higgs mass in the Standard Model. Upper picture: fermion loop (contributions from heavy fermions, like top quark and τ lepton), lower picture: gauge boson loop (contributions from heavy gauge bosons W and Z).

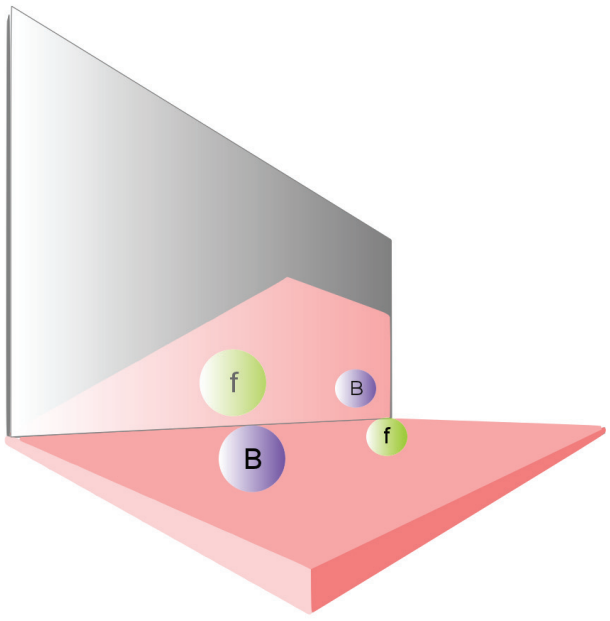

Figure 2.6: Supersymmetry is a symmetry between fermions and bosons. SUSY generators transform a fermion into a boson and vice versa.

spins. Therefore its key relation has to be given by an anti-commutator relation:

$$\{Q_\alpha, Q_{\dot{\alpha}}\} = 2\sigma^\mu_{\alpha\dot{\alpha}} P_\mu, \tag{2.38}$$

where P_μ is a space time translation [54].
What makes SUSY an attractive model of new physics is that it naturally solves many problems of the Standard Model at once if one assumes the SUSY particle masses to be at the TeV scale. This will be further explained in the next section.

2.2.1 Motivation for Supersymmetry

Gravity

A thing that has not been mentioned in the context of the standard model is gravity, the fourth fundamental force. That is because there is no possibility to include gravity into the Standard Model. The carrier of gravity, the so-called graviton, is a spin 2 particle. Thus the graviton exists in another representation of the Poincare group, which are particles of spin 1 and can therefore not been unified (according to the "'no-go theorem" by Coleman and Mandula) [54–56].
In SUSY the embedding of gravity into a fundamental theory is getting possible due to the SUSY breaking operators. If one applies such a SUSY operator on the graviton the following chain can be obtained:

$$\text{spin } 2 \rightarrow \text{spin } \frac{3}{2} \rightarrow \text{spin } 1 \rightarrow \text{spin } \frac{1}{2} \rightarrow \text{spin } 0$$

From this one can see that SUSY connects all spin states arising in nature [54].

Unification of the coupling constants

Contrary to the SM in SUSY the unification of the gauge couplings is possible. In Fig. 2.7 it is shown that due to the contribution of the SUSY particles at a scale of about [57] $M_{\text{SUSY}} = 10^{3.4\pm0.9\pm0.4}$ GeV, the coupling constants unify at a scale of $M_{\text{GUT}} = 10^{15.8\pm0.3\pm0.1}$ GeV [53]. It is amazing that SUSY masses at exactly this scale are also able to restore the hierarchy problem.

The Hierarchy Problem

In SUSY the radiative corrections mentioned in Sect. 2.1.4 include fermions additional to bosons and bosons additional to fermions with the same attribute as their SM partners (see Sect. 2.2.3). This leads to a cancellation of the quadratic divergences, because according to the Feynman rules they contribute with different signs

$$\Delta M_H \equiv \mathcal{O}(\alpha) \left| M_{\text{boson}} - M_{\text{fermion}} \right| \equiv \mathcal{O}\left(10^{-2}\right) M_{\text{SUSY}}.$$

Therefore if one assumes the radiative corrections to the Higgs mass not to be larger than a few hundred GeV, the mass of the SUSY particles should be at the scale

$$M_{\text{SUSY}} \leq 10^3 \text{ GeV},$$

which was already predicted by the unification argument [53, 54].

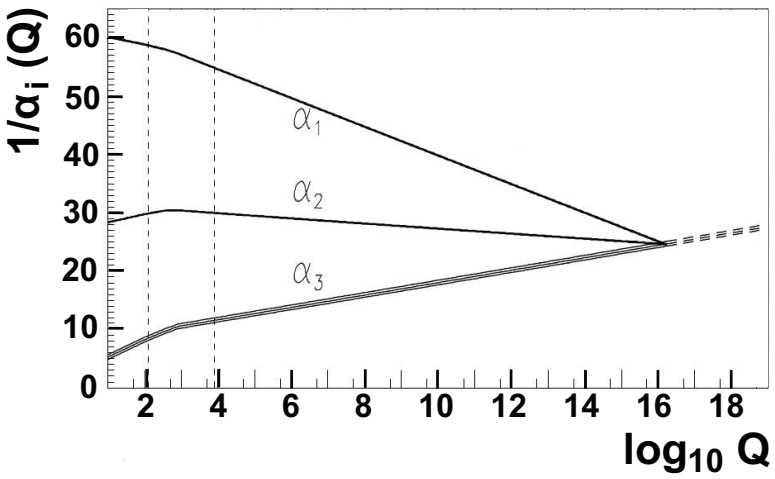

Figure 2.7: Dependence of gauge couplings in a supersymmetric model with $M_{\text{SUSY}} = \mathcal{O}\left(10^3 GeV\right)$ on the energy scale. α_1 is the electromagnetic, α_2 the weak and α_3 the strong coupling. μ is the energy scale [53].

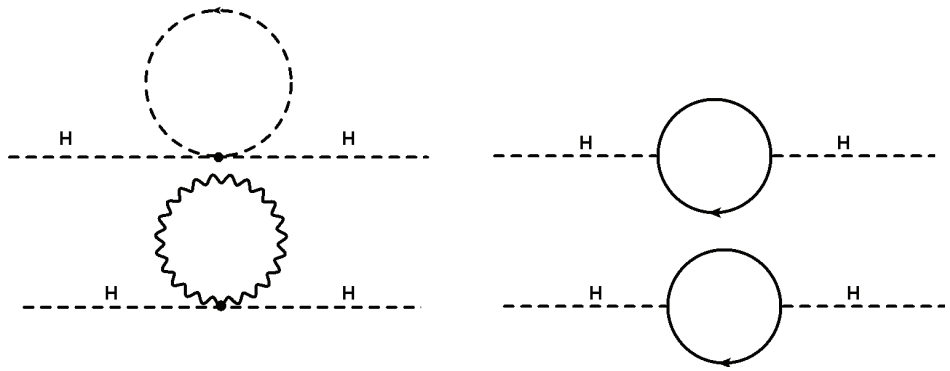

Figure 2.8: Corrections to the Higgs mass in including the SUSY contributions. Upper picture: standard model fermion and its scalar SUSY partner (contributions from top, stop quark, squark, tau, and stau), lower picture: Standard Model gauge boson and SUSY partners (contribution of heavy gauge bosons W and Z and gauginos wino and zino).

2.2.2 The SUSY formalism

As mentioned earlier, SUSY transforms fermions into bosons and vice-versa:

$$F \to \delta F = \epsilon B$$
$$B \to \delta B = \epsilon F,$$

where F is a fermion state, B a boson state, $\hat{F}$ and $\hat{B}$ the corresponding operators , δ the transformation operator and ϵ is an infinitesimal transformation parameter. Bosons correspond to commuting and fermions to anti-commuting operators:

$$\left[\hat{B}, \hat{B}\right] = 0$$
$$\{\hat{F}, \hat{F}\} = 0.$$

Thus the fermion has to have Fermi state statistics (a state can only be taken by one particle) and bosons to have a Bose state statistics. Therefore, the SUSY generators have to be fermionic, for example it has to change two properties of the particle:

1. The spin of the particle has to be changed by a half-odd number ($1 \to \frac{1}{2}$, $\frac{3}{2} \to 1$)
2. The statistics of the particle have to be changed from Fermi to Bose statistics or vice versa.

Hence, SUSY generators have to be anti-commuting [54, 56].

The SUSY Algebra

The Poincare group includes Lorentz transformations ($M_{\mu\nu}$) and space translations (P_μ). To extend the Poincare group to the Super-Poincare group, one additionally needs internal symmetry operators B_r and the already mentioned spinoral SUSY generators Q^i and $\bar{Q}^i$. With these additional generators the Super-Poincare-Lie-Algebra appears as [19, 54]:

$$\begin{aligned}
&[P_\mu, P_\nu] = 0 \\
&[P_\mu, M_{\rho\sigma}] = i\left(g_{\mu\rho}P_\sigma - g_{\mu\sigma}P_\rho\right) \\
&[M_{\mu\nu}, M_{\rho\sigma}] = i\left(g_{\nu\rho}M_{\mu\sigma} - g_{\nu\sigma}M_{\mu\rho} - g_{\mu\rho}M_{\nu\sigma} + g_{\mu\sigma}M_{\nu\rho}\right) \\
&[B_r, B_s] = iC^t_{rs}B_t \\
&[B_r, P_\mu] = [B_r, M_{\mu\sigma}] = 0 \\
&\left[Q^i_\alpha, P_\mu\right] = \left[Q^i_{\dot{\alpha}}, P_\mu\right] = 0 \\
&\left[Q^i_\alpha, M_{\mu\nu}\right] = \frac{1}{2}\left(\sigma_{\mu\nu}\right)^\beta_\alpha Q^i_\beta \qquad \left[\bar{Q}^i_\alpha, M_{\mu\nu}\right] = -\frac{1}{2}\bar{Q}^i_{\dot{\beta}}\left(\sigma_{\mu\nu}\right)^{\dot{\beta}}_{\dot{\alpha}} \\
&\left[Q^i_\alpha, B_r\right] = \left(b_r\right)^i_j Q^j_\alpha \qquad \left[\bar{Q}^i_{\dot{\alpha}}, B_r\right] = -\bar{Q}^j_{\dot{\alpha}}\left(b_r\right)^i_j \\
&\{Q^i_\alpha, \bar{Q}^j_{\dot{\beta}}\} = 2\delta^{ij}\left(\sigma^\mu\right)_{\alpha\dot{\beta}}P_\mu \\
&\{Q^i_\alpha, Q^j_\beta\} = 2\epsilon_{\alpha\beta}Z^{ij} \qquad \{\bar{Q}^i_{\dot{\alpha}}, \bar{Q}^j_{\dot{\beta}}\} = -2\epsilon_{\dot{\alpha}\dot{\beta}}Z^{ij} \\
&[Z_{ij}, \text{anything}] = 0 \\
&Z_{ij} = a^r_{ij}b_r \qquad Z^{ij} = Z^\dagger_{ij} \qquad \alpha = \beta = \dot{\alpha} = \dot{\beta} = 1, 2 \qquad j = 1, 2, ..., N,
\end{aligned} \tag{2.39}$$

State	Expression	N_{States}
vacuum	$\|E,\lambda\rangle$	1
1 particle	$\bar{Q}_i \|E,\lambda\rangle = \left\|E,\lambda+\frac{1}{2}\right\rangle_i$	$\begin{pmatrix} N \\ 1 \end{pmatrix} = N$
2 particles	$\bar{Q}_i\bar{Q}_j \|E,\lambda\rangle = \|E,\lambda+1\rangle_{ij}$	$\begin{pmatrix} N \\ 2 \end{pmatrix} = \frac{N(N-1)}{2}$
...	...	...
N particles	$\bar{Q}_1\bar{Q}_2...\bar{Q}_N \|E,\lambda\rangle = \left\|E,\lambda+\frac{N}{2}\right\rangle_i$	$\begin{pmatrix} N \\ N \end{pmatrix} = 1$

Table 2.1: Number of SUSY states in models with different number of SUSY generators [54].

where Z_{ij} are so-called central charges and α, β, $\dot{\alpha}$ and $\dot{\beta}$ are the spinorial indexes. N is the number of SUSY generators. The easiest case is the so-called $N = 1$ like in the MSSM supersymmetry with only one SUSY generator. If $N > 1$ the model is called extended supersymmetry [54].
Tab. 2.1 shows the number of states for a system with energy E and a vacuum helicity of λ. Due to the Pauli principle no state can be populated for twice. This causes an upper limit for possible SUSY states in a model with a given N. Additionally, due to the fact that the SUSY generators commute with the Hamiltonian the energy does not change by applying the SUSY generator to a state with given energy E. Thus there is a given sequence of a total number of fermions and an equal number of bosons [54].
The theory forming the basis of this thesis is an $N = 1$ theory (simple SUSY). There are two kinds of multiplets given in this model:

1. The chiral multiplets with helicity ground state $\lambda = 0$ containing a spin-$\frac{1}{2}$ fermion and a scalar as physical states: (ϕ, ψ)

2. The vector multiplet with helicity ground state $\lambda = \frac{1}{2}$ containing a spin-$\frac{1}{2}$ fermion and a spin-1 boson: (λ, A_μ).

As the number of fermions is equal to the number of bosons in supersymmetric model, the SM cannot be a SUSY theory on its own. It has to be extended by new particles (Sect. 2.2.3) [54].

Superspace

To extend space to a superspace two spinorial degrees of freedom have to be added. For this purpose the two Grassmanian variables θ and $\bar{\theta}$ are introduced. These variables anti-commute with each other:

$$\{\theta_\alpha, \theta_\beta\} = 0, \quad \{\bar{\theta}_{\dot{\alpha}}, \bar{\theta}_{\dot{\beta}}\} = 0, \quad \text{where } \alpha, \beta = 1, 2 \text{ and } \dot{\alpha}, \dot{\beta} = 1, 2. \tag{2.40}$$

For this reason the product of Grassmanian variables is equal zero: $\theta_\alpha\theta_\alpha = \bar{\theta}_{\dot{\alpha}}\bar{\theta}_{\dot{\alpha}} = 0$.
A field depending on x^μ, θ and $\bar{\theta}$ is called superfield. While P^μ (momentum operator) generates just a shift in space-time $\phi(x) \to \phi(x + \delta x)$, the supercharges Q and $Q^\dagger$ generate

shifts in spinorial arguments and also space-time shifts (equation 2.39) [54].
In quantum mechanics the momentum operator can always be written in the representation of space-time coordinates:

$$P^{\mu} = i\partial^{\mu}.$$

In analogy to quantum mechanics the SUSY charges can be written in the representation of the introduced Grassmanian variables:

$$\begin{aligned} Q_{\alpha} &= \frac{\partial}{\partial\theta_{\alpha}} - i\sigma^{\mu}_{\alpha\dot{\alpha}}\bar{\theta}^{\dot{\alpha}}\partial_{\mu} \\ Q^{\dagger}_{\dot{\alpha}} &= -\frac{\partial}{\partial\bar{\theta}_{\dot{\alpha}}} + i\theta^{\alpha}\sigma^{\mu}_{\alpha\dot{\alpha}}\partial_{\mu}, \end{aligned} \tag{2.41}$$

where σ^{μ} are the Pauli matrices defined in A.1. The additional terms of the space-time derivatives describe the additional space-time shift caused by the SUSY charges [54].

Superfields and Superpotentials

A chiral superfield is expressed in superspace as a field $\Phi(x,\theta)$ independent of $\bar{\theta}$. Because of the nil-potency of the Grassmanian variables the chiral field can be expanded as [23]:

$$\Phi(x,\theta) = \phi(x) + \theta\chi(x) + \frac{1}{2}\theta\theta F(x), \tag{2.42}$$

where ϕ, χ and F are component fields. By applying a SUSY transformation

$$\begin{aligned} \delta\Phi &= \left(-i\xi^{a}Q_{a} - i\xi^{\star}_{a}\bar{Q}^{a}\right)\Phi \\ &\equiv \delta_{\xi}\phi + \theta^{a}\delta_{\xi}\chi_{a} + \frac{1}{2}\theta\theta\delta_{\xi}F, \end{aligned}$$

on the superfield Φ, the transformations of the component fields can be approximated as:

$$\begin{aligned} \delta_{\xi}\phi &= \sqrt{2}\xi\chi \\ \delta_{\xi}\chi &= i\sqrt{2}\sigma^{\mu}\bar{\xi}\partial_{\mu}\phi + \sqrt{2}\xi F \\ \delta_{\xi}F &= i\sqrt{2}\sigma^{\mu}\partial_{\mu}\phi. \end{aligned} \tag{2.43}$$

The change in the field F is just a total derivative, thus it vanishes under integration over space-time. Therefore, the SUSY action automatically appears to be invariant for this so-called auxiliary field.
The other two fields have the same number of bosonic and fermionic degrees of freedom. Under the applied SUSY transformation they transform among themselves. They are the so-called supersymmetric partners. χ can be thought of as a Standard Model fermion with its newly introduced SUSY partner ϕ [54, 58].
The products of two chiral superfields appear to have three kinds of terms:

1. Terms independent of θ: $\phi_i\phi_j$
2. Linear terms: $\theta\left(\chi_i\phi_j + \chi_j\phi_i\right)$
3. Bi-linear terms: $\frac{1}{2}\theta\theta\left(\phi_iF_j + \phi_jF_i - \chi_i\chi_j\right)$

All other terms vanish because of the nil-potency of the Grassmanian numbers. The product can also be expressed in terms of the component fields

$$\Phi_i \Phi_j = \phi_i j + \theta \chi_{ij} + \frac{1}{2}\theta\theta F_{ij},$$

where

$$\begin{aligned} \phi_{ij} &= \phi_i \phi_j, \\ \chi_{ij} &= \chi_i \phi_j + \phi_j \chi_i, \\ F_{ij} &= \phi_i F_j + \phi_j F_i - \chi_i \chi_j. \end{aligned}$$

The so-called quadratic superpotential can be defined as:

$$\begin{aligned} W_{\text{quad}} &= \frac{1}{2} M_{ij} \Phi_i \Phi_j |_F \\ &= M_{ij} \phi_i F_j - \frac{1}{2} M_{ij} \chi_i \chi_j. \end{aligned} \tag{2.44}$$

The fact that the superpotential is the F component of a superfield guarantees that the action is always invariant [58].
A cubic superpotential can also be introduced:

$$\begin{aligned} W_{\text{cubic}} &= \frac{1}{6} y_{ijk} \Phi_i \Phi_j \Phi_k |_F \\ &= \frac{1}{2} y_{ijk} \phi_i \phi_j F_k - \frac{1}{2} y_{ijk} \chi_i \chi_j \phi_k. \end{aligned} \tag{2.45}$$

In fact all SUSY interactions can be expressed in terms of these superpotentials:

$$W = \frac{1}{2} M_{ij} \Phi_i \Phi_j + \frac{1}{6} y_{ijk} \Phi_i \Phi_j \Phi_k + \ldots, \tag{2.46}$$

In the Lagrangian an integration over the Grassmanian numbers θ_1 and θ_2 ensures that only the F components of the superpotential are taken into account. This guarantees that all considered SUSY interactions have a SUSY invariant action [58].
To construct gauge invariant interactions of the introduced chiral superfields vector superfields are needed. The massless $U(1)$ field (spin 1) has two degrees of freedom just like a potential supersymmetric spin-$\frac{1}{2}$ partner, the so-called gaugino λ. Additionally, it has to have the same "internal" quantum numbers like the photon to be placed in the same supermultiplet. For that reason it has to:

- have no coupling to the photon,
- be electrically neutral
- and have a vanishing mass.

To also be able to get a valid off-shell supermultiplet notation for the vector supermultiplet an additional auxiliary field $D(x)$ has to be introduced, which is able to compensate the third degree of freedom of the spin-1 gauge boson [58].

The transformations of the component fields under a SUSY transformation can be estimated to be [58]

$$\begin{aligned}
\delta_\xi A^\mu &= \xi^\dagger \bar{\sigma}^\mu \lambda + \lambda^\dagger \bar{\sigma}^\mu \xi \\
\delta_\xi \lambda &= \frac{1}{2} i \sigma^\mu \bar{\sigma}^\nu \xi F_{\mu\nu} + \xi D \\
\delta_\xi \lambda^\dagger &= -\frac{1}{2} i \xi^\dagger \bar{\sigma}^\nu \sigma^\mu F_{\mu\nu} + \xi^\dagger D \\
\delta_\xi D &= -i \left(\xi^\dagger \bar{\sigma}^\mu \partial_\mu \lambda - (\partial_\mu \lambda)^\dagger \bar{\sigma}^\mu \xi \right).
\end{aligned}$$

These kinds of fields can be arranged together in vector superfields [23]. These Hermitian fields can be expanded in terms of the Grassmanian variables as:

$$\begin{aligned}
V\left(x,\theta,\bar{\theta}\right) =& C(x) + i\theta\chi(x) - i\bar{\theta}\bar{\chi}(x) \\
&+ \frac{i}{2}\theta\theta\left[M(x) + iN(x)\right] - \frac{i}{2}\bar{\theta}\bar{\theta}\left[M(x) + iN(x)\right] \\
&+ \theta\sigma^\mu\bar{\theta}A_\mu(x) + i\theta\theta\bar{\theta}\left[\lambda(x) + \frac{i}{2}\bar{\sigma}^\mu\partial_\mu\chi(x)\right] \\
&- i\bar{\theta}\bar{\theta}\theta\left[\lambda(x) + \frac{i}{2}\sigma^\mu\partial_\mu\bar{\chi}(x)\right] \\
&+ \frac{1}{2}\theta\theta\bar{\theta}\bar{\theta}\left[D(x) + \frac{1}{2}\Box C(x)\right].
\end{aligned} \tag{2.47}$$

In this expression all fields but A_μ and λ are unphysical and can be eliminated by a good choice of the gauge. E.g. in the Wess-Zumino gauge:

$$C = \chi = M = N = 0, \tag{2.48}$$

only physical degrees of freedom and the auxiliary field D remain [54]. Under an Abelian supergauge transformation the field given in equation 2.47 transforms as:

$$V \to V + \Phi + \Phi^\dagger, \tag{2.49}$$

where Φ and $\Phi^\dagger$ are chiral superfields as given in equation 2.42. This transformation behaviour looks for the physical component fields like an ordinary SM gauge transformation [54].
To formulate a supergauge theory, one needs the kinetic term of the vector superfield, namely the superfield strength tensor given by:

$$\begin{aligned}
W_\alpha &= -\frac{1}{4}\bar{D}^2 e^V D_\alpha e^{-V} \\
\bar{W}_\alpha &= -\frac{1}{4} D^2 e^V \bar{D}_\alpha e^{-V}.
\end{aligned} \tag{2.50}$$

D is the supercovariant derivative. In the Wess-Zumino gauge (equation 2.48) this is a polynomial in the component fields.
To generalise this result to non-Abelian gauge groups an additional group index has to be introduced running from one to the number of group generators (for $SU(N)$ this number is $N^2 - 1$). The difference of a non-Abelian and an Abelian gauge field is given by the

structure constant term in the field tensor (equation 2.18). In this context the superfield strength tensor includes an additional summation over the group generators [54]:

$$W_\alpha = t_a \left(i\lambda^a_\alpha + \theta_\alpha D^a \left(\sigma^\mu \sigma^\nu \theta\right)_\alpha F^a_{\mu\nu} + \theta^2 \sigma^\mu D_\mu \bar{\lambda}^a \right),$$

where

$$F^a_{\mu\nu} = \partial_\mu A^a_\nu - \partial_\nu A^a_\mu + f_{abc} A_\mu A_\nu, \qquad \text{and} \qquad D_\mu \bar{\lambda}^a = \partial \bar{\lambda}^a + f^{abc} A^b_\mu \bar{\lambda}^c.$$

SUSY Lagrangians

If the Lagrangian of a theory is known, the action can be calculated by a space time integration. Thus the last step to build a supersymmetric model is to construct a Lagrangian taking all aspects of the theory into account.
In supersymmetry the Lagrangians are polynomials of superfields. Like in the Standard Model (chapter 2.1) first the matter fields are introduced and the gauge fields are introduced later by adding gauge invariant interaction terms and the corresponding kinetic terms of the gauge fields.
The most general supersymmetric space time Lagrangian is [21, 54]:

$$\begin{aligned} \mathcal{L} = &\int d^2\theta d^2\bar{\theta} \Phi^\dagger_i \Phi_i \\ &+ \int d^2\theta \left[\lambda_i \Phi_i + \frac{1}{2} m_{ij} \Phi_i \Phi_j + \frac{1}{3} y_{ijk} \Phi_i \Phi_j \Phi_k \right] + \text{h.c.} \end{aligned} \tag{2.51}$$

The first term is the kinetic term of the fields included in the chiral supermultiplet. The other terms are the superpotential like introduced in equation 2.46. In this context products of chiral and anti-chiral fields cannot be introduced, because these would destroy the chiral superfield behaviour of the superpotential [54].
Expanding the superfields, performing integration taking into account the Grassmanian integration rules (equation A.4) and using the following constraints on the auxiliary fields

$$\begin{aligned} \frac{\partial \mathcal{L}}{\partial F^\star_k} &= F_k + \lambda^\star_k + m^\star_{ik} A^\star_i + y_{ijk} A^\star_i A^\star_j = 0, \\ \frac{\partial \mathcal{L}}{\partial F_k} &= F_k + \lambda_k + m_{ik} A_i + y_{ijk} A_i A_j = 0 \end{aligned}$$

lead to the well known expression

$$\begin{aligned} \mathcal{L} = &i\partial_\mu \bar{\psi}_i \bar{\sigma}^\mu \psi_i + A^\star_i \Box A_i - \frac{1}{2} m_{ij} \psi_i \psi_j - \frac{1}{2} m^\star_{ij} \bar{\psi}_i \bar{\psi}_j \\ &- y_{ijk} \psi_i \psi_j A_k - y^\star_{ijk} \bar{\psi}_i \bar{\psi}_j A^\star_k - V(A_i, A_j), \end{aligned}$$

where $V = F^\star{}_k F^k$ is the scalar potential. This is the free Lagrangian for chiral superfields. Like in the Standard Model gauge invariant interactions have to be included to describe the interactions between particles [54].
Using the Wess-Zumino gauge (equation 2.48) the kinetic terms of the Abelian gauge fields can be expressed as [22]:

$$W^\alpha W_\alpha|_{\theta\theta} = -2i\lambda\sigma^\mu D_\mu \bar{\lambda} - \frac{1}{2} F_{\mu\nu} F^{\mu\nu} + \frac{1}{2} D^2 + i \frac{1}{4} F_{\mu\nu} F^{\rho\sigma} \epsilon_{\mu\nu\rho\sigma}, \tag{2.52}$$

where D_μ is the usual covariant derivative (equation 2.25). Considering the supergauge transformations

$$\begin{aligned}\Phi &\to e^{-ig}\Lambda\Phi,\\ \Phi^\dagger &\to \Phi^\dagger e^{ig}\Lambda^\dagger,\\ V &\to V + i(\Lambda - \Lambda^\dagger),\end{aligned}$$

where Λ is the gauge parameter (a chiral field) one obtains the gauge invariant kinetic terms:

$$\Phi_i^\dagger \Phi_i|_{\theta\theta\bar\theta\bar\theta} \to \Phi_i^+ e^{gV}\Phi_i|\theta\theta\bar\theta\bar\theta. \tag{2.53}$$

The complete SUSY Lagrangian with $U(1)$ interactions can then easily be constructed out of equation 2.51 and 2.52 [54]:

$$\begin{aligned}\mathcal{L}_{inv} =& \frac{1}{4}\int d^2\theta W^\alpha W_\alpha + \frac{1}{4}\int d^2\bar\theta \bar W^{\dot\alpha}\bar W_{\dot\alpha} + \int d^2\theta d^2\bar\theta \Phi_i^\dagger e^{gV}\Phi_i\\ &+ \int d^2\theta(\frac{1}{2}m_{ij}\Phi_i\Phi_j + \frac{1}{3}y_{ijk}\Phi_i\Phi_j\Phi_k) + \text{h.c.}.\end{aligned} \tag{2.54}$$

In non-Abelian theories this is:

$$\begin{aligned}\mathcal{L}_{\text{SUSY YM}} =& \frac{1}{4}\int d^2\theta \text{tr}\left(W^\alpha W_\alpha\right) + \frac{1}{4}\int d^2\bar\theta \text{tr}\left(\bar W^{\alpha}\bar W_{\alpha}\right)\\ &+ \int d^2\theta d^2\bar\theta \bar\Phi_{ia}(e^{gV})^a_b\Phi_i^b\\ &+ \int d^2\theta W\left(\Phi_i\right) + \int d^2\bar\theta \bar W\left(\bar\Phi_i\right)\end{aligned} \tag{2.55}$$

The last missing part of the Lagrangian is the scalar potential. It does not need to be introduced non-intuitively like in the Standard Model, but it consists of the D- and F-contributions of the superpotential:

$$\begin{aligned}V &= V_D + V_F\\ V_D = \frac{1}{2}D^aD^a \qquad &\text{and} \qquad V_F = F_i^\star F_i.\end{aligned} \tag{2.56}$$

The only remaining degrees of freedom are the field contents, the values of the gauge couplings, the Yukawa coupling and the masses [54].

Soft Symmetry Breaking

In pure SUSY models the masses of the contents of a supermultiplet are degenerated. Thus SUSY has to be broken in any way. Here it is important not to spoil the cancellation of quadratic divergences (Sect. 2.2.1). Therefore SUSY has to be broken spontaneously like the SM gauge sector (Sect. 2.1.3). For this purpose new particles or interactions have to be introduced at high mass scales.
From the commutator rule for SUSY generators (equation 2.39) the vacuum expectation value of the energy can be calculated to be [56, 58]

$$\langle 0|\, H\, |0\rangle = \frac{1}{2}\left(\left|Q_1^\dagger\,|0\rangle\right|^2 + \left|Q_1\,|0\rangle\right|^2 + ...\right).$$

It can be seen, that the vacuum of a SUSY invariant theory is zero. This has striking consequences for spontaneous symmetry breaking: The vacuum can only be non-invariant ($Q_a \left|0\right\rangle \neq 0$), only if the minimum of the potential is positive ($\left\langle 0\right| H \left|0\right\rangle > 0$). For this reason the Mexican hat potential cannot be used in these theories. An answer could be found in meta-stable states. These could have occurred in the early universe caused by finite-temperature effects [56].
Breaking a global symmetry implies a massless Nambu-Goldstone mode with the same quantum numbers as the broken symmetry generator (here Q_a). Therefore it should be a massless, neutral Weyl fermion in our case, which is called goldstino:

$$\tilde{G} = \begin{pmatrix} \frac{\langle D^a \rangle}{\sqrt{2}} \\ \langle F_i \rangle \end{pmatrix},$$

where F_i and D^a are the auxiliary fields of the chiral and a vector supermultiplet, respectively [56].
For the masses obtained by the symmetry breaking the following sum rule can be derived:

$$\sum m^2_{\text{real scalars}} = 2 \sum m^2_{\text{fermions}}, \tag{2.57}$$

where the sum runs over all particles with the same quantum numbers. This is in many cases bad for phenomenology, for example it requires light scalar partners for SM fermions.
In general SUSY breaking appears like gauge symmetry breaking: One has to find fields with non-zero vacuum expectation values (vevs), which are breaking the symmetry. Thus in case of SUSY they have to fulfil the following equation:

$$\phi'(x) = i\left[Q, \phi(x)\right]. \tag{2.58}$$

To keep the theory Lorentz invariant only auxiliary fields can acquire non-zero vevs (in both chiral and vector supermultiplets). This leads to two different possibilities of SUSY breaking [58].
The first type is the so-called O'Raifearlaigh breaking, or "F-type SUSY breaking"[2] [59]. Here a set of chiral supermultiplets and a superpotential are picked in a way that the equations

$$F_i = -\frac{\delta W^\star}{\delta \phi^{\star i}} = 0$$

have no simultaneous solutions. As simplest example the superpotential can be chosen in a way that[54]:

$$W(\phi) = \lambda A_3 + m A_1 A_2 + g A_3 A_1^2, \tag{2.59}$$

where A_i are complex scalar fields. Therefore the three auxiliary fields are

$$\begin{aligned} F_1^\star &= m A_2 + 2 g A_1 A_3 \\ F_2^\star &= m A_1 \\ F_3^\star &= \lambda + g A_1^2. \end{aligned} \tag{2.60}$$

It is easy to determine, that $F_1^\star$ and $F_2^\star$ cannot vanish at the same time. Thus SUSY is broken. If m^2 becomes larger than $g \cdot \lambda$, the absolute minimum is at $A_2 = A_1 = 0$ with

[2] Because it drives SUSY breaking via vevs of the auxiliary fields of chiral supermultiplets.

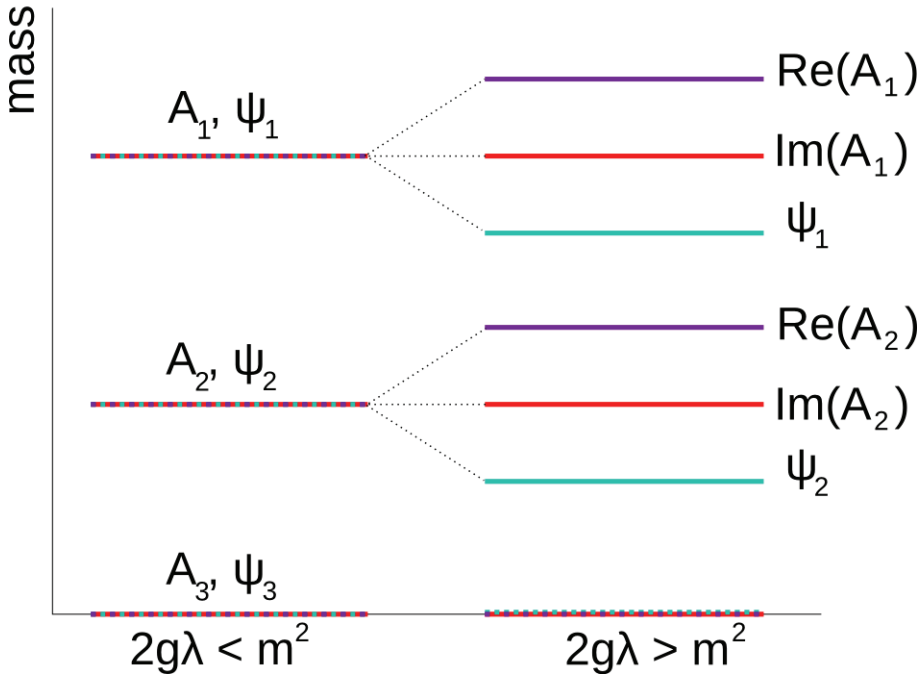

Figure 2.9: Mass spectrum in case of an F-type SUSY breaking before and after breaking. Compare [54].

an undetermined A_3. This is a so-called flat direction, a common feature of this kind of symmetry breaking. An expansion around $A_1 = 0$ causes two scalar masses and one Weyl fermion (the goldstino) to vanish and the other masses to get different values. A typical the mass spectrum in this case is shown in Fig. 2.9 [54].
The second type of SUSY breaking is the so-called Fayet-Iliopoulos mechanism, or "D-type SUSY breaking" [3] [24]. Here auxiliary fields of vector multiplets are having non-zero vevs:

$$\langle 0| D |0\rangle \neq 0. \tag{2.61}$$

To be more precise, a auxiliary field of the $U(1)$ gauge multiplet has to get a non-zero vev. This is because a SUSY invariant term is given by

$$\Delta\mathcal{L} = -\xi D,$$

where ξ is of dimension mass^2. But this term is not gauge-invariant in non-Abelian theories and can therefore not be introduced.
The auxiliary part of the scalar potential (equation 2.56) is then given by:

$$V_D = \xi D - \frac{1}{2}D^2 - g\sum_i q_i D\,|A_i|^2 \tag{2.62}$$

[3] Because it drives SUSY breaking via vevs of the auxiliary fields of vector supermultiplets.

and the equation of motion for D is [56]:

$$D = \xi - g \sum_i q_i \left|A_i\right|^2 \text{[4]}. \tag{2.63}$$

Suppose the scalar fields A_i have all non-zero superpotential masses m_i. The scalar potential can be written as:

$$V = \sum_i \left|m_i\right|^2 \left|A_i\right|^2 + \frac{1}{2}\left(\xi - g \sum_i q_i \left|A_i\right|^2\right)^2. \tag{2.64}$$

In this case the potential cannot vanish and thus SUSY is broken. The minimum can always be obtained for equation 2.61. The simplest case is $\left|m_i\right|^2 > g q_i \xi$ for each i. Then the minimum is at $A_i = 0$ and so $D = \xi$. In this case the $U(1)$ symmetry remains unbroken. The SUSY breaking in this case generates squared masses for the scalar fields of $\left|m_i\right|^2 - g q_i \xi$, for their fermionic partners of $\left|m_i\right|^2$ and the goldstino mass vanishes.
Difficulties occur in the application of SUSY models like the MSSM (Sect. 2.2.3). Here the only natural $U(1)$ symmetry is the $U(1)_Y$. But this cannot be used for SUSY breaking, because squarks and sleptons do not have any superpotential mass terms. Some of them would get non-zero vevs, which would violate fundamental quantum numbers. Colour and electromagnetic charge would be broken, but not SUSY. That is why Fayet-Iliopoulus terms in $U(1)_Y$ have to be sub-dominant or even absent compared to other sources of SUSY breaking. This could be only eluded by triggering SUSY breaking with other $U(1)$ symmetries. These are yet unknown, because they are spontaneously broken at high mass scales. Thus they are so far unexplored or simply do not affect SM particles. It stays difficult to get appropriate masses especially for the gaugino sector using the Fayet-Iliopoulus method. Therefore in most cases the F-term SUSY breaking mechanism is strongly preferred [56].

2.2.3 The MSSM

In Sect. 2.2.1 many reasons for a supersymmetric extension of the SM have been given. The MSSM [60–63], namely the minimal supersymmetric Standard Model, extends the SM minimally by introducing just as many new particles and interactions as necessary. Except the introduction of two Higgs doublets is a direct supersymmetrisation of the standard model [64].
In SUSY models the number of fermionic degrees of freedom has to be equivalent to the number of bosonic degrees of freedom, which is not directly fulfilled in the SM[5]. Thus the standard model has to be extended because it is not a priory supersymmetric [54].
To do a minimal extension the following aspects have to be taken into account:

- Since the SM fermions do not have the same quantum number as the SM bosons a set of new fermionic partners have to be introduced.
- Higgs bosons have to have non-zero vevs. For that reason they are no accurate superpartners for SM quarks and leptons (a combination would lead to a spontaneous violation of the baryon- and lepton-number).

[4] The scalar fields A_i are all charged under $U(1)$ with the charge q_i. Due to gauge invariance they have to come in pairs with opposite sign charges.

[5] In the SM there are 90 fermionic and 28 bosonic degrees of freedom.

Names		spin 0	spin 1/2	$SU(3)_c$,	$SU(2)_L$,	$U(1)_Y$
squarks, quarks (3 families)	Q	$\left(\tilde{u}_L, \tilde{d}_L\right)$	(u_L, d_L) or (χ_u, χ_d)	3,	2,	$\frac{1}{3}$
	$\bar{u}$	$\tilde{\bar{u}}_L = \tilde{u}_R^\dagger$	$\bar{u}_L = (u_R)^c$ or $\chi_{\bar{u}} = \psi_u^c$	$\bar{3}$,	1,	$-\frac{4}{3}$
	$\bar{d}$	$\tilde{\bar{d}}_L = \tilde{d}_R^\dagger$	$\bar{d}_L = (d_R)^c$ or $\chi_{\bar{d}} = \psi_d^c$	$\bar{3}$,	1,	$\frac{2}{3}$
sleptons, leptons (3 families)	L	$(\tilde{\nu}_{eL}, \tilde{e}_L)$	(ν_{eL}, e_L) or (χ_{ν_e}, χ_e)	1,	2,	-1
	$\bar{e}$	$\tilde{\bar{e}}_L = \tilde{e}_R^\dagger$	$\bar{e}_L = (e_R)^c$ or $\chi_{\bar{e}} = \psi_e^c$	1,	1,	2
Higgs, Higgsino	H_u	(H_u^+, H_u^0)	$\left(\tilde{H}_u^+, \tilde{H}_u^0\right)$	1,	2,	1
	H_d	(H_d^0, H_d^-)	$\left(\tilde{H}_d^0, \tilde{H}_d^-\right)$	1,	2,	-1

Table 2.2: Chiral Superfields in the MSSM: They are obtained from an extension of the SM fermions and the introduction of two Higgs supermultiplets [58].

- The SM Yukawa interactions are only invariant under $U(1)$ if the conjugate Higgs doublet is taken into account. In SUSY this is not possible, because antichiral superfields are not allowed in the superpotential. Therefore a second Higgs doublet has to be introduced.
- Triangle singularities: In the Standard Model these cancel between quarks and leptons of each generation, since the sum of their hypercharges cancels. In SUSY additional to each Higgs boson an higgsino is introduced, which is a chiral particle and also contributes to the chiral anomaly. Thus the two Higgs doublets introduced have to have opposite hypercharges.

To summarise, the MSSM associates known bosons with new fermions and known fermions with new bosons [54]. Two Higgs doublets with opposite hypercharge have to be introduced.

Particle Content of the MSSM

In the previous section it is shown how the MSSM is built up. The resulting chiral superfields in the MSSM and their component fields as well as their quantum numbers are shown in Tab. 2.2, the gauge supermultiplet fields in Tab. 2.3.

The SUSY partners of the SM particles are not discovered yet. For that reason SUSY must be broken (with a mechanism able to obtain higher masses for the SUSY partners.). The Higgs doublets in Tab. 2.2 both have four degrees of freedom (like two times the SM Higgs). Three degrees of freedom are known to be absorbed as longitudinal degrees of freedom for the three weak gauge bosons. Therefore in the MSSM five degrees of freedom are left after spontaneous symmetry breaking. So the model includes five Higgs bosons (in the Standard Model it was just one) [54]. The properties of these Higgs bosons will be discussed in Sect. 2.2.4.

Names	spin 1/2	spin 1	$SU(3)_c$,	$SU(2)_L$,	$U(1)_Y$
gluinos, gluons	$\tilde{g}$	g	8,	1,	0
winos, W bosons	$\tilde{W}^{\pm}$, $\tilde{W}^0$	$W^{\pm}$, W^0	1,	3,	0
bino, B boson	$\tilde{B}^0$	B^0	1,	1,	0

Table 2.3: Vector Superfields in the MSSM: They are obtained from an extension of the SM gauge bosons [58].

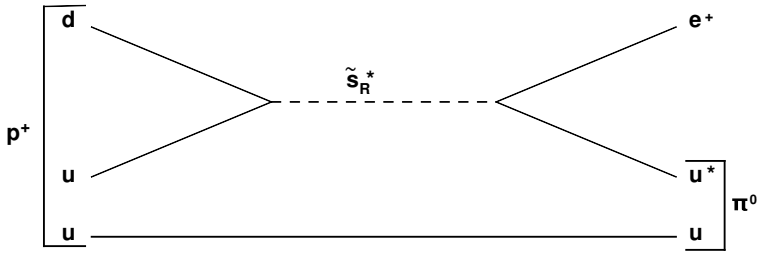

Figure 2.10: Example for proton decay : The proton decays into a positron and a pion via a virtual strange squark.

The R-Parity and its Consequences

In the original MSSM new interaction terms not included in the SM would be possible:

$$W_{NR} = \underbrace{\epsilon_{ij}\left(\lambda^{L}_{abc} L^i_a L^j_b e^c_d + \lambda^{L\prime}_{abc} L^i_a Q^j_b d^c_d + \mu'_a L^i_a H^j_u\right)}_{\not{L}} + \underbrace{\lambda^{B}_{bd} u^c_a d^c_b d^c_d}_{\not{B}} . \tag{2.65}$$

They violate lepton and baryon number which is not discovered so far. Thus these terms must be suppressed or even absent. An example for a process which even violates both L and B is proton decay. If $\lambda^{L\prime}$ and λ^{B} would be unsuppressed the lifetime of the proton would be very short.

An example for such a proton decay process is shown in Fig. 2.10. Here the proton decays into a positron e^+ and a pion π^0. Other possible decay products are: e^+K^0, $\mu^+\pi^0$, μ^+K^0, $\nu\pi^+$, νK^+ and the rest of it. Which process is dominant depends on which components in $\lambda^{L\prime}$ and λ^{B} are the largest ones.

In such models assuming squark masses of about 1 TeV the lifetime of the proton would be a tiny fraction of a second [56]. But in observations the lifetime of the proton has been proven to be larger than 10^{32} years. Therefore these terms have to be strongly suppressed.

The most obvious idea would be to introduce B and L conservation in the MSSM. However, this would be unmotivated[6] and additionally there are hints that they must be violated by non-perturbative electroweak effects [56]. Thus a new symmetry has to be introduced in

[6] In the SM L an B conservation is introduced intrinsically, because B and L violating terms are non-renormalisable.

the MSSM [63, 65–68].
Technically this is a global $U(1)_R$ invariance:

$$U(1)_R: \qquad \theta \to e^{i\alpha}\theta \qquad \Phi \to e^{in\alpha}\Phi$$

A superfield has the quantum number $R = n$. To preserve the $U(1)_R$ invariance the superpotential must have the quantum number $R = 2$ (to get $W_{NR} = 0$). That is why there must be $R = 1$ for all Higgs superfields and $R = \frac{1}{2}$ for all quark and lepton fields. However, it comes out that this condition is too restrictive because of the gaugino mass term[7]. For that reason the R-symmetry is reduced to a discrete group Z_2, the so called R-parity. The R-parity can be obtained from its discrete quantum numbers as follows:

$$R = (-1)^{3(B-L)+2S}, \tag{2.66}$$

if S is the spin of the particle. It can be seen that R-parity adjusts a positive sign to an ordinary SM particle and a negative sign to its SUSY partner. If R-parity is assumed to be conserved the W_{NR} terms become strongly constrained [54]:

$$\lambda^{L}_{abc}, \lambda^{L\prime}_{abc} < 10^{-4} \qquad \lambda^{B}_{abc} < 10^{-9}$$

R-parity conservation has three striking consequences for the MSSM:

- The lightest particle with an odd quantum number (the LSP[8]) is absolutely stable. No matter how large its mass is. If this particle is also chosen to be electrically and strongly neutral it provides a perfect candidate for dark matter (Sect. 2.3).
- Each heavier particle has to decay into a state containing an odd number of $R = -1$ particles.
- In colliders sparticles will be produced in even numbers [54].

As a consequence the interactions of SUSY partners can be obtained by "replacing an even number of particles by their superpartners for each SM vertex". This allows for constructing for example Feynman diagrams of SUSY particle production at hadron colliders. The restriction for SUSY particle production at a collider is the center of mass energy:

$$m^{\text{max}}_{\text{sparticle}} \leq \frac{\sqrt{s}}{2}$$

As an example in Fig. 2.11 the possible production channels for a gluino pair at a hadron collider (out of gluons) are given. In this way all possible production channels at hadron colliders can be figured out. Tab. 2.4 shows all possible production channels at hadron colliders. Particles produced this way decay in cascades up to the point when the LSP is reached which does not further decay due to R-parity conservation. In most cases the lightest neutralino is the LSP, which cannot be detected. Thus in all SUSY events a high missing transverse energy will be measured. The other parts of the topology depend strongly on the mass hierarchy and the event measured. For that reason they will not further be discussed in this context [54].

[7] Lorentz- and gauge invariance can only be obtained for $\alpha = \pi$ R-invariance.
[8] Lightest Supersymmetric Particle.

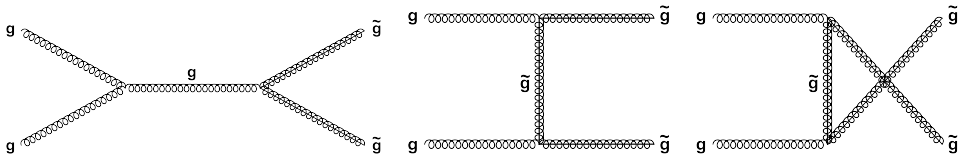

Figure 2.11: Different production channels for gluino pairs.

Initial State	Final States		
	Hadronic Particles	Sleptons	Gauginos
$q\bar{q}$	$\tilde{g}\tilde{g}$, $\tilde{q}_i\bar{\tilde{q}}_j$	$\tilde{l}_i^+\tilde{l}_j^-$, $\tilde{\nu}_l\bar{\tilde{\nu}}_l$	$\tilde{\chi}_i^+\tilde{\chi}_j^-$, $\tilde{\chi}_i^0\tilde{\chi}_j^0$
$u\bar{d}$		$\tilde{l}_l^+\tilde{\nu}_l$	$\tilde{\chi}_i^+\tilde{\chi}_j^0$
$d\bar{u}$		$\tilde{l}_l^-\bar{\tilde{\nu}}_l$	$\tilde{\chi}_i^-\tilde{\chi}_j^0$
qq	$\tilde{q}_i\tilde{q}_j$		
gq	$\tilde{g}\tilde{q}_i$		
gg	$\tilde{g}\tilde{g}$, $\tilde{q}_i\bar{\tilde{q}}_j$		

Table 2.4: All possible production channels of SUSY particles at hadron colliders: Initial states can be up-, down-quarks, gluons and sea quarks. At LHC energies the parton density functions of gluons are leading.

The MSSM Superpotential

The MSSM Lagrangian consists of two parts:

- $\mathcal{L}_{\text{SUSY}}$, which is the SUSY generalisation of the Standard Model
- $\mathcal{L}_{\text{Break}}$ depicting the breaking of supersymmetry

$\mathcal{L}_{\text{SUSY}}$ again consist of two parts:

$$\mathcal{L}_{\text{SUSY}} = \mathcal{L}_{\text{gauge}} + \mathcal{L}_{\text{Yukawa}}$$

where

$$\mathcal{L}_{\text{gauge}} = \sum_{SU(3),SU(2),U(1)} \frac{1}{4}\left(\int d^2\theta \text{tr} W^\alpha W_\alpha + \int d^2\bar{\theta} \text{tr}\bar{W}^{\dot{\alpha}}\bar{W}_{\dot{\alpha}}\right) + \sum_{\text{matter}} \int d^2\theta d^2\bar{\theta}\Phi_i^\dagger \exp\left(g_3\hat{V}_3 + g_2\hat{V}_2 + g_1\hat{V}_1\right)\Phi_i$$

and

$$\mathcal{L}_{\text{Yukawa}} = \int d^2\theta \left(W_R + W_{NR}\right) + \text{h.c.} \tag{2.67}$$

W_R is here the R-parity conserving part and W_{NR} the R-parity breaking part [54]. It can be constructed from four terms:

$$W_R = \epsilon_{ij}\left(y_{ab}^u Q_a^j u_b^c H_u^i + y_{ab}^d Q_a^j d_b^c H_d^i + y_{ab}^L L_a^j e_b^c H_d^i + \mu H_d^i H_u^j\right), \tag{2.68}$$

where $i, j = 1, 2, 3$ are $SU(2)$ and $a, b = 1, 2, 3$ generation indices. The colour indices are suppressed. The Yukawa couplings are y^u, y^d and y^L[9]. The first three terms are similar to the Standard Model (the ordinary SM model fields have just been replaced by superfields) [54]. The last term implying Higgs mixing is something new (in the SM there was just one Higgs doublet). It is the SUSY equivalent of the Higgs bosonmass term. The terms $H_u^\star H_u$ and $H_d^\star H_d$ are forbidden, because they would make the superpotential non-analytic in the chiral superfields[10] [56].
After H_u and H_d get ves the Yukawa matrices imply the particle masses and the CKM mixing [56].

SUSY Breaking and arising sparticle masses in the MSSM

From non-observation of SUSY partners and the fact that D-term vevs for $U(1)_Y$ do not lead to a satisfactory mass spectrum (discussed in Sect. 2.2.2) it is clear, that the MSSM has to be extended by SUSY violating terms. As solution a hidden sector[11] is introduced. The soft terms in the visible sector arise from indirect interactions with the hidden sector. To conclude the symmetry breaking occurs in the hidden sector, which couples not or very weakly to particles in the visible sector. The two sectors share some interactions, the so-called messengers, which mediate SUSY breaking from the hidden to the visible sector. This is illustrated in Fig. 2.12
There are three main mechanisms how SUSY breaking could be described in principle fixing the messenger particles:

- Gravity mediation (SUGRA) [69–76]
- Gauge mediation [77–82]
- Anomaly mediation [83, 84]

As the first one is the mechanism the models used in this work are based on it will be further discussed now [54]. The other ones can be looked up in [54, 56, 58, 64].
In SUGRA mechanisms effective non-renormalisable interactions are arising at low energies. Here the two sectors interact via gravity. There are two types of scalar fields developing non-zero vevs:

- Moduli fields T coming from the compactification from higher dimensions
- Dilation fields S, which are parts of the SUGRA supermultiplet

These two types of fields obtain non-zero vevs from their F-components (F_T,F_S) and cause SUSY to be spontaneously broken. The spontaneous symmetry breaking leads to Goldstone fermions. Here the so-called super-Higgs effect appears, where the fermionic degrees of freedom from the Goldstone fermions are absorbed into the additional components of the spin-$\frac{3}{2}$ gravitino getting mass [54].

[9] y^u, y^d and y^L are 3×3 operators in family space.
[10] In the first part of this section this reason for two Higgs doublets was already discussed.
[11] Hidden because the energies are that high, that this sector will not be achievable by collider experiments in the near future.

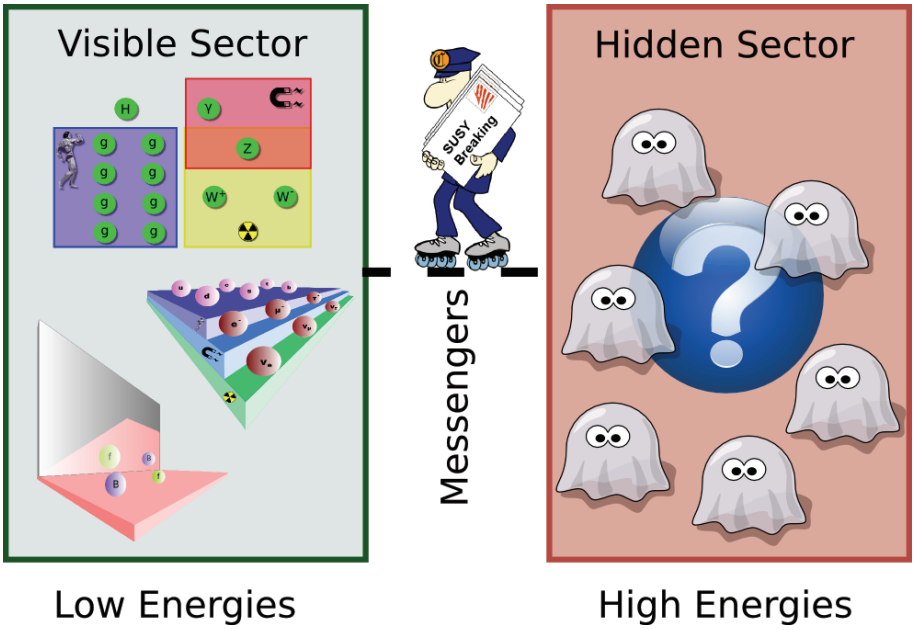

Figure 2.12: The two sectors of the MSSM: The SUSY breaking is mediated from the hidden sector to the visible sector by messenger particles. The content of the hidden sector is unknown. In supergravity the messengers would be gravitinos and gravitons.

A SUSY breaking mediated via gravitational interactions leads to SUSY breaking masses of the order of:

$$M_{\text{SUSY breaking}} \sim \frac{\langle F_T \rangle}{M_{\text{Planck}}} + \frac{\langle F_S \rangle}{M_{\text{Planck}}} \sim m_{3/2}. \tag{2.69}$$

The resulting effective low energy theory contains the explicit soft symmetry breaking terms:

$$\mathcal{L}_{\text{soft}} = -\sum_i m_i^2 \left|A_i\right|^2 - \sum_i M_i^2 \left(\lambda_i \lambda_i + \bar{\lambda}_i \bar{\lambda}_i\right) - \mathcal{B} W^{(2)}(A) - \mathcal{A} W^{(3)}(A), \tag{2.70}$$

where $W^{(2)}(A)$ and $W^{(3)}(A)$[12] are the quadratic and the cubic part of the superpotential and the mass parameters are given by

$$m_i^2 \sim \left(\frac{\langle F_S \rangle}{M_{\text{Planck}}}\right)^2 \sim m_{3/2}^2 \qquad M_i \sim \frac{\langle F_S \rangle}{M_{\text{Planck}}} \sim m_{3/2},$$
$$\mathcal{B} \sim \left(\frac{\langle F_T \rangle}{M_{\text{Planck}}}\right)^2 \sim m_{3/2}^2 \qquad \mathcal{A} \sim \frac{\langle F_{T,S} \rangle}{M_{\text{Planck}}} \sim m_{3/2}.$$

For SUSY masses of about 1 TeV this results in vevs of $\sqrt{\langle F_{T,S} \rangle} \sim 10^{11}$ GeV [54].
The current work is based on so-called mSUGRA[13] models where additional boundary conditions are introduced which unify not only the couplings (Fig. 2.7) but also the masses

[12] A_i depict still complex scalar fields.
[13] Minimal Supergravity.

at the GUT scale:

$$
\begin{aligned}
&g_1 = g_2 = g_3 = g_{\text{GUT}},\\
&M_1 = M_2 = M_3 = m_{1/2},\\
&m^2_{Q_i} = m^2_{u_i} = m^2_{d_i} = m^2_{L_i} = m^2_{E_i} = m^2_{H_u} = m^2_{H_d} = m^2_0,\\
&A_t = A_b = A_\tau = A_0.
\end{aligned}
$$

The fifth parameter is the Higgs mass parameter μ. The masses of the two Higgs doublets (m_{H_u} and m_{H_d}) are related to μ as (can be derived from eq. 2.78):

$$\frac{m_Z^2}{2} = -\mu^2 - \frac{m_{H_d} - m_{H_u}\tan^2\beta}{\tan^2\beta - 1}. \tag{2.71}$$

With the assumption of the unification boundary condition the masses of the two Higgs doublets are fixed. Therefore μ gets fixed by eq. 2.71 up to its sign. This results in models with the five free parameters: m_0, $m_{1/2}$, A_0, $\tan\beta = \frac{v_1}{v_2}$ and sgn(μ).
The two main sources of mass terms are coming from the soft terms and additionally from the D-terms. With given m_0, $m_{1/2}$, μ, Y_t, Y_b, Y_τ, $\mathcal{A}$ and $\mathcal{B}$ the mass matrices for all particles can be determined.
From these GUT scale masses the renormalisation group equations mentioned in [64] can be solved and the results can be substituted into the mass matrices. In this way the mass spectrum of supersymmetric particles can be predicted [64].
The higgsino mass matrix is non-diagonal, which implies that the higgsinos mix with each other. The mass terms in the Lagrangian can be written as

$$\mathcal{L}_{\text{gaug-h}} = \frac{1}{2}M_3\bar{\lambda}_a\lambda_a - \frac{1}{2}\bar{\chi}M^{(0)}\chi - \left(\bar{\psi}M^{(c)}\psi\text{h.c.}\right),$$

where λ_a depicts the eight Majorana gluino fields, χ the neutral gauginos and Higgsinos

$$\chi = \begin{pmatrix} \tilde{B}^0 \\ \tilde{W}^3 \\ \tilde{H}_u^0 \\ \tilde{H}_d^0 \end{pmatrix}$$

and ψ the charged gaugino and Higgsino

$$\psi = \begin{pmatrix} \tilde{W}^+ \\ \tilde{H}^+ \end{pmatrix}.$$

Their mass matrices are:

$$
\begin{aligned}
M^{(0)} &= \begin{pmatrix} M_1 & 0 & -M_Z\cos\beta\sin\theta_W & M_Z\sin\beta\sin\theta_W \\ 0 & M_2 & M_Z\cos\beta\cos\theta_W & -M_Z\sin\beta\cos\theta_W \\ -M_Z\cos\beta\sin\theta_W & M_Z\cos\beta\cos\theta_W & 0 & -\mu \\ M_Z\sin\beta\sin\theta_W & -M_Z\sin\beta\cos\theta_W & \mu & 0 \end{pmatrix}\\
M^{(c)} &= \begin{pmatrix} M_2 & \sqrt{2}M_W\sin\beta \\ \sqrt{2}M_W\cos\beta & \mu \end{pmatrix},
\end{aligned}
\tag{2.72}
$$

where $\tan\beta = \frac{v_1}{v_2}$ is the ratio of the two Higgs vevs and θ_W the electroweak mixing angle. The mass eigenstates which would be measured at a particle detector are called neutralino and chargino. Their masses can be determined by diagonalisation of the mass matrices [54].
Squarks and sleptons have non-negligible Yukawa couplings leading to a mixing between the electroweak eigenstates. The mass matrices of the third generation particles can be written as:

$$\begin{pmatrix} m^2_{\tilde{t}_L} & m_t\left(A_t - \mu\cot\beta\right) \\ m_t\left(A_t - \mu\cot\beta\right) & m^2_{\tilde{t}_R} \end{pmatrix} \\ \begin{pmatrix} m^2_{\tilde{b}_L} & m_b\left(A_b - \mu\tan\beta\right) \\ m_b\left(A_b - \mu\tan\beta\right) & m^2_{\tilde{b}_R} \end{pmatrix}, \\ \begin{pmatrix} m^2_{\tilde{\tau}_L} & m_\tau\left(A_\tau - \mu\tan\beta\right) \\ m_\tau\left(A_\tau - \mu\tan\beta\right) & m^2_{\tilde{\tau}_R} \end{pmatrix} \tag{2.73}$$

where

$$\begin{aligned} m^2_{\tilde{t}_L} &= m^2_{\tilde{Q}} + m^2_t + \frac{1}{6}\left(4M^2_W - M^2_Z\right)\cos^2\beta, \\ m^2_{\tilde{t}_R} &= m^2_{\tilde{u}} + m^2_t - \frac{2}{3}\left(M^2_W - M^2_Z\right)\cos^2\beta, \\ m^2_{\tilde{b}_L} &= m^2_{\tilde{Q}} + m^2_b - \frac{1}{6}\left(2M^2_W + M^2_Z\right)\cos^2\beta, \\ m^2_{\tilde{b}_R} &= m^2_{\tilde{d}} + m^2_b + \frac{1}{3}\left(M^2_W - M^2_Z\right)\cos^2\beta, \\ m^2_{\tilde{\tau}_L} &= m^2_{\tilde{L}} + m^2_\tau - \frac{1}{2}\left(2M^2_W - M^2_Z\right)\cos^2\beta, \\ m^2_{\tilde{\tau}_R} &= m^2_{\tilde{e}} + m^2_\tau + \left(M^2_W - M^2_Z\right)\cos^2\beta.. \end{aligned}$$

The indices R and L describe the handedness of the sparticles. Each expression exists of three parts: The first coming from the soft terms (solution of the renormalisation group equations), the second part is the usual quark mass and the last part coming from the D-terms of the potential.
The mass eigenstates of the sparticles are written as $m_{\tilde{t}_1}$, $m_{\tilde{t}_2}$, $m_{\tilde{b}_1}$, $m_{\tilde{b}_2}$, $m_{\tilde{\tau}_1}$ and $m_{\tilde{\tau}_2}$ and can be obtained by diagonalising the mass matrices. The new indices depict the change to mass eigenstates. For the lighter generations the Yukawa coupling becomes small and thus the mixing is negligible [54].

2.2.4 The Higgs Sector in the MSSM

As mentioned in Sect. 2.2.3 in SUSY two Higgs doublets [85–88] with opposite hypercharge exist:

$$\begin{aligned} H_u &= \begin{pmatrix} H^+_u \\ H^0_u \end{pmatrix} \qquad y = 1 \\ H_d &= \begin{pmatrix} H^0_d \\ H^-_d \end{pmatrix} \qquad y = -1 \end{aligned}.$$

There are several terms of scalar fields in the classical potential:

- Quadratic terms from SUSY-invariant contributions:
  $|\mu|^2 \left(|H_u^+|^2 + |H_d^-|^2 + |H_u^0|^2 + |H_d^0|^2\right)$
- Quadratic terms from SUSY breaking:
  $-m_{H_u}^2 \left(|H_u^+|^2 + |H_u^0|^2\right) - m_{H_d}^2 \left(|H_d^-|^2 + |H_d^0|^2\right)$
  $-\left(b\left(H_u^+ h_d^- - H_u^0 H_d^0\right) + \text{h.c.}\right)$
- Cubic SUSY-invariant D-terms:
  $\frac{1}{2}\sum_G \sum_\alpha \sum_{ij} g_G^2 \left(\phi_i^\dagger T_G^\alpha \phi_i\right)\cdot\left(\phi_j^\dagger T_G^\alpha \phi_j\right)$, where $\phi_{i,j}$ depicts the different Higgs doublets, G runs over the involved groups[14] and alpha over the involved group generators.

The complete scalar potential can then be expressed as [58]:

$$\begin{aligned}\mathcal{V} = &\underbrace{\left(|\mu|^2 + m_{H_u}^2\right)}_{m_1^2}\left(|H_u^+|^2 + |H_u^0|^2\right) + \underbrace{\left(|\mu|^2 + m_{H_d}^2\right)}_{m_2^2}\left(|H_d^0|^2 + |H_d^-|^2\right)\\ &+ \left(b\left(H_u^+ H_d^- - H_u^0 H_d^0\right) + \text{h.c.}\right)\\ &+ \frac{g^2 + g'^2}{8}\left(|H_u^+|^2 + |H_u^0|^2 - |H_d^0|^2 - |H_d^-|^2\right)^2\\ &+ \frac{g^2}{2}\left(H_u^+ H_d^{0\star} + H_u^0 H_d^{-\star}\right)^2.\end{aligned} \tag{2.74}$$

The minimum of this potential has to break $SU(2)_L \times U(1)_y$ down to $U(1)_{em}$. Therefore H_u^+ is chosen to vanish at the minimum. This results in two possible solutions:

1. $h_d^- = 0$
2. $b + \frac{g^2}{2} H_d^{0\star} H_u^{0\star} = 0$

The second case makes b to become $g^2 |H_u^0|^2 |H_d^0|^2$ which is positive. This makes the second case to be unfavourable for symmetry breaking. Therefore the first case is chosen which results in a negative b-contribution. The fact that the electrically charged components of the two Higgs doublets do not acquire vevs holds electromagnetism off spontaneous symmetry breaking [58].
With this knowledge one can concentrated on the neutral component of the scalar potential:

$$\mathcal{V}_n = m_1^2 |H_u^0|^2 + m_2^2 |H_d^0|^2 - \left(b H_u^0 H_d^0 + \text{h.c.}\right) + \underbrace{\frac{g^2 + g'^2}{8}}_{\approx 0.065}\left(|H_u^0|^2 - |H_d^0|^2\right)^2. \tag{2.75}$$

In contrast to the SM the coefficient of the cubic term is fixed by precision measurements of the electroweak couplings.
If b is chosen to be a positive, real number $H_u^0 H_d^0$ also has to be positive and real for the minimum of ten scalar potential. Thus the vevs of H_u^0 and H_d^0 have to have either equal or opposite phases.
If $H_u^0 = H_d^0$ is chosen the potential is only bounded from below if:

$$m_1^2 + m_2^2 > 2b > 0. \tag{2.76}$$

[14] Here G comprises $SU(2)_L$ and $U(1)_y$.

For this reason m_1^2 and m_2^2 cannot be negative at the same time. Otherwise there will not be a maximum in the origin.
If m_1^2 and m_2^2 are both positive there is a minimum in the origin unless:

$$m_1^2 \cdot m_2^2 < b^2. \tag{2.77}$$

This condition for the origin to be a saddle point is automatically satisfied if m_1^2 or m_2^2 is negative.
To fulfil the conditions 2.76 and 2.77 the squared masses of the two Higgs doublets have to be different. In the theories studied in this thesis the masses should unify at the GUT scale. Thus the difference is driven by the renormalisation group equations. In most cases $m_{H_u}^2$ becomes negative [58].
The actual masses of the weak gauge bosons can be obtained by substituting the covariant derivative of $SU(2)_L \times U(1)_y$ given in equation 2.25 into the kinetic term of the Higgs fields

$$\left(D_\mu H_u\right)^\dagger \left(D_\mu H_u\right) + \left(D_\mu H_d\right)^\dagger \left(D_\mu H_d\right).$$

After insertion of the vevs of the Higgs bosons and definition of the Z state as:

$$Z^\mu = \frac{1}{\sqrt{g^2 + g'^2}} \left(-g' B^\mu + g A_3^\mu\right)$$

the masses of the weak gauge bosons can be obtained as:

$$\begin{aligned} m_Z^2 &= \frac{1}{2}\left(g^2 + g'^2\right) \cdot \left(v_u^2 + v_d^2\right) \\ m_W^2 &= \frac{1}{2} g \cdot \left(v_u^2 + v_d^2\right). \end{aligned} \tag{2.78}$$

The squared sum of the Higgs vacuum expectation values is precisely known from electroweak measurements:

$$\left(v_u^2 + v_d^2\right) = 174 \text{ GeV}. \tag{2.79}$$

Therefore only the ratio is of further interest, which is defined as

$$\tan\beta \equiv \frac{v_u}{v_d}. \tag{2.80}$$

If the vevs of the Higgs particles are chosen to be positive and real the angle b must be between 0 and $\frac{\pi}{2}$ [58].
In the Standard Model a single Higgs doublet with four degrees of freedom leads after spontaneous symmetry breaking. Three of the four degrees of freedom are absorbed as longitudinal degrees of freedom by the weak gauge bosons to one Higgs particle. The two Higgs doublets of the MSSM lead in the same way to five Higgs particles. Their masses can be obtained again by expanding the potential about the minimum for all possible non-vanishing components of the Higgs doublets. This time two kinematic terms have to be taken into account:

$$\mathcal{L}_{12} = \partial_\mu \phi_1 \partial^\mu \phi_1 + \partial_\mu \phi_2 \partial^\mu \phi_2 - \mathcal{V}\left(\phi_1, \phi_2\right).$$

The minimum of the potential $\mathcal{V}\left(\phi_1, \phi_2\right)$ is at $\phi_1 = v_1$, $\phi_2 = v_2$. As next step the potential is expanded around the minimum and the fields get redefined as:

$$\begin{aligned} \tilde{\phi}_1 &= \sqrt{2}\left(\phi_1 - v_1\right), \\ \tilde{\phi}_2 &= \sqrt{2}\left(\phi_2 - v_2\right). \end{aligned}$$

The Lagrangian is:

$$\mathcal{L}_{12,\text{ quad}} = \frac{1}{2}\partial_\mu\tilde{\phi}_1\partial^\mu\tilde{\phi}_1 + \frac{1}{2}\partial_\mu\tilde{\phi}_2\partial^\mu\tilde{\phi}_2 - \frac{1}{2}\begin{pmatrix}\tilde{\phi}_1 & \tilde{\phi}_2\end{pmatrix} M^2 \begin{pmatrix}\tilde{\phi}_1 \\ \tilde{\phi}_2\end{pmatrix}, \tag{2.81}$$

where

$$M^2 = \frac{1}{2}\begin{pmatrix} \frac{\partial^2\mathcal{V}}{\partial\phi_1\partial\phi_1}(v_1,v_2) & \frac{\partial^2\mathcal{V}}{\partial\phi_1\partial\phi_2}(v_1,v_2) \\ \frac{\partial^2\mathcal{V}}{\partial\phi_1\partial\phi_2}(v_1,v_2) & \frac{\partial^2\mathcal{V}}{\partial\phi_2\partial\phi_2}(v_1,v_2)\end{pmatrix}$$

is the squared mass matrix in interaction space. The Lagrangian can be transformed into mass space by diagonalising the mass matrix via an orthogonal transformation:

$$\begin{pmatrix}\phi_+ \\ \phi_-\end{pmatrix} = \begin{pmatrix}\cos\alpha & -\sin\alpha \\ \sin\alpha & \cos\alpha\end{pmatrix}\begin{pmatrix}\tilde{\phi}_1 \\ \tilde{\phi}_2\end{pmatrix}. \tag{2.82}$$

The eigenstates of the squared mass matrix can then be interpreted as the squared masses of the Higgs particles [58].
Applied to the pair of fields $\left(\mathrm{Im}(H_u^0), \mathrm{Im}(H_d^0)\right)$ the potential can be calculated to be:

$$\begin{aligned}\mathcal{V}_A =& m_1^2\left(\mathrm{Im}(H_u^0)\right)^2 + m_2^2\left(\mathrm{Im}(H_d^0)\right)^2 + 2b\left(\mathrm{Im}(H_u^0)\right)\left(\mathrm{Im}(H_d^0)\right) \\ &+ \frac{g^2+g'^2}{8}\left(\left(\mathrm{Re}(H_u^0)\right)^2 - \left(\mathrm{Re}(H_d^0)\right)^2 + \left(\mathrm{Im}(H_u^0)\right)^2 - \left(\mathrm{Im}(H_d^0)\right)^2\right)^2.\end{aligned} \tag{2.83}$$

The eigenvalues of the squared mass matrix can then be determined as

$$m_+^2 = 0 \qquad m_-^2 = \frac{2b}{\sin 2\beta},$$

where the vanishing mass eigenvalue is associated to the longitudinal mode of the Z^0 boson. The orthogonal combination originates the so-called pseudo-scalar Higgs boson A^0 with the mass [58]:

$$m_{A^0} = \sqrt{\frac{2b}{\sin 2\beta}}. \tag{2.84}$$

The charged Higgs bosons arise from the electrically charged components of the two doublets $\left(H_u^+, H_d^-\right)$. The Lagrangian involving these components is

$$\begin{aligned}\mathcal{L}_{\text{ch, quad}} =& \left(\partial_\mu H_u^+\right)^\dagger\left(\partial_\mu H_u^+\right) + \left(\partial_\mu H_d^-\right)^\dagger\left(\partial_\mu H_d^-\right) \\ &- \frac{\partial^2\mathcal{V}}{\partial H_u^+\partial H_d^-}(H_u^+)^\dagger H_u^+ - \frac{\partial^2\mathcal{V}}{\partial H_d^-\partial H_u^+}(H_d^-)^\dagger H_d^- \\ &- \frac{\partial^2\mathcal{V}}{\partial H_u^+\partial H_d^-}H_u^+H_d^- - \frac{\partial^2\mathcal{V}}{\partial(H_u^+)^\dagger\partial(H_d^-)}(H_u^+)^\dagger(H_d^-)^\dagger.\end{aligned}$$

By expanding the potential around the minimum $H_u^0 = v_u$, $H_d^0 = v_d$, $H_u^+ = H_d^- = 0$ and diagonalisation of the squared mass matrix two eigenstates can be evaluated: A vanishing one , which represents the longitudinal mode of the W^+ boson and a mass:

$$m_{H^+} = \sqrt{m_W^2 + m_{A^0}^2}, \tag{2.85}$$

which represents the charged Higgs boson H^+. From the conjugated state the longitudinal mode of the W^- and the negatively charged Higgs boson, H^- with the same mass (equation 2.85) arise [58].
The last two Higgs bosons come from the real parts of the neutral doublet components $\left(\mathrm{Re}(H_u^0) - v_u, \mathrm{Re}(H_d^0) - v_d\right)$. This coupled pair is of the same form as $\left(\mathrm{Im}(H_u^0), \mathrm{Im}(H_d^0)\right)$ and its potential is similar to the potential given in equation 2.83[15]. From the eigenvalues of the mass matrix obtained by evaluating the potential around the minimum again the masses of the two neutral Higgs bosons can be determined as [58]:

$$\begin{aligned} m_{h^0} =& \sqrt{\frac{1}{2}\left(m_{A^0}^2 + m_{Z^0}^2 - \sqrt{\left(m_{A_0}^2 + m_Z^2\right)^2 - 4m_{A^0}^2 m_Z^2 \cos^2 2\beta}\right)}, \\ m_{H^0} =& \sqrt{\frac{1}{2}\left(m_{A^0}^2 + m_{Z^0}^2 + \sqrt{\left(m_{A_0}^2 + m_Z^2\right)^2 - 4m_{A^0}^2 m_Z^2 \cos^2 2\beta}\right)}. \end{aligned} \tag{2.86}$$

From limit considerations of $m_{A^0}^2$ the upper limit on m_{h^0} can be estimated as:

$$m_{h^0} \leq m_Z \left|\cos 2\beta\right| \leq m_Z. \tag{2.87}$$

Without significant one-loop corrections on m_{h^0} this region would already be excluded by the experimental limit on the Standard Model Higgs boson of [89]

$$m_H \geq 114.4 \text{ GeV}.$$

The significant contributions come from the not exact cancellation of the top quark and the top squarks loops[16]. Without top squark mixing the mass limit becomes:

$$m_{h^0}^2 \leq m_Z^2 + \frac{3m_t^4}{2\pi^2\left(v_u^2 + v_d^2\right)} \ln\left(\frac{m_S}{m_t}\right), \tag{2.88}$$

where

$$m_S^2 = \frac{1}{2}\left(m_{\tilde{t}_1}^2 + m_{\tilde{t}_2}^2\right). \tag{2.89}$$

This leads already for a top squark mass of 500 GeV to a realistic Higgs limit of:

$$m_h^2 \leq \left(115 \text{ GeV}\right)^2. \tag{2.90}$$

If squark mixing is taken into account the top squark mass can even be smaller [58].
The coupling of SUSY Higgs bosons to fermions can be obtained from the Yukawa terms. Taking the obtained values of the weak gauge boson masses (equation 2.78) into account the Yukawa coupling to Standard Model matter particles can in the mass basis be written as:

$$\begin{aligned} y_{u,c,t} =& \frac{g m_{u,c,t}}{\sqrt{2} m_W \sin\beta} \\ y_{d,s,b} =& \frac{g m_{d,s,b}}{\sqrt{2} m_W \cos\beta} \\ y_{e,\mu,\tau} =& \frac{g m_{e,\mu,\tau}}{\sqrt{2} m_W \cos\beta}. \end{aligned} \tag{2.91}$$

[15] Instead of the imaginary parts the real parts with a shift of $v_{u/d}$ is taken.
[16] The contributions of the top and stop contributions would cancel in exact SUSY like introduced in Sect. 2.1.4.

The coupling can then be obtained by the expansion of H_u^0 and H_d^0 about their vevs introducing afterwards the physical states:

$$\begin{pmatrix} h^0 \\ H^0 \end{pmatrix} = \sqrt{2} \begin{pmatrix} \cos\alpha & -\sin\alpha \\ \sin\alpha & \cos\alpha \end{pmatrix} \begin{pmatrix} \mathrm{Re}(H_u^0) - v_u \\ \mathrm{Re}(H_d^0) - v_d \end{pmatrix}. \tag{2.92}$$

The Yukawa couplings of the neutral Higgs bosons to the SM fermions are then determined to be:

- for the top quark [58]:

$$-\left(\frac{g m_t}{2 m_W}\right) \bar{\psi}_t \psi_t \left(\frac{\cos\alpha}{\sin\beta} h^0 + \frac{\sin\alpha}{\sin\beta} H^0\right) \tag{2.93}$$

- for the bottom quark [58]:

$$-\left(\frac{g m_b}{2 m_W}\right) \bar{\psi}_b \psi_b \left(\frac{\sin\alpha}{\cos\beta} h^0 + \frac{\cos\alpha}{\cos\beta} H^0\right) \tag{2.94}$$

- for the tau lepton [58]:

$$-\left(\frac{g m_\tau}{2 m_W}\right) \bar{\psi}_\tau \psi_\tau \left(\frac{\sin\alpha}{\cos\beta} h^0 + \frac{\cos\alpha}{\cos\beta} H^0\right). \tag{2.95}$$

The coupling to the pseudo-scalar Higgs boson can be determined in the same way. Because of its pseudo-scalar character an additional factor of γ^5 has to be introduced. The Yukawa coupling of A^0 to the SM fermions are:

- for the top quark [58]:

$$-\left(\frac{g m_t}{2 m_W}\right) \cot\beta \bar{\psi}_t \gamma^5 \psi_t A^0 \tag{2.96}$$

- for the bottom quark [58]:

$$-\left(\frac{g m_b}{2 m_W}\right) \tan\beta \bar{\psi}_b \gamma^5 \psi_b A^0 \tag{2.97}$$

- for the tau lepton [58]:

$$-\left(\frac{g m_\tau}{2 m_W}\right) \tan\beta \bar{\psi}_\tau \gamma^5 \psi_\tau A^0. \tag{2.98}$$

The couplings to the gauge bosons can be determined by the $SU(2)_L \times U(1)_y$ gauge invariance. The couplings to the neutral Higgs bosons result in:

- For W-bosons [58]:

$$\frac{g m_W}{2} \left(W_\mu^1 W^{1\mu} + W_\mu^2 W^{2\mu}\right) \left(\sin(\beta-\alpha) h^0 + \cos(\beta-\alpha) H^0\right) \tag{2.99}$$

- For Z-bosons [58]:

$$\frac{g m_Z}{2\cos\theta_W} Z_\mu Z^\mu \left(\sin(\beta-\alpha) h^0 + \cos(\beta-\alpha) H^0\right). \tag{2.100}$$

At tree level the pseudo-scalar Higgs boson does not couple to pairs of weak gauge bosons. In the limit of heavy pseudo-scalar Higgs bosons the mixing of the neutral Higgs bosons behaves as

$$\begin{array}{ll} \sin\alpha \approx -\cos\beta & \sin(\beta-\alpha) \approx 1 \\ \cos\alpha \approx \sin\beta & \cos(\beta-\alpha) \approx 0 \end{array}$$

and for this reason the couplings of the h^0 become similar to the SM Higgs couplings, while the couplings of H^0 become similar to the ones of the A^0 boson[17] [58].
The decay widths of SUSY Higgs bosons can be calculated from an integration on the transition matrix squared. This transition matrix includes the Yukawa coupling and summations over spins and colours, over phase space. The partial width of the A^0 for a decay into bottom quarks for example is [58]:

$$\Gamma\left(A^0 \to b\bar{b}\right) = \frac{3g^2 m_b^2 \tan^2\beta}{32\pi m_W^2} m_{A^0} \sqrt{1 - \frac{4m_b^2}{m_{A^0}^2}}. \tag{2.101}$$

[17] For the gauge bosons the H^0 decouples in this limit.

2.3 Dark Matter

Although SUSY is not verified yet there are already measurements constraining SUSY theories. The most important ones will be introduced in this section In the year 1933 the Swiss astronomer Fritz Zwicky discovered while examining the Coma galaxy cluster that the outer galaxies were orbiting too fast around the centre of the cluster to keep in line [16]. But in fact they did. His way out was to postulate a non-illuminating, heavy kind of matter whose Newtonian force binds the outer galaxies to the cluster, so-called Dark Matter. Another evidence for DM was given in 1974 when Ostriker and Einasto proposed independently the existence of giant DM haloes around galaxies containing most of the total mass of the galaxies [90, 91].
In current time the existence of dark matter is well established although its nature is still unknown. Some theories what dark matter could be made of will be further discussed in the following section [92].

2.3.1 Dark Matter Candidates

There are various theories existing what Dark Matter (DM) could be made of [92, 93]. The most important ones will be presented here:

- Modified Newtonian Mechanics (MONDs) is the from first point of view the most obvious DM theory: The concept of Dark Matter arises from the fact that observations of kinematic effects in gravitational systems are not consistent with the predictions from Newton's laws. For that reason the most obvious solution without an introduction of DM is to introduce violations of Newton's law or in general relativity [92, 94, 95].
  Though it is very difficult to find modifications which change gravity on the scales of DM problems while not changing anything on "ordinary" scales, where Newtonian theories are incredibly successful in describing physical systems. Although MONDs are very successful in describing rotation curves of galaxies they have currently been proven to be not efficient for the description of temperature profiles of the galaxy clusters Virgo, Abell 2199 and Coma [92, 96].

- Baryonic Dark Matter: The baryonic matter content of the universe is higher that the contribution of luminous baryons. For that reason there must also be a baryonic amount of DM. These "hidden baryons" can for example be interstellar or intergalactic gas[18] or massive and compact halo objects, so-called MACHOs[19] [97]
  The Cosmic Microwave Background spectrum is sensitive to the total energy density as well as to the baryonic matter content. In the measurements of WMAP [17] the baryonic matter content appears to account for 4 -5% of the Universe while the fraction of DM is 23%.Therefore the contingent of baryonic matter is not enough to explain Dark Matter [92, 97].

- Kaluza-Klein Dark Matter: A unification of electromagnetism with gravity can be obtained via the introduction of additional dimensions which appear at high energies,

[18] This kind of matter can be detected because it absorbs light from distant quasars.
[19] MACHOs can be measured via microlensing from far away stars.

so-called unified extra dimensions (UED) [98]. In these models SM particles propagate in the extra dimensions and get therefore additional contributions to their kinetic energy. For each extended field a set of Fourier expanded modes exist, so-called Kaluza - Klein states (KK). In 3 + 1 space-time the KK states appears as tower of states with masses increasing with their mode number. All of these states have the same quantum numbers. The lightest KK particle (LKP) is associated with the first KK excitation of the photon. This mode provides a perfect DM candidate. In case of KK Dark Matter the annihilation is not suppressed by helicity. Therefore there would be a lot more annihilation relics in the universe than for example in case of SUSY Dark Matter [92, 99].

- Massive Neutrinos have the advantage that they are known to exist. In the SM neutrinos are treated like mass-less particles, which is in most cases a well working approach because the mass of the neutrino is indeed proven to be very small[100]:

$$m_{\nu_e} < 2.05 \text{ eV} \qquad \text{at a } 95\% \text{ CL}^{20} \tag{2.102}$$

The existence of a not-vanishing neutrino mass could be proven by the existence of neutrino flavour oscillations observed in KAMIOKANDE [101], SNO [102], K2K [103] and KARMEN [104]. From the cosmic microwave background an upper constraint on the sum of all neutrino masses can be given as [17]:

$$\sum_{i=1}^{3} m_{\nu_i} = 0.67 \text{ eV}. \tag{2.103}$$

From the fact that neutrinos are massive it follows that they must have been thermally produced in the early universe and started to freeze-out at energies of about 1 MeV. Therefore the Relic Density made up from neutrinos can be calculated from:

$$\Omega_\nu h^2 = \sum_{i=1}^{3} \frac{m_{\nu_i}}{93 \text{ eV}}. \tag{2.104}$$

Together with the constraint on the sum of the neutrino masses given in eq. 2.103 this leads to an upper limit on the possible neutrino Relic Density of:

$$\Omega_\nu h^2 =\lesssim 0.007 \tag{2.105}$$

which is not enough to make up all Relic Density in the Universe [92].

- WIMPzillas: In these theories Dark Matter particles are assumed to be thermal relics of the early Universe with high masses of up to 340 TeV. The cosmic microwave background measurement of WMAP has set an upper limit of 34 TeV[105].
These super-heavy DM candidates are called WIMPzillas and they have masses larger than 10^{10} sun masses. Thus they have not been in thermal equilibrium during the freeze-out. So their Relic Density does not depend on an annihilation cross section. They have been produced for example gravitationally between inflationary and matter-dominated Universe or via oscillations of the inflationary potential during the defrost phase after inflation[92, 106].

[20] From tritium β-decay experiments.

- Axions have been introduced to solve the strong CP problem. Their masses where proven by laboratory searches, stellar cooling and the dynamics of supernova 1987 A to be very small [107]:

$$m_a \lesssim 0.01 \text{ eV}. \tag{2.106}$$

  However this does not cause problems in assuming it as Dark Matter candidate because its coupling to standard model matter is very weak. Due to this fact axions were never in thermal equilibrium with other particles in the early Universe and today it behaves like a perfect DM candidate [92, 107, 108].

- Neutralinos are the most promising DM candidates, because the introduction of SUSY beyond providing a perfect dark matter candidate solves also other particle physics problems (Sect. 2.2.1). In the R-parity conserving MSSM SUSY particles are only produced and destroyed in pairs. Therefore the LSP can be assumed to be due to R-parity conservation stable. In mSUGRA models the LSP is the lightest neutralino[21] which is a Majorana particle. Due to the results of SUSY breaking mechanisms (Sect. 2.2.2) the neutralino is assumed to be non-relativistic at the freeze-out time. As partner of the mixture of photon, Z-boson and neutral Higgs particles is electromagnetically neutral and therefore it does not radiate. It survived the long time period between freeze-out and present time. Its annihilation cross section explains very well the Relic Density measured in WMAP for a large range of SUSY parameter-space. This is the theory forming the basis of our study [54, 92].

2.3.2 The Cosmological History of Dark Matter

Dark matter is assumed to consist of weakly interacting, massive particles (WIMPs). Presumably these particles have been in thermal equilibrium. Their Relic Density was fixed when these particle froze out of the thermal equilibrium. The number density of the WIMPs in this epoch can be described by the Boltzmann equation:

$$\frac{dn_\chi}{dt} = -3Hn_\chi - \langle\sigma v\rangle \cdot \left(n_\chi^2 - n_{\chi,\text{eq}}^2\right), \tag{2.107}$$

where $H = \frac{\dot{R}}{R}$ is the Hubble expansion[22], $\langle\sigma v\rangle$ the thermal average over the WIMP annihilation cross section and $n_{\chi,\text{eq}}$ is the number density in the thermal equilibrium. In the Boltzmann equation (eq. 2.107) there are two terms contributing to the change of number density in time. The term including the Hubble constant represents the decreasing of the number density while the Universe expands and the second term describes the change caused by the WIMP annihilation.
In a static Universe the Hubble expansion would be zero. For that reason the Boltzmann equation could be reduced to

$$\frac{dn_\chi}{dt} = -\langle\sigma v\rangle \cdot \left(n_\chi^2 - n_{\chi,\text{eq}}^2\right).$$

The solution of this equation would be an exponential decrease starting from the number density in thermal equilibrium. There would be no dark matter left in the present Universe

[21] In most mSUGRA models the lightest neutralino has large contributions from the photino. In some models it gets additional Higgsino contributions.
[22] the expansion rate of the Universe.

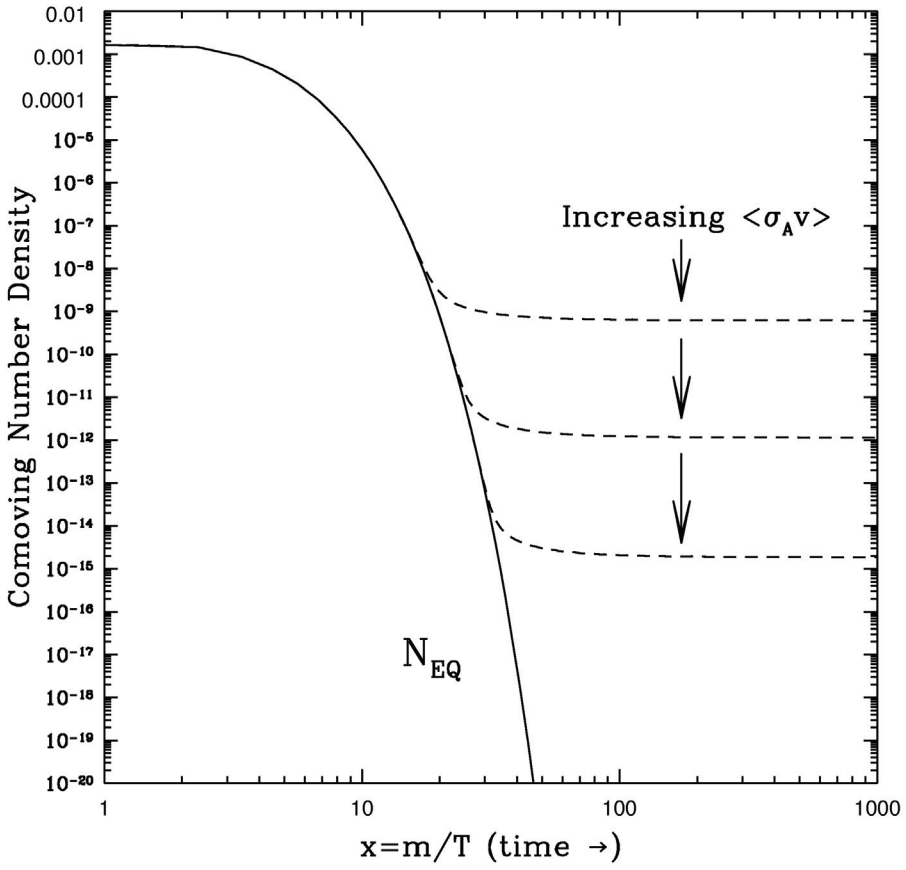

Figure 2.13: Numerical solutions of the Boltzmann equation. Taken from [18].

[54].
In an expanding Universe the Hubble expansion does not vanish. At early times after the decoupling from the plasma the cross section term would still dominate the Boltzmann equation. Therefore at these times the behaviour of DM would not differ in static and dynamic models. As long as the temperature of the Universe is higher then the WIMP mass the scale radius $R \propto \frac{1}{T}$ leads for the WIMP number density to a cubic dependence on the temperature. Therefore at this time the annihilation rate decreases with T^3. This continues up to the point where the number density drops below the expansion rate ($H \langle n_\chi \sigma v \rangle$). At this time the WIMPs fall out of the thermal equilibrium forming a constant number density in the present Universe [18, 92]. In Fig. 2.13 the time evolution of the number density is shown for different annihilation cross sections. The number density in the present Universe (Relic Density) is related to the annihilation cross section:

$$\Omega_\chi h^2 \approx \left(\frac{3 \cdot 10^{-27} cm^3 s^{-1}}{\langle \sigma v \rangle} \right) \tag{2.108}$$

In the WMAP experiment the cosmic microwave background has been measured very precisely. From this data a global fit has been done, where one of the parameters has been the Relic Density of DM. Combined with other data sets the measurement results in

a Relic Density value of [17]:

$$\Omega_\chi h^2 = 0.1131 \pm 0.0034. \tag{2.109}$$

CHAPTER 3

The MOPS software package

"The best way to predict the future is to implement it." D. Heinemeier Hansson

The MOPS (Minimisation Of chi square functions for Parameters in Supersymmetric models) package is a modular software package developed to run χ^2 minimisations in multi-dimensional SUSY parameter spaces. The input is taken from micrOMEGAs [109]. For the minimisation MINUIT [110] or a Markov Chain Monte Carlo [27] method can be chosen.

3.1 Some Simple Statistics

An aim of this thesis is the estimation of the probability of occurrence of certain mSUGRA models. Therefore, first a definition of probability and a way to calculate it has to be given. In the current section this is done.

3.1.1 Frequentist Probability Interpretation and Probability Density

Frequentists define probability as a limiting relative frequency. The elements of the set space S are thought of as possible outcomes of a measurement, assumed to be repeatable. A subset A of S, a so-called event, corresponds to the occurrence of any outcomes in the subset.
The probability for the event A is defined as:

$$P(A) = \lim_{n\to\infty} \frac{\text{number of occurrences of outcome } A \text{ in } n \text{ measurements}}{n}, \tag{3.1}$$

where

$$P(S) = 1.$$

The conditional probability $P(A|B)$[1] is the number of cases, where both A and B occur divided by the number of cases in which B occurs regardless of whether A occurs. So $P(A|B)$ gives the frequency of A with the sample space B [111].
In an experiment with a single continuous variable as outcome the probability of the observed value to be within the interval $[x, x+dx]$ is $f(x)\,dx$, where $f(x)$ is the probability density function (pdf). So $f(x)\,dx$ gives the fraction of times x is observed in the interval $[x, x+dx]$ in the limit that the total number of observations in infinitely large. The pdf is normalised such that

$$\int_S f(x)\,dx = 1.$$

The expectation value of a random variable x (also called population mean) can be calculated from the pdf by

$$E[x] = \int_{-\infty}^{\infty} x f(x)\,dx = \mu.$$

The variance of this mean is

$$\sigma_x^2 = E\left[x^2\right] - (E[x])^2.$$

According to problems where n variables are measured (the sample space becomes multidimensional) the quantities can be written in multidimensional random vectors. The definitions, given in this section, stay similar [111].

[1] $P(A|B)$: "A causes B".

3.1.2 Chi Square Functions and the Least Square Method

A typical example for a probability distribution is the so-called chi square distribution. If z is a continuous variable ($0 \leq z \leq \infty$) its chi-square distribution is defined by:

$$f(z;n) = \frac{1}{2^{n/2}\Gamma\left(\frac{n}{2}\right)} \cdot z^{\frac{n}{2}-1} e^{-\frac{z}{2}}, \tag{3.2}$$

where $n = 1, 2, ...$ is the number of degrees of freedom and Γ is the gamma function (Sect. A.3).
The mean and the variance of the gamma function can be calculated to be

$$E[z] = \int_0^\infty \frac{1}{2^{\frac{n}{2}}\Gamma\left(\frac{n}{2}\right)} z^{\frac{n}{2}-1} e^{-\frac{z}{2}} dz = n$$
$$V[z] = \int_0^\infty (z-n)^2 \frac{1}{2^{\frac{n}{2}}\Gamma\left(\frac{n}{2}\right)} z^{\frac{n}{2}-1} e^{-\frac{z}{2}} dz = 2n.$$

Given N independent, Gaussian random variables x_i, with known mean μ_i and variance σ_i the variable:

$$z = \sum_{i=1}^{N} \frac{(x_i - \mu_i)^2}{\sigma_i^2} \tag{3.3}$$

is distributed for N degrees of freedom according to a χ^2 distribution [111].
The method of least squares is, like the maximum likelihood method (sec A.4), a method to optimise the parameters $\vec{\theta}$ of a given model in a way to fit a sample of experimental data in the best possible way. It can also be taken to give an estimate of the goodness-of-fit of the hypothesis function $\lambda(\vec{x};\vec{\theta})$. Following this method

$$\log L(\vec{\theta}) = -\frac{1}{2} \sum_{i=1}^{N} \frac{(y_i - \lambda(x_i;\theta))^2}{\sigma_i^2}$$

has to be maximised. Therefore the chi square function:

$$\chi^2\left(\vec{\theta}\right) = \sum_{i=1}^{N} \frac{(y_i - \lambda(x_i;\theta))^2}{\sigma_i^2} \tag{3.4}$$

has to be minimised to get the least square estimators $\hat{\theta}_1, ..., \hat{\theta}_m$. These are the parameters of the chi square function at its minimum and therefore they build the best possible model. A single term of the chi square function $\frac{y_i - \lambda(x_i;\vec{\theta})}{\sigma_i}$ gives a measure of the deviation between the ith measurement y_i and the function $\lambda(x_i; \vec{theta})$. For that reason the complete chi-square function is a measure of the total agreement between the observed data and hypothesis [111].
If y_i are independent Gaussian random variables with known variance σ_i^2, the hypothesis λ is linear in θ_i and the functional form of the hypothesis is correct the minimum of the chi square function is distributed according to 3.2 with $N - m$ degrees of freedom. Then a measure for the goodness of fit is given by

$$\frac{\chi^2}{n_{\text{dof}}} = \frac{\chi^2}{N-m}.$$

If the $\frac{\chi^2}{n_{\text{dof}}} \sim 1$ the distribution is as expected. On the other hand if it is much more than one the hypothesis has to be doubted. For this case a measure of reliability of the hypothesis can be given by quoting a significance level (or a P-value):

$$P = \int_{\chi^2}^{\infty} f\left(z; n_{\text{dof}}\right) dz. \tag{3.5}$$

The P-value gives the probability for obtaining a result compatible with the hypothesis in question or less than the one actually observed [111].

3.2 The Brute Force Scan Method

The brute force scan method is the simplest method to scan a certain parameter space. Here a given interval for a parameter is divided into a given number of equidistant steps. This procedure is done for each parameter, which should be included into the parameter scan. Now the likelihood function for each point can be calculated. Afterwards the point with the best likelihood value is chosen. In the neighbourhood of this point the procedure is repeated for a smaller area and smaller step sizes. This is called step-refining. The procedure of step-refining can be repeated for several times. In our case it was repeated until $\tan\beta$ was known with a precision of 10^{-3}.
The advantage of this method is, that it is not very complicated and therefore it is not sensitive to effects from the limits of parameter space or local irregularities. Its disadvantage is the time and effort. The computing time increases with $2^{n_{\text{para}}}$ where n_{para} is the number of parameters. For that reason it is not useful for multidimensional fits with a given amount of computing power. However, it can be used to obtain an overview over low-dimensional projections of parameter spaces if a scan with more sophisticated methods like Markov Chain Monte Carlo (MCMC) is planned.

3.3 Markov Chain Monte Carlo

Markov Chain Monte Carlo (MCMC) [27] is a Monte Carlo (MC) integration using Markov chains for the sampling. In general MC integrations approximate expectations by forming sample averages over samples from a required distribution. It is done by drawing samples $\{X_t, t = 1, ..., n\}$ of a given pdf. Afterwards the expectation value of a function $f(x)$ can be calculated by averaging over the function values of the determined samples:

$$E\left[f(X)\right] \approx \frac{1}{n} \sum_{t=1}^{n} f(X_t). \tag{3.6}$$

MCMC in special utilises Markov Chains to draw these samples. This method can be used to integrate over high-dimensional parameter spaces. The Metropolis-Hastings algorithm is the most popular algorithm because it is easy to implement. Therefore this method will be introduced in this section [28].
In general there are two sampling methods: randomly or adaptively. The Gibbs sampler for example is a random sampler. The hit-and-run algorithm is an example for an adaptive sampler. It chooses a random sampling direction out of $\mathbb{R}^k$ and then samples a point into

this direction starting from the current point. The more general adaptive direction sampling (ADS) chooses points on the basis of previously sampled points. A special example for an ADS is the snooker algorithm, which will be further discussed in this section.
The most popular sampling method, the so-called Gibbs sampling, moves the directions parallel to the coordinate axes, which is not sufficient in order to obtain rapid mixing[2]. Therefore this algorithm was not used in this scope [28].

3.3.1 Markov Chains

A Markov Chain is a set of random variables $\{X_0, X_1, ...\}$, such that at each time t the next state X_{t+1} only depends on the immediately previous state X_t. The function $P(X_{t+1}|X_t)$ the point X_{t+1} is sampled from is called transition kernel of the chain.
After a certain amount of time the chain might converge to a stationary distribution $\phi(.)$, which does not depend on time t or on the starting point X_0. For that reason after the so-called burn-in, the chain has "forgotten" its starting point. From the output of the Markov Chain the expectation value of the function $f(x)$ can be calculated using the ergodic average:

$$\bar{f} = \frac{1}{n-m} \sum_{t=m+1}^{n} f(X_t), \tag{3.7}$$

where m is the number of burn-in iterations [28].
To converge to a stationary distribution the chain has to be

- **irreducible:** Any non-empty set of points with positive probability can be reached from all possible starting points.
- **aperiodic:** It must not oscillate between different sets of states in a periodic movement.
- **positive recurrent:** If the starting point X_0 is sampled from the pdf $\pi(.)$ all following points will also be distributed according to $\pi(.)$ [28].

3.3.2 The Metropolis-Hastings Algorithm

The first idea how to technically construct such a Markov Chain was given by Hastings in 1970 [112] based on an idea of Metropolis (1953) [113]. If one assumes a state X_t as current point the Metropolis-Hastings algorithm chooses the next state by first sampling a candidate point Y from a proposal distribution $q(.|X_t)$. The proposed point is then accepted, meaning $X_{t+1} = Y$, with a probability of:

$$\alpha(X, Y) = \min\left(1, \frac{\pi(Y)q(X|Y)}{\pi(X)q(Y|X)}\right). \tag{3.8}$$

If the point does not get accepted the new point is chosen to be the current point $X_{t+1} = X_t$.
The Metropolis-Hastings algorithm is popular because of its simplicity [28].

[2] Mixing means that the proposal function becomes close to the real pdf.

3.3.3 The Snooker Algorithm

In ADS algorithms directions for next points can be chosen on basis of previously sampled points. This procedure is called adaption. At each iteration a set of m points $\{X_t^1, X_t^2, ...X_t^m\}$ called the current set gets stored. An iteration of ADS comprises:

1. A random point X_t^c gets selected out of the current set,
2. A sample direction in parameter space e_t gets chosen,
3. A scalar r_t from a given density $f(r)$ is sampled,
4. The new point can be calculated by $X_{t+1}^c = X_t^c + r_t e_t$,
5. all other points stay unchanged.

An example for such an ADS algorithm is the snooker algorithm [28]. Here a second point, the so-called anchor point X_t^i is chosen out of the current set. The sampling direction is then calculated from:

$$e_t = X_t^i - X_t^c. \tag{3.9}$$

In case of the snooker algorithm the probability density is given by:

$$f(r) \propto \pi(X_t^c + re_t) \left|1 - r\right|^{k-1}. \tag{3.10}$$

Therefore X_{t+1}^c finally can be found on the straight line through the two points X_t^i and X_t^c. The general idea is to use the fact that as the algorithm proceeds the sampling directions become more likely to touch regions of high probability, because the current point as well as the anchor point tend to become more and more likely. The advantage of the snooker algorithm is that it is very robust. Its small disadvantage is that it treats computing resources wastefully, but with modern computers this point gets less problematic [28].

3.4 Implementation of the MOPS package

The classes of the MOPS package are shown in Fig. 3.1. There are two interface classes. One of them, MicroClass, connects the package to micrOMEGAs[114]. It is structured as a wrapper class interfacing all functions of micrOMEGAs to C++. The second interface gives the possibility to read information from a configuration file where all informations of the different constraints are stored. This enables the user to change for example mean values without the need of a recompilation. The configuration class includes two functions:

- `Parameter get_parameter(string)` searches a parameter in the internally stored parameter list and returns it. The parameter list is filled when the constructor of the class is called.
- `get_parameters()` returns a reference to the whole list of parameters.

Two container classes are implemented. The first one is called `Constraint` and can be used to store constraints. To achieve the possibility to store constraints with measured means as well as upper and lower limits on variables a special technique is applied called factory method. The constructor of the class is kept private and can be called by four

different member functions, which make it possible to store these different data types in a unique format. The functions are
`Constraint_lower_boundary(string,double,double)`,
`Constraint_upper_boundary(string,double,double)`,
`Constraint_meassured_mean(string,double,double)`
and `Constraint_direct_search(string)`.
Constraints from direct DM searches are kept separately because, here the exclusion limit is a function of an internal parameter of MOPS.
The second container can be used to store the input parameters. Its name is `Parameter`. This class is kept very simple. It just includes the constructor where the starting values get stored, the usual get functions and a function to check if the given starting point is within physical limits.
The `ChiSquare` class is implemented to calculate the χ^2 value for a a list of constraints. This list can be filled using `add_constraint(const Constraint&)`. The function double `calc_chisquare(MicroClass*)` calculates the χ^2 value based on the `MicroClass` object whose pointer is passed to it.
At last there is the Chain class. This class includes the Markov Chain. A `ChiSquare` object used for the χ^2 calculation at the different point has to be passed to the class constructor. The function `get_acceptance()` calculates the acceptance rate of the current point. Which is used in `set_step_sizes(ParamVector)` to decide if the step size has to be increased or lowered. Here, the step size is increased by a factor of 3/2, if the acceptance rate is greater than 30% and lowered by a factor of 2/3 if the acceptance rate is less than 20%.
The type `ParamVector` is a vector of the C++ library Eigen. This library is specially constructed for the treatment of physical vectors. It is optimised for 2^n entries.
The function `decide(ParamVector,double)` decides based on a Metropolis Hastings sampler if the point is taken as a point of the Markov Chain or it gets rejected. The parameters given to the function `decide(ParamVector,double)` are the suggested point previously calculated with `suggest_point()` and its χ^2 value which has to be previously calculated with double `calc_chi2(ParamVector)`. The current point is internally stored.
To enable people to use Minuit[110] within this framework an FCN function is implemented which is an instance of FCNBase and uses the output of ChiSquare as function values.
The MOPS package is implemented in a modular way which means each part can be extracted and used in another framework.

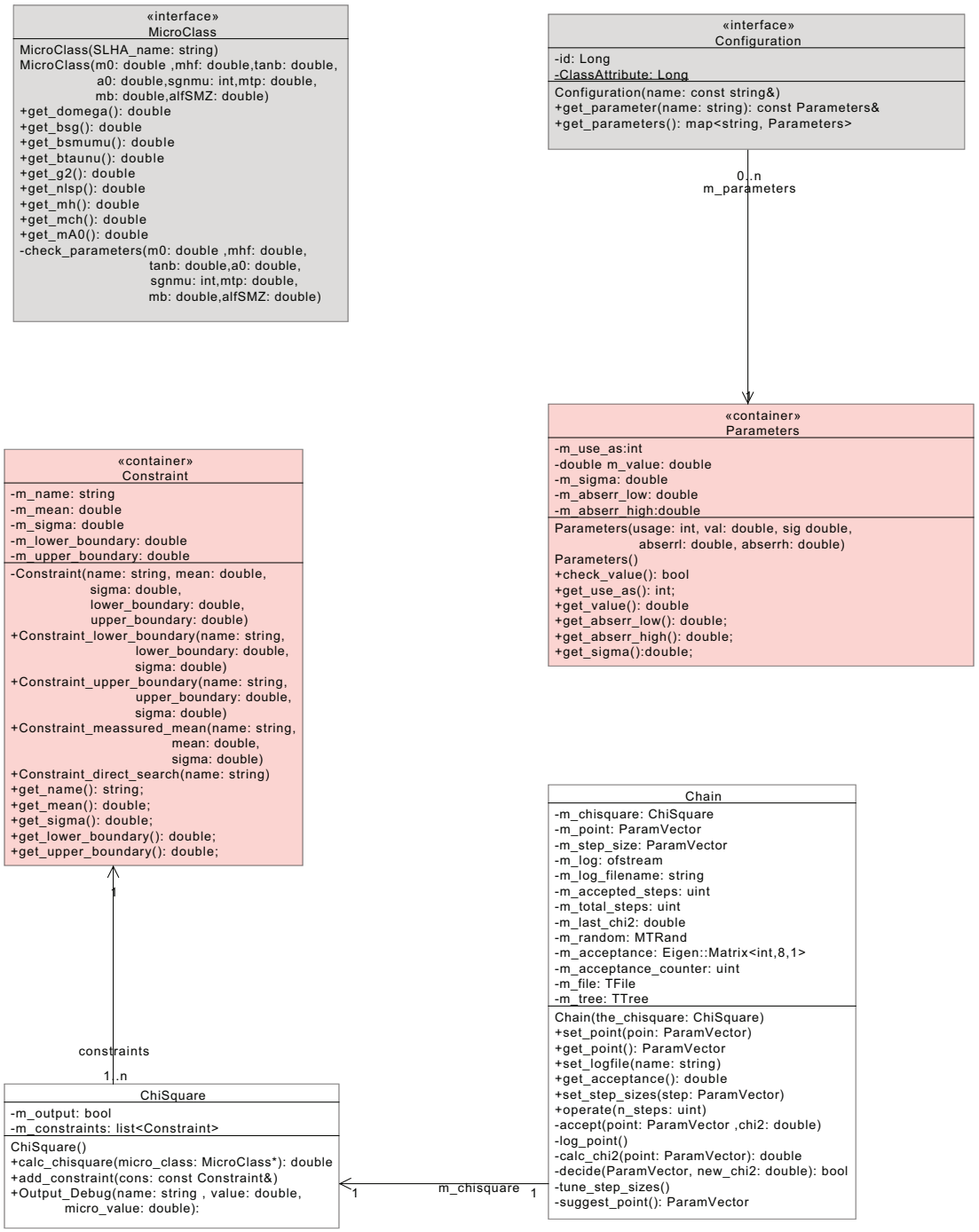

Figure 3.1: Class diagram of the MOPS package.[3]

CHAPTER 4

Results

”Die Natur ist so gemacht, daß sie verstanden werden kann. Oder vielleicht sollte ich richtiger sagen, unser Denken ist so gemacht, daß es die Natur verstehen kann.” W. Heisenberg

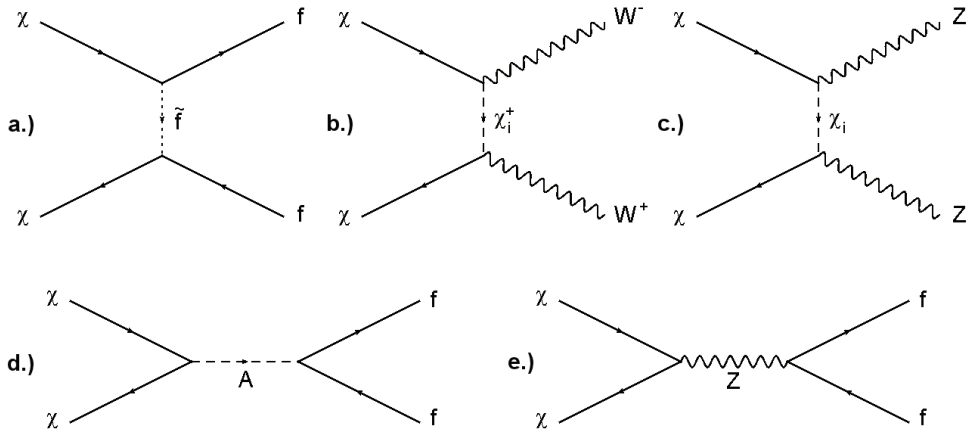

Figure 4.1: Neutralino Annihilation channels: a.) Via a sfermion, b.) via charginos, c.) via neutralinos, d.) via the pseudo-scalar Higgs e.) via the Z boson.

4.1 Is it possible to measure the Relic Density at the LHC?

4.1.1 Annihilation of SUSY Dark Matter

In cMSSM models the lightest neutralino is a perfect candidate for DM, because it is electrically neutral, weakly interacting and massive, a so-called WIMP. The neutralino is a Majorana particle with spin 1/2. Due to R-parity conservation only a pair of neutralinos can annihilate into SM particles. The products of the various annihilation processes can be leptons, bosons or high energetic photons. In Fig. 4.1 the Feynman diagrams of the main annihilation channels are given [92]. The annihilation cross section via the sfermion channel mainly depends on the particle masses [116]:

$$\sigma_f \propto \left(\frac{m_\chi m_f}{m_{\tilde{f}}^2} \right)^2 .$$

It is inversely proportional to the fourth power of the mass of the sfermion and to the neutralino mass squared. Thus this channel is only possible in regions with small sfermion masses.
In the channels where the weak gauge bosons are final products the annihilation depends on the ratio of the mass of the virtual particle and the LSP mass and the ratio of the gauge boson mass and the LSP mass:

$$\sigma_{W/Z} \propto \left(\frac{1}{1 + \left(m_{\chi_i^+/\chi_i}/m_\chi \right)^2 - \left(m_{W/Z}/m_\chi \right)^2} \right)^2 . \tag{4.1}$$

This process is a weak process, so the rate is small compared to other channels.
The annihilation via the pseudo-scalar Higgs boson depends on m_A and m_χ:

$$\sigma_A \propto \left(\frac{1}{4m_\chi^2 - m_A^2} \right)^2 . \tag{4.2}$$

The highest value for the cross section can be obtained on the resonance where the mass of the neutralino is half the mass of the pseudo-scalar Higgs boson. There are always two solutions fitting the WMAP Relic Density located in the order of 50 GeV at the left and at the right side of the resonance. The mass of the pseudoscalar Higgs boson depends on $\tan\beta$. Therefore the cross section depends implicitly on $\tan\beta$.
So the annihilation cross section for this diagram increases with increasing $\tan\beta$.
Another resonance diagram is given by the annihilation via the Z^0 boson. This diagram only depends on the LSP mass and the mixing matrix element of the neutralino [116]:

$$\sigma_Z \propto \left(\frac{m_f \cdot m_\chi}{4m_\chi^2 - m_Z^2} N_{3/4}^2 \right)^2 .$$

In most regions of the cMSSM parameter space the neutralino-neutralino-Z^0 coupling corresponds to the coupling of photons to the Z^0. This coupling does not exist in the SM. Therefore the neutralino only couples via its higgsino component. This higgsino mixing is usually small and in special regions like the focus point region [117, 118] the co-annihilation via neutralinos or charginos unusually dominates. Solutions fitting the WMAP constraint can be found for a neutralino mass close to the mass of the Z boson or in the focus point region. Thus it only appears in a narrow region of parameter space.
Another possible contribution to the neutralino annihilation comes from so-called co-annihilation channels. In the affected SUSY models the mass of the next to lightest SUSY particle and the mass of the LSP get nearly degenerated. In the early Universe this causes the LSP and the NLSP to freeze-out from the thermal equilibrium at the same time. Therefore the LSP can also annihilate with the NLSP instead of only pairwise. Thus the annihilation cross section increases drastically. Co-annihilation regions are fine areas very close to the areas where the NLSP reverses roles with the LSP. The most important co-annihilation area in cMSSM is the stau co-annihilation region which is close to the not DM consistent region where the SUSY partner of the τ-lepton becomes the LSP [119–123]. Another co-annihilation region is located close to the region forbidden by electroweak symmetry breaking. Here the NLSP is a chargino or neutralino.
Fig. 4.2 gives again an overview which diagram appears where in the cMSSM mass plane. For different values of $\tan\beta$ the annihilation via A^0 makes a coverage of the whole mass plane possible, because the pseudo-scalar Higgs mass can be tuned to the resonance.

4.1.2 Determination of $\tan\beta$ and m_A from the WMAP constraint

As previously discussed the annihilation of DM particles in the early Universe in combination with the expansion of the Universe yields a constant DM density called the Relic Density. The Relic Density shrinks with increasing annihilation cross sections. Due to the fact that the Relic Density value of $\Omega_\chi h^2 = 0.1131 \pm 0.0034$ measured by WMAP [17] is small compared to the values in the early Universe the annihilation cross section has to be high. This is the case for areas where special annihilation diagrams enhance the annihilation cross section.
If the mass of the pseudoscalar Higgs boson is adjusted to $2 \cdot m_\chi$ the cross section can be adapted to the WMAP results for each mass parameter point. This can be done by an adjustment of the cMSSM parameter $\tan\beta$ (see Figure 4.2). The result for such an attempt is show in Fig. 4.3. It is shown that for each point in the mass parameter plane a

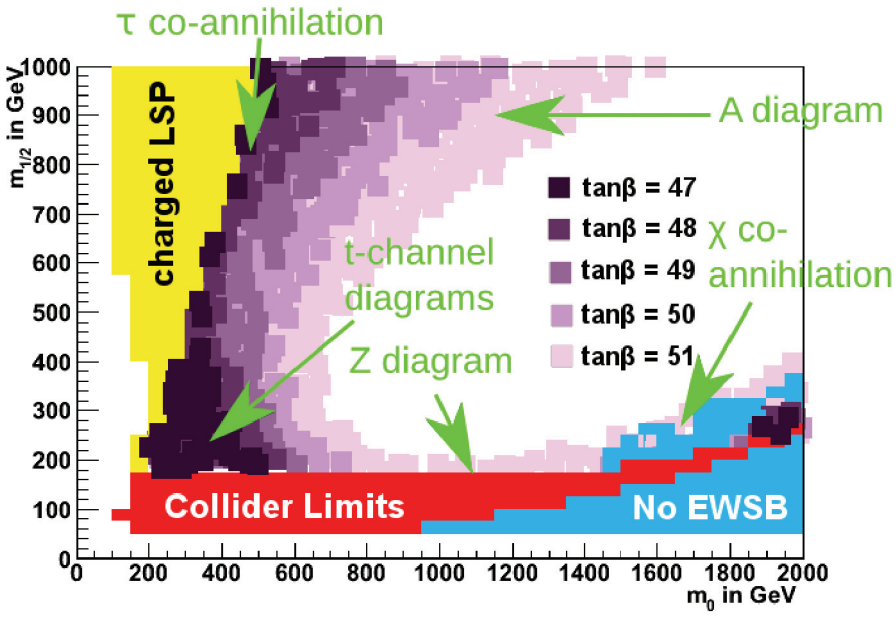

Figure 4.2: Neutralino annihilation channels in the cMSSM mass plane. DM consistent regions (pink - violet) for different values of $\tan\beta$ and excluded regions (yellow: excluded by charged LSP, red: excluded by direct collider searches, blue: excluded by breakdown of electroweak symmetry breaking): The t-channel diagrams (via virtual χ^+, χ^0 and $\tilde{f}$) appear for small mass parameters. They are partially excluded by collider limits. The τ co-annihilation channel appears close to the region of charged LSPs. Close to the region where electroweak symmetry breaking fails the chargino co-annihilation takes place. The resonance annihilation via Z^0 bosons appears if the neutralino mass is close to $m_Z/2$. The annihilation cross section via pseudo-scalar Higgs bosons increases with increasing $\tan\beta$. For this reason the DM consistent region caused by this diagram varies strongly with variation of $\tan\beta$.

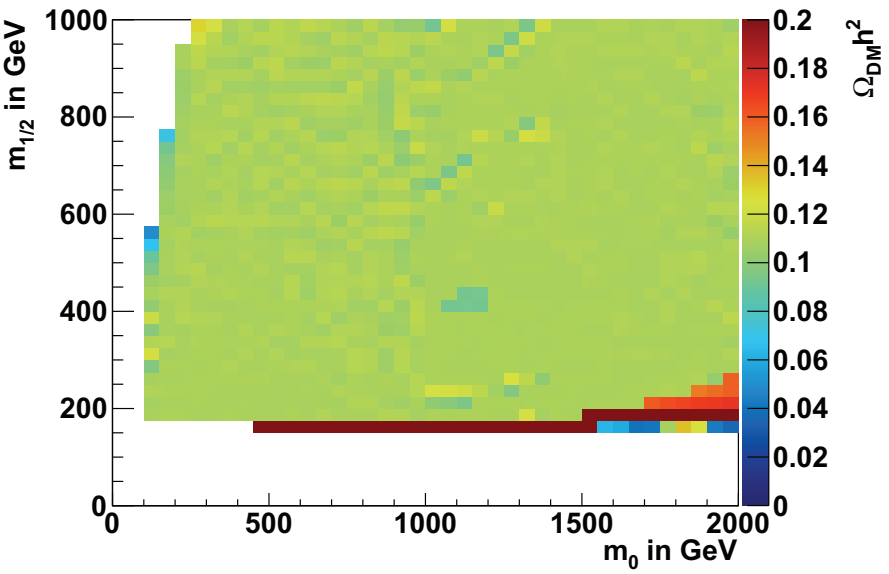

Figure 4.3: Results of the WMAP fit: The Relic Density values resulting from the fit are shown. All of them are close to the WMAP value given in eq. 2.109.

solution fitting the WMAP constraint can be found.
eq. 4.2 can be reformulated as

$$\sigma_A \propto \frac{1}{\left(4m_\chi^2\left(\frac{m_A}{2m_\chi}\right)^2 - 1\right)^2}.$$

Thus to obtain high annihilation cross sections the mass ratio $\frac{m_A}{2m_\chi}$ has to be close to one. In Fig. 4.4 the mass ratios corresponding to the Relic Density solutions in Fig. 4.3 are shown. In areas where other annihilation diagrams contribute to the relic density the mass ratio reaches values of 1.5 or more. For the rest of the mass parameter plane the ratio is close to one enhancing the cross section of the annihilation diagram via the pseudoscalar Higgs boson.
Taking eq. 2.84 and 2.76 into account m_A can be calculated from $\sqrt{m_1^2 + m_2^2}$. The RGEs of m_1^2 and m_2^2 get negative corrections depending on the Yukawa couplings of the top- and the bottom-quark, Y_t and Y_b [58, 64]. These are related as:

$$\frac{Y_b}{Y_t} = \frac{m_b}{m_t} \cdot \tan\beta. \tag{4.3}$$

To obtain small masses of m_A the ratio of the Yukawa couplings has to be close to 1 and therefore $\tan\beta$ becomes about 50.
The dependence of the mass of the pseudoscalar Higgs boson on $\tan\beta$ is shown exemplary for the mass parameters $m_0 = 1000$ GeV and $m_{1/2} = 500$ GeV in Fig. 4.5. It looks the same for the whole cMSSM mass parameter plane. Concluding, to get pseudoscalar Higgs masses small enough to be two times the LSP mass $\tan\beta$ has to be large.

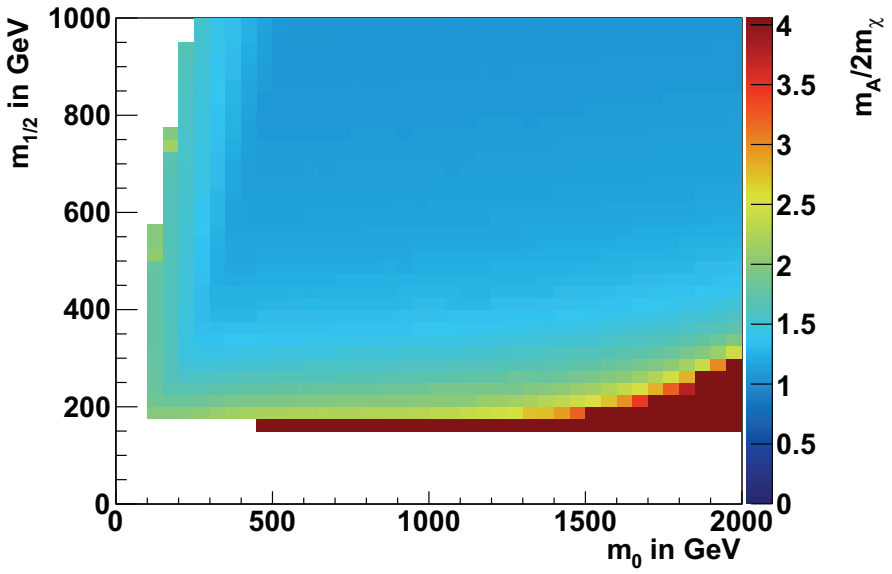

Figure 4.4: Ratio $\frac{m_A}{2m_\chi}$ for the WMAP fit. If the ratio is close to one the cross section of the annihilation diagram via the pseudoscalar Higgs boson is close to the resonance.

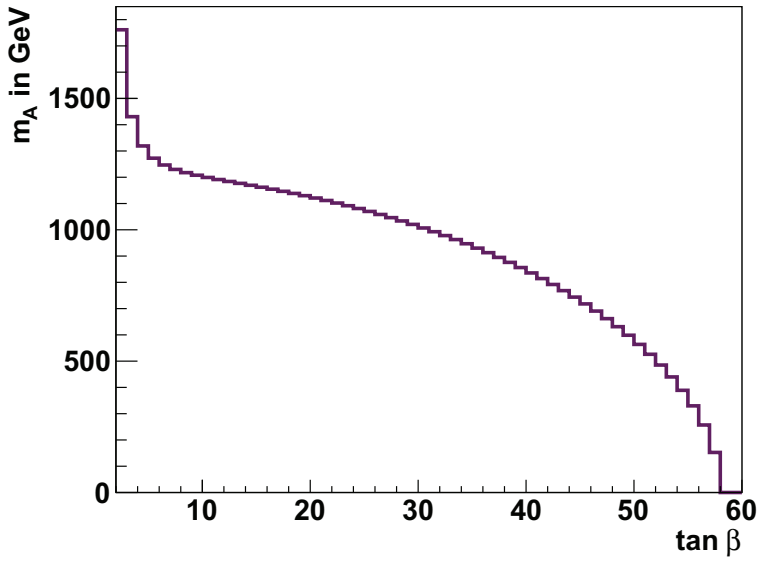

Figure 4.5: Dependence of m_A on $\tan\beta$ for $m_0 = 1000$ GeV and $m_{1/2} = 500$ GeV. The mass of the pseudoscalar Higgs boson shrinks with increasing values of $\tan\beta$. The same behaviour is found for all points in the m_0-$m_{1/2}$ plane.

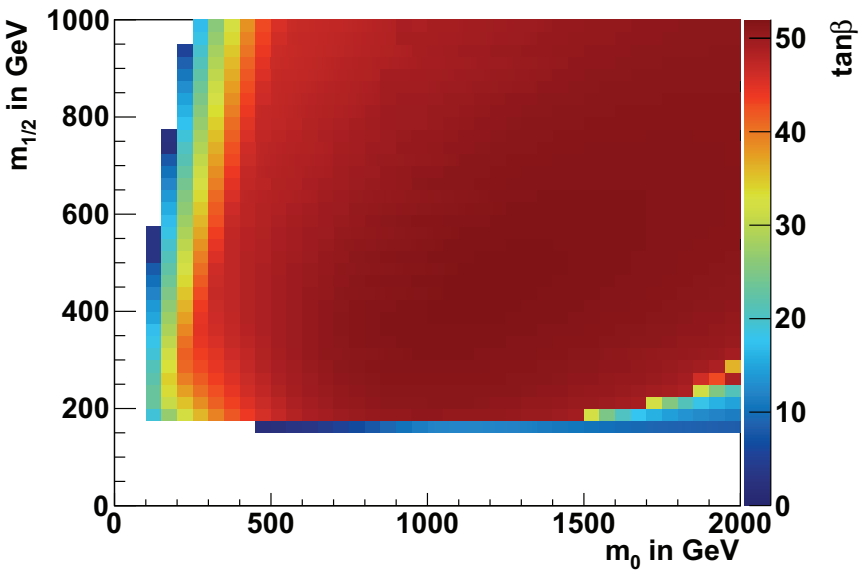

Figure 4.6: Values of $\tan\beta$ obtained by the WMAP fit: Values of high $\tan\beta$ are favoured in areas of the parameter space where the annihilation channel via the pseudoscalar Higgs boson dominates.

The analysis done in this thesis uses this fact by adjusting $\tan\beta$ instead of the mass of the pseudoscalar Higgs boson directly. This is done this way because the mass of the pseudoscalar Higgs boson is connected to the masses of the other SUSY particles via the renormalisation group equations and the condition of mass unification at the GUT scale. By changing just the mass of the pseudoscalar Higgs boson the resulting model would not be within the cMSSM framework anymore.
To find WMAP consistent solutions for the Relic Density $\tan\beta$ is varied on the interval $[1, 56]$ up to a precision of $\Delta\tan\beta = 10^{-3}$. The resulting $\tan\beta$ values are plotted in Fig. 4.6. Apparently, for the regions of parameter space where none of the the other diagrams is dominant enough to drive the Relic Density to the value expected from WMAP $\tan\beta$ appears to get high. This is because of the strong dependence of the annihilation cross section on the mass of the pseudoscalar Higgs boson and thus on $\tan\beta$. Such high values of $\tan\beta$ enhance the production cross section of the pseudoscalar Higgs boson at the LHC and would therefore abet a discovery [124].
To illustrate the influence of the annihilation via pseudoscalar Higgs bosons in Fig. 4.7 the dependence of the Relic Density on $\tan\beta$ is shown. This is done for a point where the annihilation cross section is purely influenced by the annihilation via the pseudoscalar Higgs boson and a point where the contributions from another diagram influences the cross section. If the annihilation cross section is dominated by the pseudoscalar Higgs channel there are two solutions for high $\tan\beta$ located around the A^0 resonance. In this analysis always the left one is taken. In cases where the annihilation cross sections get additional other solutions the best fit point is located around 40.
In Fig. 4.8 the obtained pseudoscalar Higgs masses are shown. In the region considered they can increase up to 1 TeV.

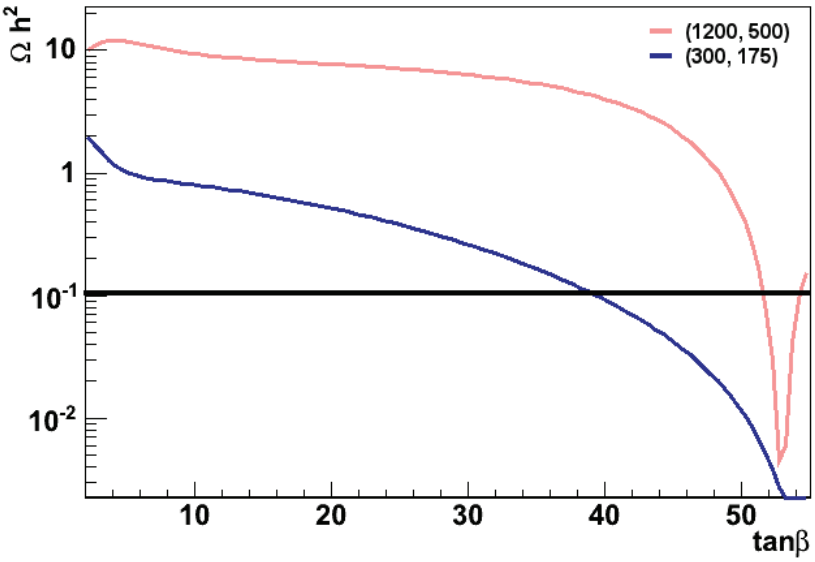

Figure 4.7: $\tan\beta$ dependence of the Relic Density: The black line shows the Relic Density expected from WMAP. The first diagram (pink) is located at a parameter point where the annihilation is dominated by the pseudoscalar Higgs channel. The other diagram (deep blue) is located at a point in parameter space, where also contributions from other diagrams become relevant.

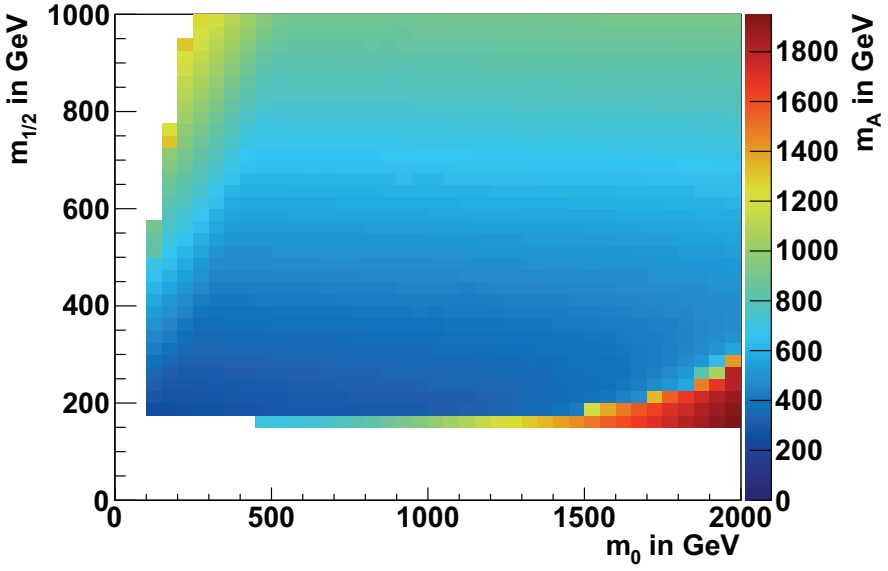

Figure 4.8: Pseudoscalar Higgs mass values obtained by the WMAP fit. All masses are below 1 TeV.

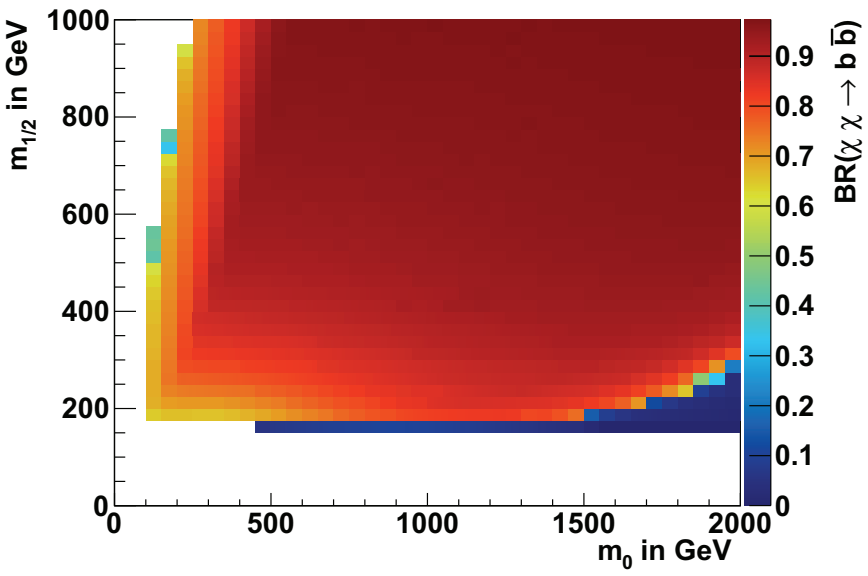

Figure 4.9: Branching ratio of annihilation via pseudoscalar Higgs bosons: The ratio $\frac{CS(\chi\chi\to A^0\to b\bar{b})}{CS(\chi\chi\to b\bar{b})}$ is calculated for each point resulting from the $\tan\beta$ optimisation.

The chosen m_A values are constant for changing m_0. They only depend on $m_{1/2}$ due to the fixed ratio of $\frac{m_A}{2m_\chi}$.
Accordingly, in areas where no other diagrams contribute to the annihilation cross section the annihilation cross section is dominated by the annihilation via the pseudoscalar Higgs boson. This is shown in Fig. 4.9. Here, the branching fraction of annihilation via the pseudoscalar Higgs boson is plotted. It can be seen that in regions where no other annihilation diagrams contribute the annihilation cross section is dominated by the annihilation via the pseudoscalar Higgs boson. Due to the fact that this makes up a large part of the parameter space the error of a Relic Density calculation can be obtained by exploring the potential errors for the observable in eq. 4.2. These are $\Delta\tan\beta$, Δm_{A^0} and Δm_{χ^0}. This will be done in the following section. For the stau co-annihilation region the predictions for Relic Density calculation at the LHC can be found in [125].

4.1.3 Estimated Uncertainty in the Relic Density Determination from LHC Data

Influence of the Neutralino Mass Uncertainty

The first point in the determination of the influence from neutralino mass uncertainties is to estimate the errors of the neutralino mass realistically. This can be achieved by getting an understanding of the mass reconstruction accurately.
In the LHC the production of superpartners can appear up to masses of about 2.5 TeV. Such heavy particles decay immediately. Depending on the mass hierarchy of the investigated model the decays appear in longer or shorter cascades. The final result of these

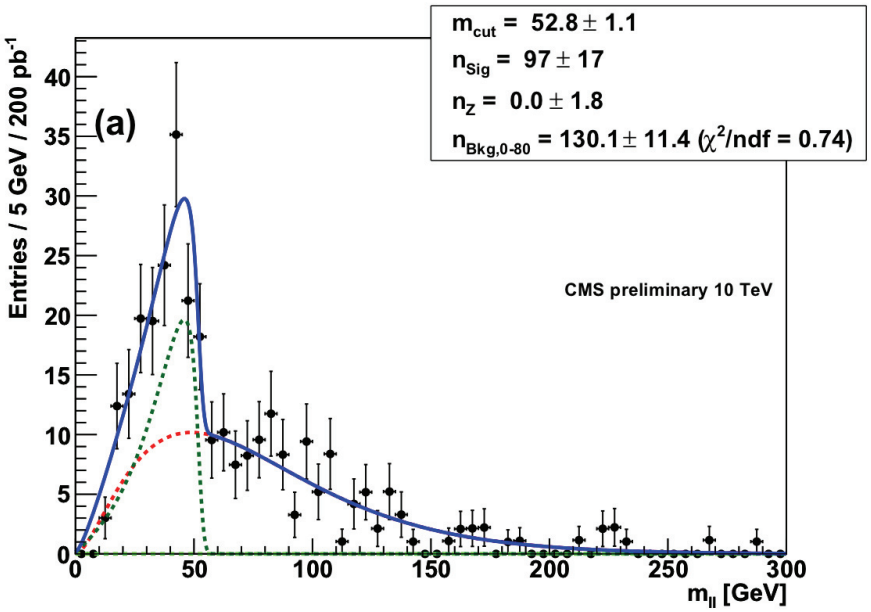

Figure 4.10: Example for Endpoint Determination: The plot shows an example for the mass edge of the parameter point $(m_0, m_{1/2}, \tan\beta, A_0, sgn(\mu)) = (200, 160, 10, -400, 1)$. The background (red dashed line) and the signal (green dashed line) distribution get fitted to the data and afterwards the endpoint can be determined from the signal distribution. Taken from [126].

cascades is due to R-parity the LSP plus SM particles. If the LSP is a dark matter candidate it is weakly interacting and therefore it escapes the detector just like the neutrino. Thus a full reconstruction is not possible. The thing that can be determined is the mass difference of the LSP and the NLSP. This can be done from invariant mass distributions of the visible particles. The escaping particle causes triangular shapes in the invariant mass spectrum. The endpoints of these shapes can be used to reconstruct the mass difference between the lightest and the second lightest neutralino. An example for such a distribution is shown in Fig. 4.10 [126]. In [126] the discovery potential at the LHC with a centre of mass energy of 10 TeV is explored. In the explored models the second lightest neutralino ($\tilde{\chi}_2^0$) decays leptonically which is useful for an accurate reconstruction. The mass hierarchy of the chosen models is not fixed, thus the leptonic neutralino decay can occur in two different scenarios: If the second lightest neutralino is the next to lightest supersymmetric particle (NLSP) a three-body-decay appears. In this scenario the endpoint is given directly by the mass difference of the LSP and the NLSP [126]:

$$m_{ll,\,\mathrm{max}} = m_{\tilde{\chi}_2^0} - m_{\tilde{\chi}_1^0}. \tag{4.4}$$

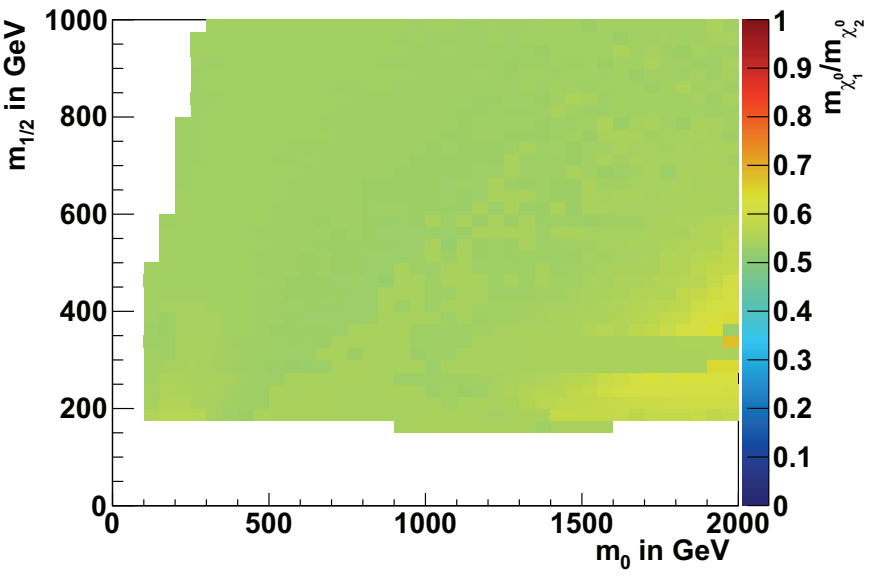

Figure 4.11: Mass ratio of the two lightest neutralinos for parameters points fulfilling the WMAP constraint.

The second possible scenario is the two-body-decay where a real slepton is produced in an intermediate step. In this case the endpoint is given by [126]:

$$(m_{\mathrm{ll,\,max}})^2 = \frac{\left(m^2_{\tilde{\chi}^0_2} - m^2_{\tilde{l}}\right) \cdot \left(m^2_{\tilde{l}} - m^2_{\tilde{\chi}^0_1}\right)}{m^2_{\tilde{l}}}. \tag{4.5}$$

In the models discussed in this thesis the couplings and masses unify at the GUT scale. This condition fixes the hierarchy between the two neutralino mass parameters [56]. Due to the fact that in most of the parameter space the lightest and the second lightest neutralino are mainly bino and wino-admixtures while the contribution from the higgsinos admixture is negligible [64] this fixes the hierarchy between the two lightest neutralinos to:

$$m_{\chi^0_1} \approx 0.5 \cdot m_{\chi^0_2}. \tag{4.6}$$

Fig. 4.11 demonstrates that this holds for the current analysis. Here, the ratio between the masses of the two lightest neutralinos has been plotted for all points fitted to the WMAP constraint. It shows that the ratio is always around 0.5 like predicted in eq. 4.6 except in the so-called focus point region, where chargino co-annihilation diagrams via contribute to the annihilation cross section. Here, the higgsino components of the two lightest neutralinos increase. This defies the assumptions in eq. 4.6 because it does not take the additional higgsino contributions into account. Anyway, this region is not taken into account in the current analysis. Only points where the annihilation via the pseudoscalar Higgs boson are assumed.
The uncertainty of the endpoint fits is not constant in the whole cMSSM mass plane, because the production cross section depends on the position in parameter space. An estimate of the uncertainty was given in Ref. [126] to be 3.5%. Therefore the uncertainty

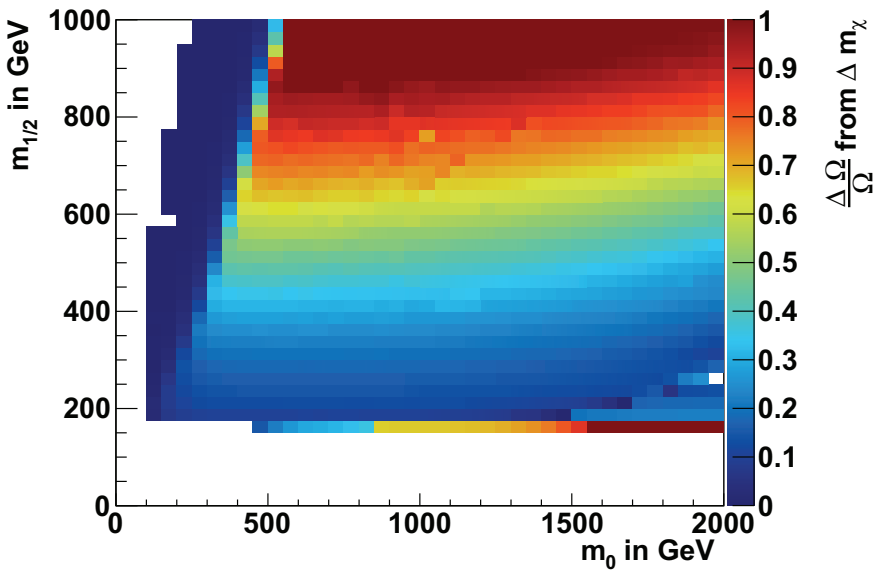

Figure 4.12: Relative error on Relic Density caused by error of m_χ .

of the neutralino mass can be assumed to be this order of magnitude.
The uncertainty of the neutralino mass causes an uncertainty in the Relic Density determination. The degree of influence of the relative neutralino mass uncertainty error on the relative Relic Density uncertainty is shown in Fig. 4.12. The error increases with increasing $m_{1/2}$ and makes the uncertainty on the Relic Density being more than 100% for $m_{1/2}$ larger than 900 GeV. Therefore it is the dominant uncertainty.

Influence of the Pseudoscalar Higgs Mass Uncertainty

The second fraction of uncertainty is caused by the mass of the pseudoscalar Higgs boson. For high values of $\tan\beta$ the dominant production channel for the pseudoscalar Higgs boson is the associated production with bottom quarks. The Feynman diagrams are shown in Fig. 4.13. For small $\tan\beta$ this channel is the second most prevalent channel. The preference of an association with bottom quarks compared to top-quarks for high values of $\tan\beta$ comes from the fact that the Yukawa coupling of the A^0 depends on $\tan\beta$ and prefers coupling to down-like quarks [88].
In addition to the measurement of the production cross section of pseudo-scalar Higgs particles the exact knowledge of the mass is of interest. For a mass detection it is beneficial to choose a decay channel into particles different from the associated particles. In case of the pseudoscalar Higgs boson these are tau-leptons. For high values of $\tan\beta$ the coupling to tau leptons is just like the coupling to bottom quarks enhanced by $\tan\beta$. Additionally, the decay to tau leptons is preferred to the decay into other leptons because of the mass dependence of the Yukawa coupling [88].
The reconstruction of the pseudoscalar Higgs boson mass in tau-decay channels can be done when the leptons are not back to back. This is ensured by cuts on the angle between the two leptons in the transverse plane [127]. The mass of the pseudoscalar Higgs bosons

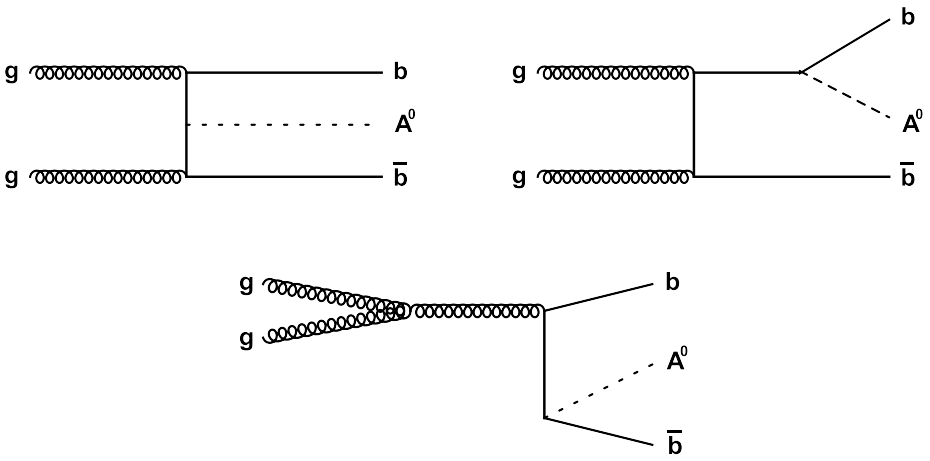

Figure 4.13: Feynman diagrams of gluon fusion. The production of the pseudoscalar Higgs boson is associated with a bottom quark pair.

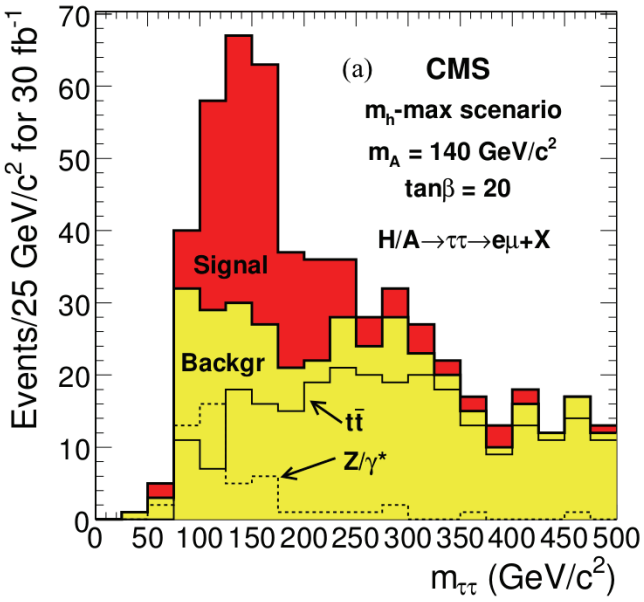

Figure 4.14: Monte Carlo study about the determination of m_A from the $\tau\tau$ reconstructed mass at the LHC. Taken from [127].

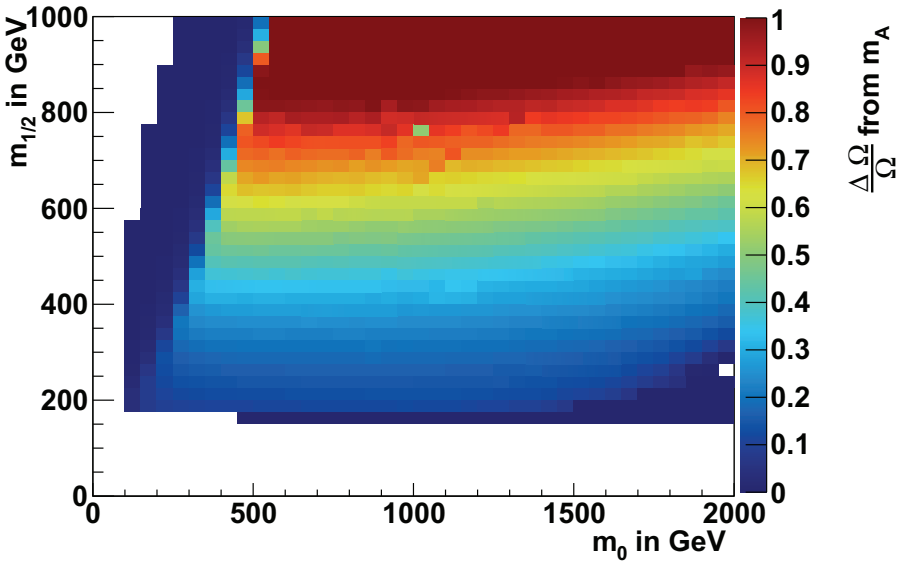

Figure 4.15: Contribution from a 3% m_A uncertainty.

is determined from the invariant mass of the tau leptons. In Fig. 4.14 an example for such an invariant mass distribution is given. In [128], [129], [130] and [131] such reconstruction processes are studied for different particle masses. The uncertainty of the mass determination can be concluded to be $\Delta m_A \approx 3\%$.
This is similar to the error estimation for m_χ. Since both enter to the fourth power in the annihilation cross section the uncertainty is similar to Fig. 4.12 as demonstrated in Fig. 4.15.

Influence of the $\tan\beta$ Uncertainty

For the determination of the contribution of $\tan\beta$ one first has to think about a method to determine $\tan\beta$ reliably from LHC data. In the previous section the mass determination of the pseudoscalar Higgs boson from gluon fusion was discussed. Also the cross section of gluon fusion can be measured directly. This parameter depends quadraticly on $\tan\beta$. Therefore it can be used to measure $\tan\beta$. In such measurements the fact that the cross section also depends on the mass of the pseudoscalar Higgs boson has to be taken into account.Thus an uncertainty in m_A is also reflected in the uncertainty of $\tan\beta$. Because of this connection the uncertainty on $\tan\beta$ has to be in combination with an uncertainty on m_A. In Fig. 4.16 the $\tan\beta$ uncertainty for a fixed combination of m_0 and $m_{1/2}$ is calculated taking an uncertainty of 10% for the cross section of the pseudoscalar Higgs production and 3% uncertainty for m_A [127] into account. This calculation is repeated for each WMAP solution. The result is illustrated in Fig. 4.17. Concluding, the uncertainty of $\tan\beta$ is about 12% which results into a contribution of about 10% to the uncertainty of the Relic Density in all areas of parameter space where the determination method is valid. This is shown in Fig. 4.18. The uncertainties from $\tan\beta$ influence the uncertainty of the Relic Density least.

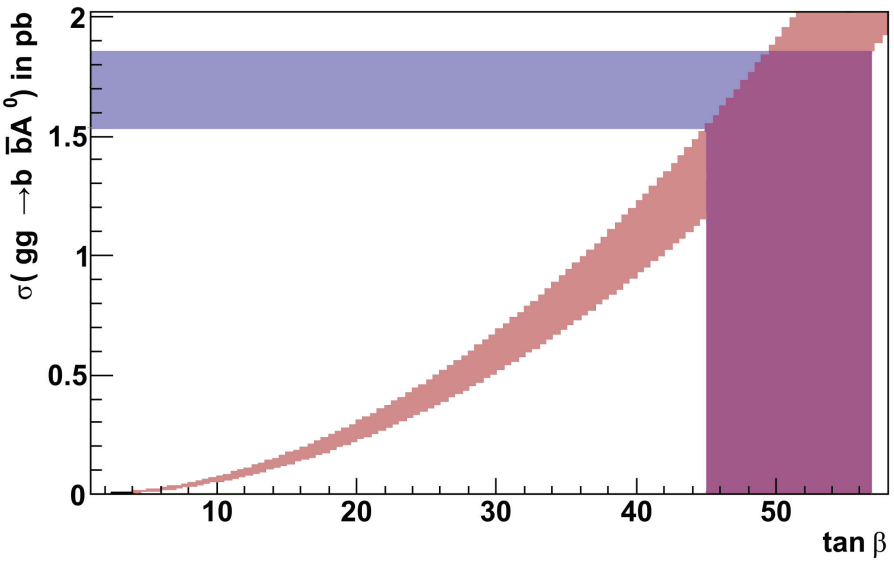

Figure 4.16: Cross section of associated A^0 production at the LHC (14 TeV centre of mass energy). The pseudoscalar Higgs mass is m_A = 500 GeV. Pink band: m_A uncertainty of 3%. Blue band: Cross section uncertainty of 10%. Purple band: Resulting uncertainty in $\tan\beta$. The cross section was calculated using CalcHEP [132].

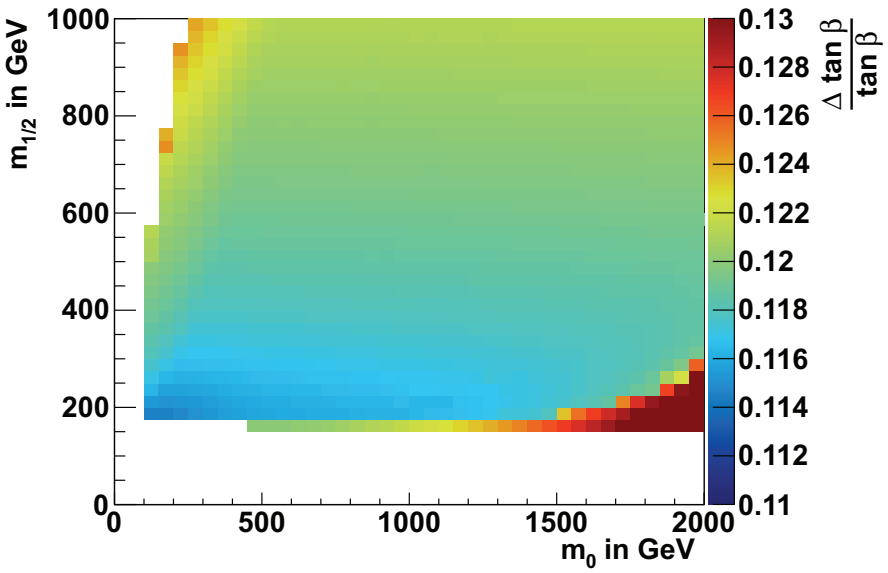

Figure 4.17: Relative error on $\tan\beta$ calculated by combining the error on the mass of the pseudoscalar Higgs boson with a 10% error on the production cross section at the LHC. The cross sections were calculated using CalcHEP [132].

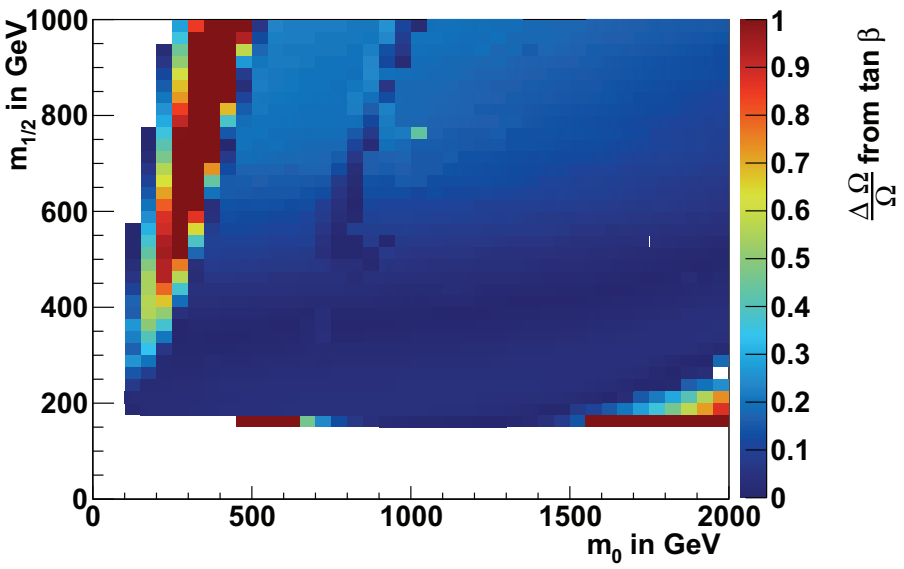

Figure 4.18: Contribution from $\tan\beta$ uncertainty like illustrated in Fig. 4.17.

Combination of Errors

These investigations can be combined in order to determine the complete uncertainty of the Relic Density determination from LHC data. The results are plotted in Fig. 4.19.
For a narrow area next to region excluded by the requirement that the LSP has to be electrically neutral, the so-called co-annihilation region, and a narrow area close to the electroweak symmetry forbidden region the method of determination fails. The reason for this is that the annihilation cross sections obtains strong contributions from other annihilation diagrams and can therefore not be calculated just from the pseudoscalar Higgs diagram.
In the regions, where the determination method is valid the Relic Density can be reconstructed up to $m_{1/2}$ = 500 GeV with an uncertainty of 20 - 60%. This is clearly much worse than the cosmological uncertainty on the Relic Density but if the LHC would find a Relic Density compatible with WMAP, it would be a hint that neutralinos are the dominant part.

4.1.4 Constraining Neutralino Masses by Relic Density

Alternatively to trying to determine the Relic Density one could determine the neutralino mass from the WMAP constraint assuming neutralinos make up all the DM. In this case one can use this constraint to constrain $m_{1/2}$ values for fixed values of m_0. This is demonstrated in Fig. 4.20. The first resonance is located at $m_Z/2$. Here the WMAP Relic Density value is driven by the decay channel via the Z-boson, which was not further studied in the current analysis since it appears in the regions excluded by the LEP limit. The second resonance is caused by the pseudoscalar Higgs. Around this resonance two solutions for the neutralino mass can be found by matching the Relic Density to the value measured by WMAP. The value of $\tan\beta$ can be determined like explained in Sect. 4.1.3.

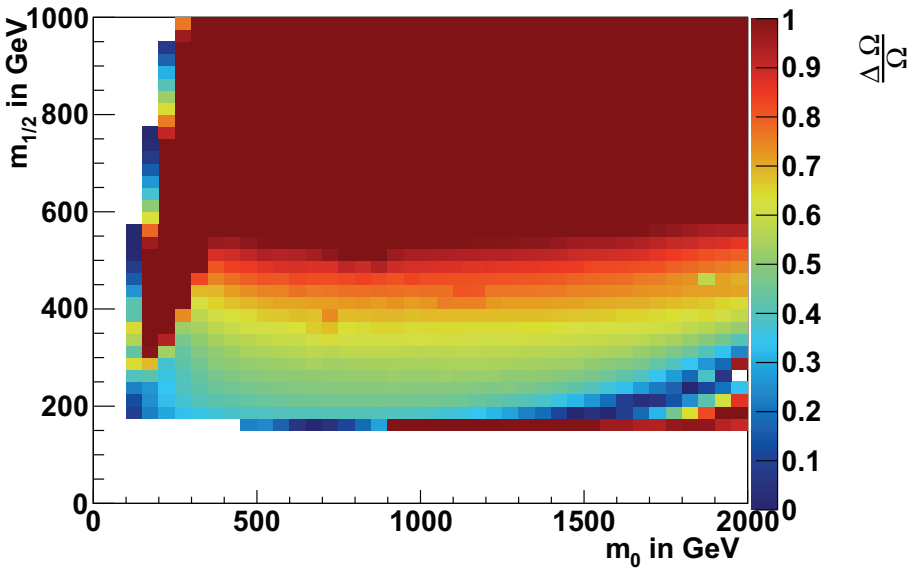

Figure 4.19: Relative Relic Density uncertainty. The following errors are taken into account: $\frac{\Delta m_\chi}{m_\chi}$ = 3.5%, $\frac{\Delta m_a}{m_A}$ = 3%, $\frac{\Delta \tan\beta}{\tan\beta}$ like given in Fig. 4.17.

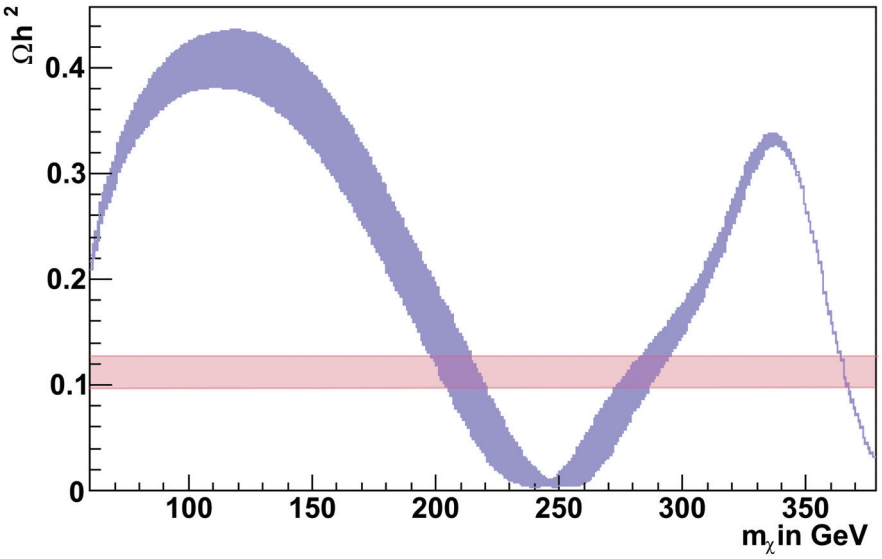

Figure 4.20: Relic Density dependence of m_χ. Pink band: uncertainty caused by an m_A uncertainty of 3%. Blue band: Uncertainty of the relic density measurement by WMAP. This plot was done for m_0 = 500 GeV.

The pink band represents the Relic Density measured by WMAP including the uncertainty of the measurement. Another quantity contributing to the uncertainty is the uncertainty of the A^0 mass. This is included in the blue band. The uncertainty in $\tan\beta$ broadens the band negligibly. If other SUSY attributes can be measured, this could resolve the ambiguities in Fig. 4.20.
Taking all uncertainties into account leads to a measurement of the neutralino mass with an uncertainty of 3 - 7%. The work of this section was done in collaboration with Tim Küstner [133].

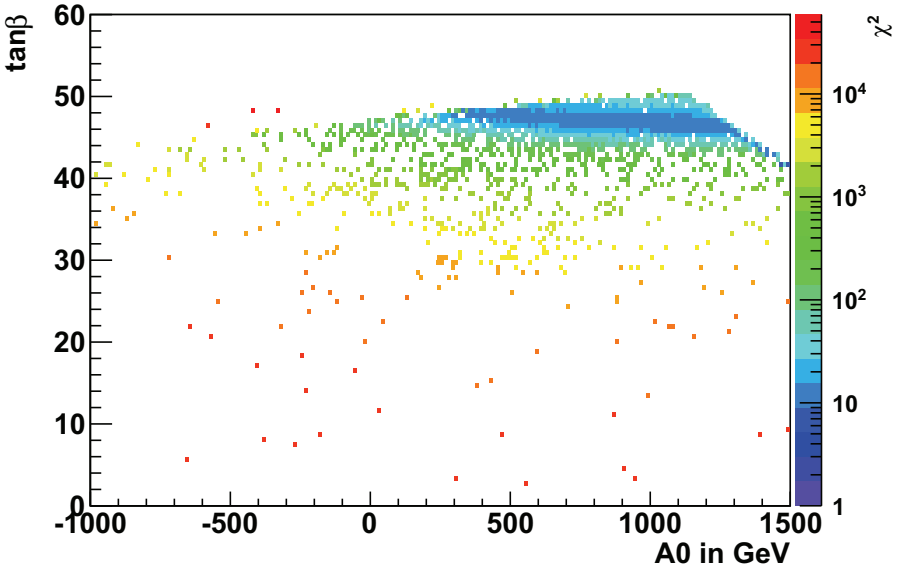

Figure 4.21: Correlation of $\tan\beta$ with A_0 for m_0 = 500 GeV and $m_{1/2}$ = 400 GeV.

4.2 Constraints on SUSY parameter space

4.2.1 Motivation

The SUSY parameter space has 105 free parameters and thus a large parameter space. Already the cMSSM with 4 continuous free parameters has as many dimensions as space-time.
However, indirect informations about SUSY can be obtained from experiments in cosmology and particle physics (flavour physics). With the constraints parts of the parameter space can already be excluded without a direct measurement at new particle accelerators. New exclusion limits can be included extending the excluded region directly. As soon as the best-fit point of a global fit gets excluded the new best-fit-point can be determined using this method.
In this study MCMC algorithms are used for global fits. The results can be compared with [134] where the same fit was done using MINUIT as minimiser. The problem arising from a global fit of the SUSY parameter space is the strong correlation between the two parameters $\tan\beta$ and A_0. To avoid a loss of good solutions the so-called multi-step fit method has been applied. Here, the variation is first done for the two strongest correlated parameters ($\tan\beta$ and A_0) keeping the other two parameters m_0 and $m_{1/2}$ fixed. This is done for all possible m_0-$m_{1/2}$ combinations for a fixed step width in the m_0-$m_{1/2}$ plane.
Then with the four main parameters close to their optimum value further minimisation can be obtained by selecting in addition the SM parameters (α_S, m_b and m_t) in the fit.

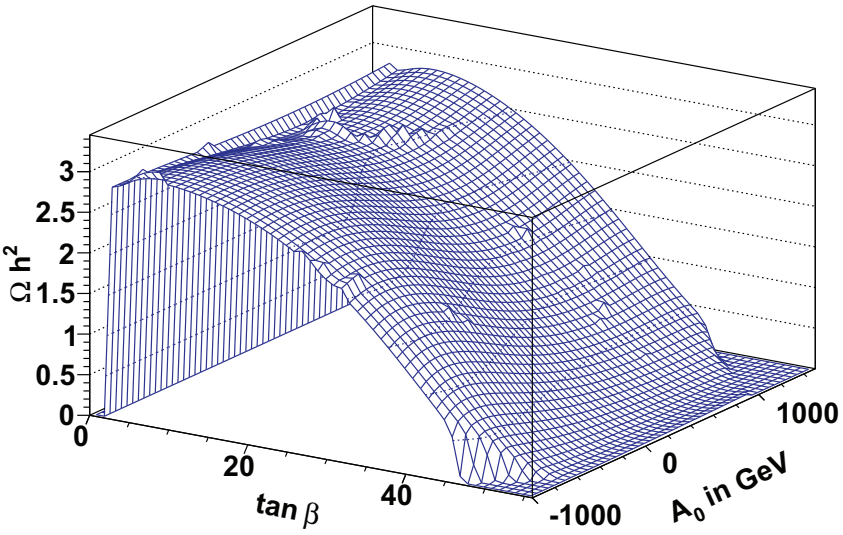

Figure 4.22: Dependence of Ω on $\tan\beta$ and A_0 for m_0 = 500 GeV and $m_{1/2}$ = 400 GeV.

However, the effect of the SM parameters is small. Therefore the are kept fixed as:

$$\begin{aligned} m_t &= 172.5 \text{ GeV} \\ m_b &= 4.25 \text{ GeV} \\ \alpha_S &= 0.1172 \end{aligned} \tag{4.7}$$

The probability of the different m_0-$m_{1/2}$ points is measured by:

$$\Delta\chi^2 = \chi^2_{\text{abs}} - \chi^2_{\text{min}}. \tag{4.8}$$

The 95% C.L. contour in this two-dimensional parameter space can be obtained by connecting points with $\Delta\chi^2 = 5.99$. Similar contours can be obtained for other confidence levels by selecting the appropriate $\Delta\chi^2$ (see Appendix). The influence of the different constraints on the exclusion curve are studied by the appropriate $\Delta\chi^2$ of each constraint. All observations discussed below have been calculated with the MOPS framework including micrOMEGAs version 2.4.1 [114, 135].

4.2.2 Relic Density Constraint

The first constraint taken into account is the compatibility of the neutralino annihilation cross section with the Relic Density obtained from WMAP. As discussed in Sect. 4.1.2 taking only the Relic Density constraint into account good solutions can be found by a simple variation of $\tan\beta$. This is because there is always a good solution in $\tan\beta$ for each arbitrary choice of A_0, which is exemplified in Fig. 4.22.
As mean for the χ^2 fit the mean of 3 years WMAP data and its experimental error have been taken [17]. The theoretical error of the Relic Density calculation is mainly caused by

QCD effects [109]. Concluding, the experimental value and its uncertainties are:

$$\Omega h^2 = 0.1131 \pm 0.0034 \pm 0.014. \tag{4.9}$$

4.2.3 $B_S \to \mu\mu$ Constraint

In the flavour physics sector of the SM there are many processes which do not appear at tree level but only in loop correction calculations. These processes are sensitive to new physics because the newly introduced particles can contribute to the loop corrections at the same order as SM particles. Furthermore, these measurements constrain SUSY models. An example for such a process is $B_S \to \mu\mu$ [64].
In the SM the cross section of the leptonic decays of B_s mesons are very small because they only occur trough penguin and box diagrams. Its value predicted by the SM is [136]:

$$Br(B_S \to \mu\mu)_{\text{SM}} = (3.2 \pm 1.5) \cdot 10^{-9} \tag{4.10}$$

which is more than ten times smaller than the discovery limit on this branching ratio so far [41]:

$$Br(B_S \to \mu\mu)_{\text{exp}} \leq 4.7 \cdot 10^{-8} \quad \text{95\% C.L.} \tag{4.11}$$

The additional SUSY contribution enhance the branching ratio by $\tan^6\beta$. The branching ratio of $B_S \to \mu\mu$ is given by[137, 138]:

$$\begin{aligned} Br(B_S \to \mu\mu) =& \frac{2\tau_B M_B^5}{64\pi} f_{B_s}^2 \sqrt{1 - \frac{4m_l^2}{M_B^2}} \\ & \left[\left(1 - \frac{4m_l^2}{M_B^2}\right) \left| \frac{(C_S - C'_S)}{(m_b + m_s)} \right|^2 + \left| \frac{(C_P - C'_P)}{(m_b + m_s)} + 2\frac{m_\mu}{M_{B_s}^2}(C_A - C'_A) \right|^2 \right], \end{aligned} \tag{4.12}$$

where M_B, τ_B and f_{B_s} are the mass, the life time and the form factor of the B meson, m_l is the lepton mass and C_S, C'_S, C_P, C'_P are the SUSY loop contributions. For large values of $\tan\beta$ the leading contribution to C_S is given by

$$\begin{aligned} C_S \simeq & \frac{G_F \alpha}{\sqrt{2}\pi} V_{tb} V_{ts}^* \left(\frac{\tan^3\beta}{4\sin^2\theta_W} \right) \left(\frac{m_b m_\mu m_t \mu}{M_W^2 M_A^2} \right) \\ & \frac{\sin 2\theta_{\tilde{t}}}{2} \left(\frac{m_{\tilde{t}_1}^2 \log\left[\frac{m_{\tilde{t}_1}^2}{\mu^2}\right]}{\mu^2 - m_{\tilde{t}_1}^2} - \frac{m_{\tilde{t}_2}^2 \log\left[\frac{m_{\tilde{t}_2}^2}{\mu^2}\right]}{\mu^2 - m_{\tilde{t}_2}^2} \right), \end{aligned} \tag{4.13}$$

where $\theta_{\tilde{t}}$ is the rotation angle between the two stop eigenstates and $m_{\tilde{t}_1/\tilde{t}_2}$ are the masses of the top squarks. The SUSY contribution proportional to the down-type fermion mass matrix. However, in the MSSM the formalism of quark mass creation is different to the one of SM. The MSSM contains two Higgs doublets: One coupling to the up-type quarks only and one coupling to the down-type quarks only. Thus flavour changing via charged Higgs bosons cannot occur at tree level but only at one-loop level because at this level a coupling of H_u to down-type fermions is induced. So the SUSY contribution to the branching ratio

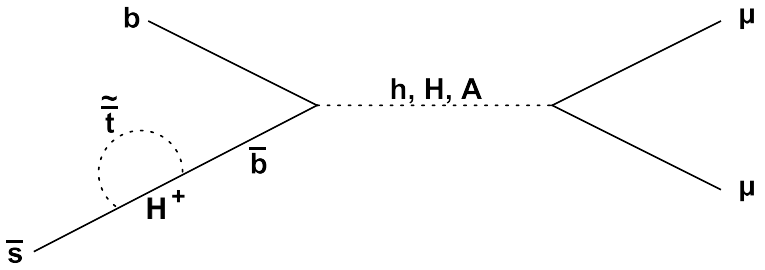

Figure 4.23: Main SUSY contribution to $B_S \to \mu\mu$: One of the two initial quarks changes its flavour via a squark loop and afterwards the two same flavour quarks annihilate to two muons.

is suppressed by a loop factor, which can be compensated by increased values of $\tan\beta$. Fig 4.23 represents such a diagram including a charged Higgs boson. Additional MSSM contributions come from diagrams, which are similar to the SM diagrams but with the SM particles replaced by their SUSY partners.

In Fig. 4.24 the branching fraction of $B_S \to \mu\mu$ is plotted for three different values of $\tan\beta$. The dark red areas correspond to values which are more or equal to the limit given in Eq. 4.11. Apparently, for small values of $\tan\beta$ the limit does not cause any χ^2 contribution. For high values of $\tan\beta$ the values conflict with the upper limit for small mass parameters. This affects the attempt to optimise $Br(B_S \to \mu^+\mu^-)$ and the Relic Density at the same time. The results for a optimisation via $\tan\beta$ with fixed A_0 = 0 GeV is given in Fig. 4.25. For very small scalar masses the optimisation works because the Relic Density prefers small values of $\tan\beta$. This is because in this region of parameter space the annihilation channel via sfermions is possible and therefore the branching ratios of processes including the pseudoscalar Higgs boson have to get smaller (compare Fig. 4.9).

For more moderate scalar masses the annihilation takes place via the pseudoscalar Higgs process. In this case the Relic Density constraint prefers high values of $\tan\beta$ while $B_S \to \mu\mu$ prefers small $\tan\beta$ for fixed values of A_0 = 0 GeV. The conflicting values of χ^2 are plotted for an example point (m_0 = 600 GeV, $m_{1/2}$ = 300 GeV) in the upper picture in Fig. 4.26. In the lower picture the two χ^2 values are plotted again for A_0 = 981 GeV. The conflict can be solved by a variation of A_0. The reason for this is that the branching ratio of $B_S \to \mu\mu$ is sensitive to A_0 because it depends on the top squark mass difference (eq. 4.13) while the Relic Density is not. This implies that the partial χ^2 can obtain a minimum for high values of A_0 like shown in Fig. 4.27. Here the χ^2 part of $B_S \to \mu\mu$ and Ωh^2 is plotted over $\tan\beta$ and A_0.

It can be ascertained that the partial χ^2 becomes larger for increasing $\tan\beta$, but it drops again if the values of A_0 are additionally driven to high values. Therefore by adding A_0 as additional variation parameter solutions for the whole m_0 - $m_{1/2}$ plane can be found.

This is demonstrated in Fig. 4.28. Additionally the resulting $\tan\beta$ and A_0 values are plotted. The values of $\tan\beta$ sometimes seem to jump. This is because at these points the second solution at the “right side“ of the A^0 resonance are chosen. Also in the previously excluded region (compare Fig. 4.25) solutions for the optimisation can be found for high values of A_0.

Concluding, if only the Relic Density and $B_S \to \mu\mu$ are used as constraints good solu-

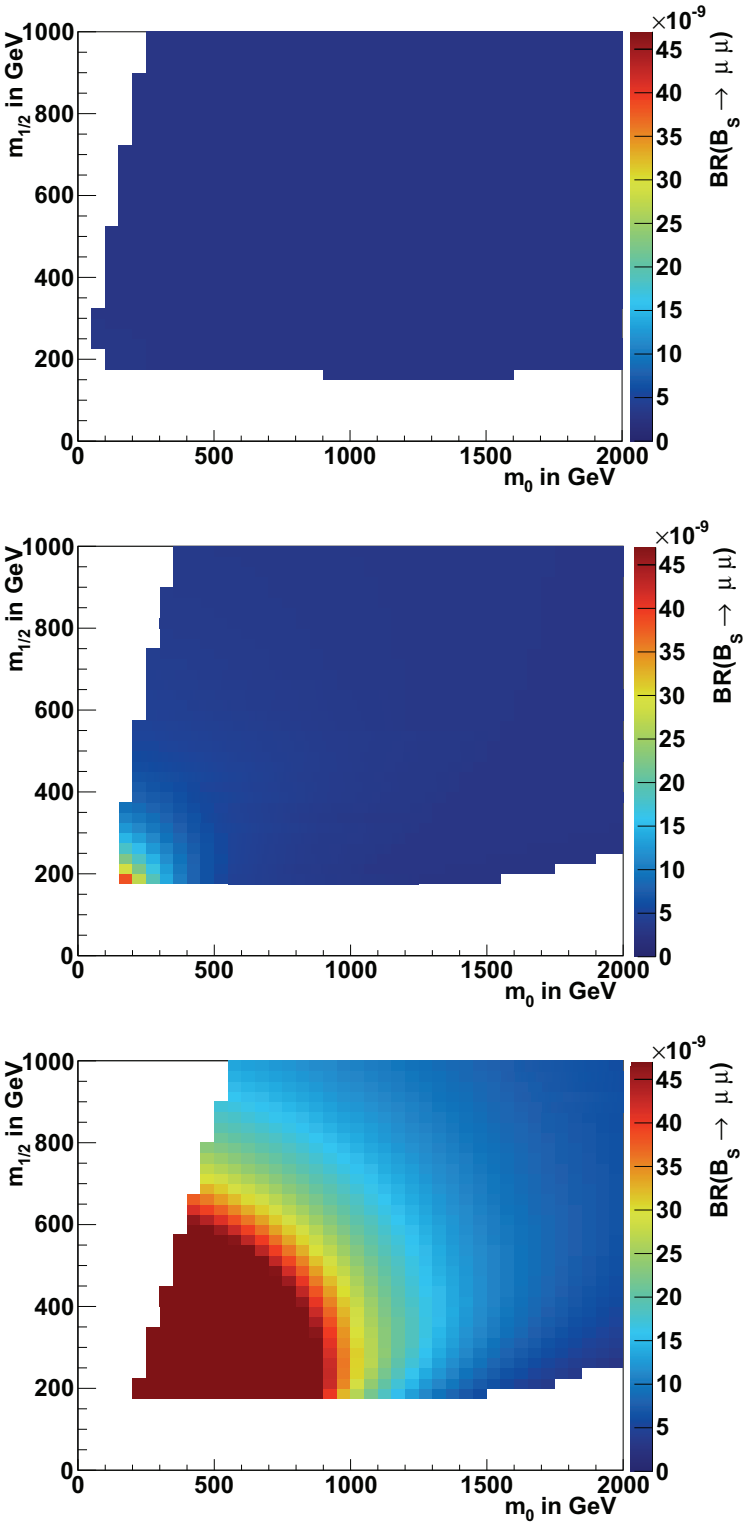

Figure 4.24: $Br(B_S \to \mu\mu)$ for $\tan\beta$ = 10 (top), 30 (middle), 50(bottom).

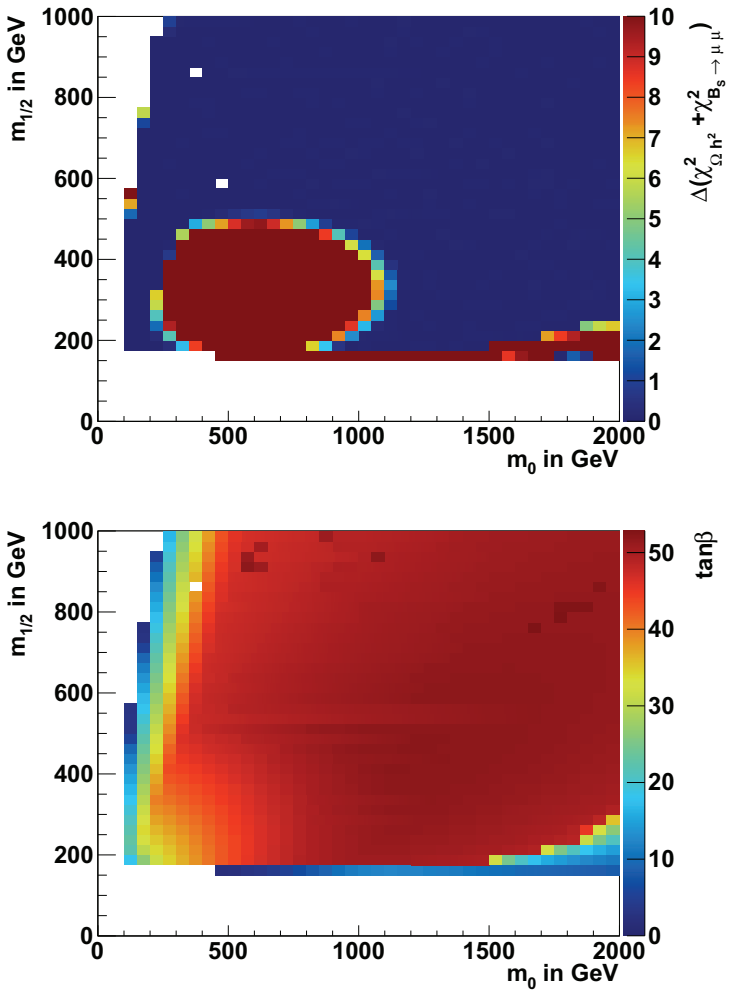

Figure 4.25: Results of the $\tan\beta$ adjustment on a combination of the WMAP and the $B_S \to \mu\mu$ constraint. Top: $\chi^2_{B_S\to\mu\mu} + \chi^2_{\Omega h^2}$. Bottom: Resulting values of $\tan\beta$.

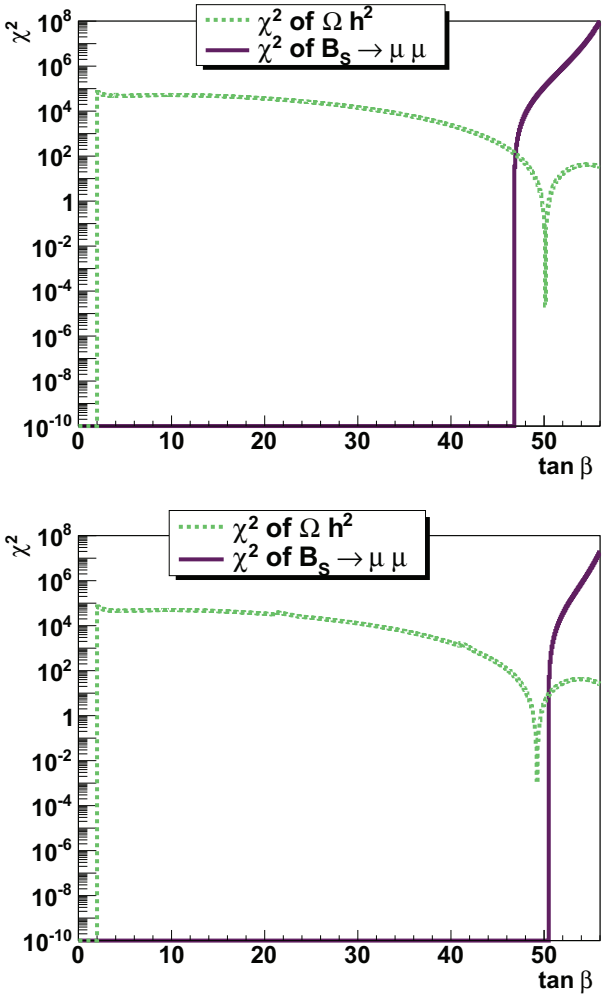

Figure 4.26: $\tan\beta$ dependence of $\chi^2_{B_S\to\mu\mu}$ and $\chi^2_{\Omega h^2}$ in comparison for A_0 = 0 GeV (top) and 981 GeV (bottom) at a point, where no solutions for a $\tan\beta$ adjustment with fixed A_0 = 0 GeV can be found: m_0 = 600 GeV, $m_{1/2}$ = 300 GeV.

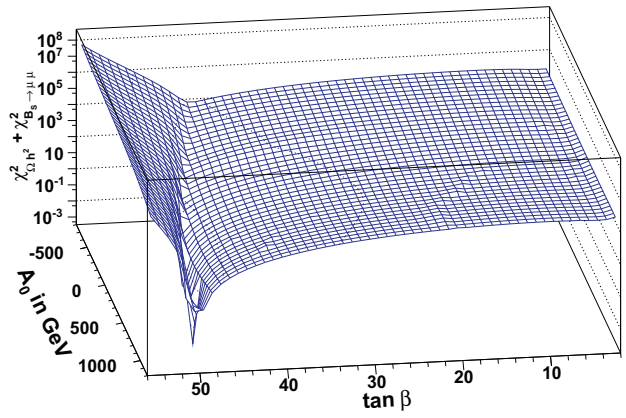

Figure 4.27: $\tan\beta$ and A_0 dependence of $\chi^2_{B_S\to\mu\mu} + \chi^2_{\Omega h^2}$. m_0 = 600 GeV, $m_{1/2}$ = 300 GeV.

tions can be found in the whole mass plane wherefore A_0 has to exceed high values for moderate values of m_0.

4.2.4 $b \to s\gamma$ Constraint

The SM contributions to the flavour changing process $b \to s\gamma$ only occur via tW^- loops. The SM branching ratio of this process is found to be [139]:

$$Br(b \to s\gamma)_{\text{SM}} = (3.15 \pm 0.23) \cdot 10^{-4}. \tag{4.14}$$

Experimentally, the branching ratio has been measured to be [140]:

$$Br(b \to s\gamma)_{\text{exp}} = (3.55 \pm 0.24 \pm 0.07) \cdot 10^{-4}. \tag{4.15}$$

which is slightly more than 1σ above the theoretical value.
In the MSSM such additional contributions come from the charged Higgs boson, from chargino-squark loops and likewise from neutralino-squark loops. Feynman diagrams of such processes are plotted in Fig. 4.29. Due to the fact that the SUSY processes are at the one-loop level (as well as the SM process) their contribution to the cross section should be in the same order of magnitude as the SM cross section. This gives a strong constraint on cMSSM models.
The branching ratio is proportional to $\mu A_t \tan\beta$. This behaviour is visualised in Fig. 4.30. Here the value of $Br(b \to s\gamma)$ has been plotted in the cMSSM mass parameter plane. Especially for the regions of low masses this yields a problem because the values of the branching ratio become very small for large values of $\tan\beta$. This is contrary to the fact that the Relic Density constraint prefers large values of $\tan\beta$ also for small (not tiny) mass parameters [64]. This conflict effects a one-dimensional optimisation process where only $\tan\beta$ becomes optimised while A_0 stay fixed (A_0 =0 GeV). An absence of solutions for small $m_{1/2}$ and small up to moderate values of m_0 is caused. The results of such an attempt can be seen in Fig. 4.31. The $\tan\beta$ values stay high because Ωh^2 accounts a much

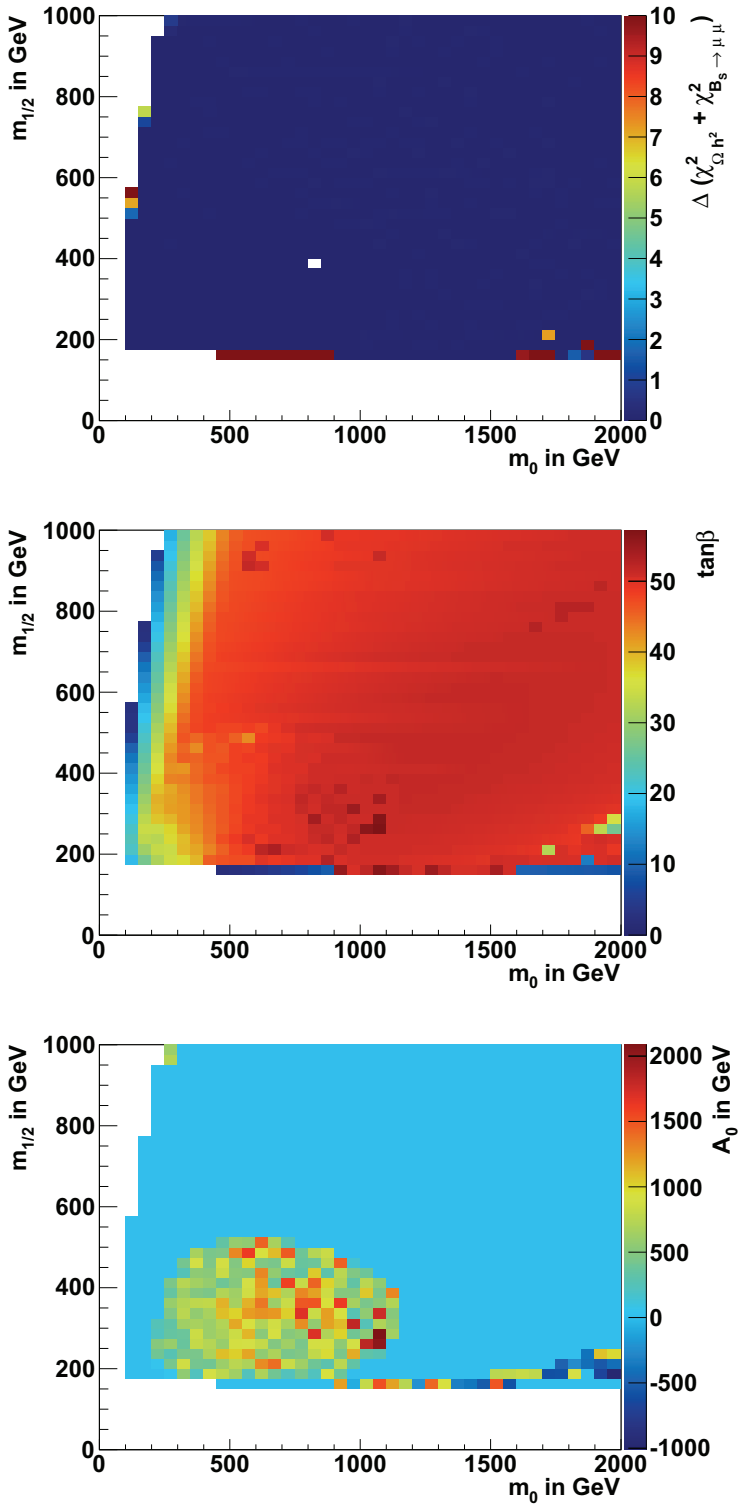

Figure 4.28: Results of two-dimensional $B_S \to \mu\mu$ optimisation: Here $\tan\beta$ and A_0 are adjusted to fit $B_S \to \mu\mu$ and the Relic Density constraint simultaneously. Upper plot: Resulting χ^2 values. Lower plots: resulting parameters $\tan\beta$ (middle) and A_0 (bottom).

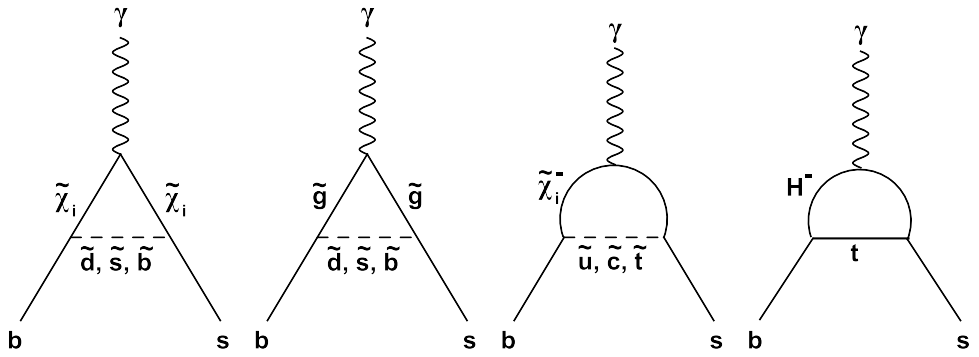

Figure 4.29: SUSY contributions to $b \to s\gamma$: Additional contributions to the SM cross section come from $\tilde{d}_i\tilde{\chi}^0_j$, $\tilde{d}_i\tilde{g}$, $\tilde{u}_i\tilde{\chi}^+_j$ and tH^-loops.

higher χ^2 contribution caused by the sharp increase in the neighbourhood of the minimum. A solution for this conflict in the choice of $\tan\beta$ ensues from the fact, that $Br(b \to s\gamma)$ also depends on A_0. Thus by the choosing high values of A_0 the conflict can be resolved at least for moderate mass parameters. The change with the choice of other values of A_0 is shown in Fig. 4.32 in comparison with the first plot of Fig. 4.30. In Fig. 4.32 $Br(b \to s\gamma)$ has been plotted for the lowest and the highest possible values of A_0 which are due to the Tachyon limit $-2 \cdot m_0$ and $3 \cdot m_0$. Beyond these values it is not ensured that all SUSY masses are positive, especially for tau squarks.
The preference of large values of A_0 is not in conflict with the the $B_S \to \mu\mu$ constraint. $Br(b \to s\gamma)$ favours slightly larger values of A_0 than needed for $B_S \to \mu\mu$ the χ^2.
The exact behaviour for a parameter point in the area which is just excluded in the one-dimensional fit is given in Fig. 4.33 (m_0 = 1000 GeV, $m_{1/2}$ = 400 GeV). The $\tan\beta$ dependence of the χ^2 contribution from $b \to s\gamma$ for four different A_0 values are shown: The A_0 value chosen in the one-dimensional optimisation (A_0 = 0 GeV), a moderate values (A_0 = 600 GeV), the A_0 preferred by $B_S \to \mu\mu$ (A_0 = 1217 GeV) and the A_0 value chosen by the final full optimisation(A_0 = 3000 GeV). Evidently, keeping in mind that high values of $\tan\beta$ are preferred by the Relic Density constraint large values of A_0 get a strong preference from the addition of the $b \to s\gamma$ constraint.
The enhancement of A_0 does not add to the χ^2 contribution of $B_S \to \mu\mu$, as shown in Fig. 4.34.
Finally, the two-dimensional optimisation shows the expected behaviour (Fig. 4.35). The excluded region can nearly be eliminated by the choice of very large A_0 values.

4.2.5 Δa_μ Constraint

The anomalous magnetic moment of the muon:

$$a_\mu = \frac{(g-2)_\mu}{2} \tag{4.16}$$

is sensitive to new physics. There is a difference of about three standard deviations between the measured and the calculated SM value [141–147]:

$$\Delta a_\mu = \left| a_\mu^{\text{exp}} - a_\mu^{\text{SM}} \right| = (30.2 \pm 8.8 \pm 2.0) \cdot 10^{-10}. \tag{4.17}$$

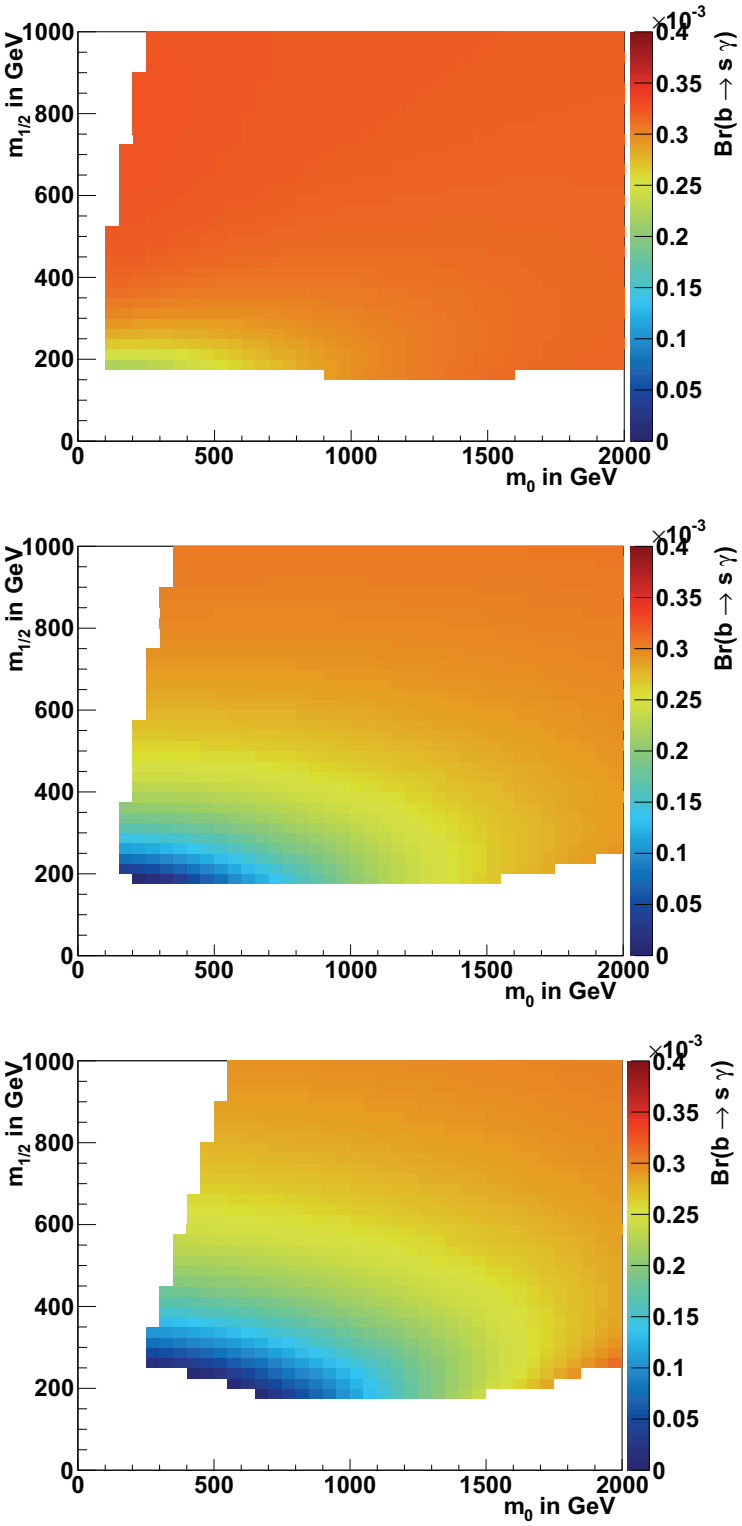

Figure 4.30: $Br(b \to s\gamma)$ for $\tan\beta$ = 10 (top), 30 (middle), 50(bottom). $A_0 = 0$ for all plots.

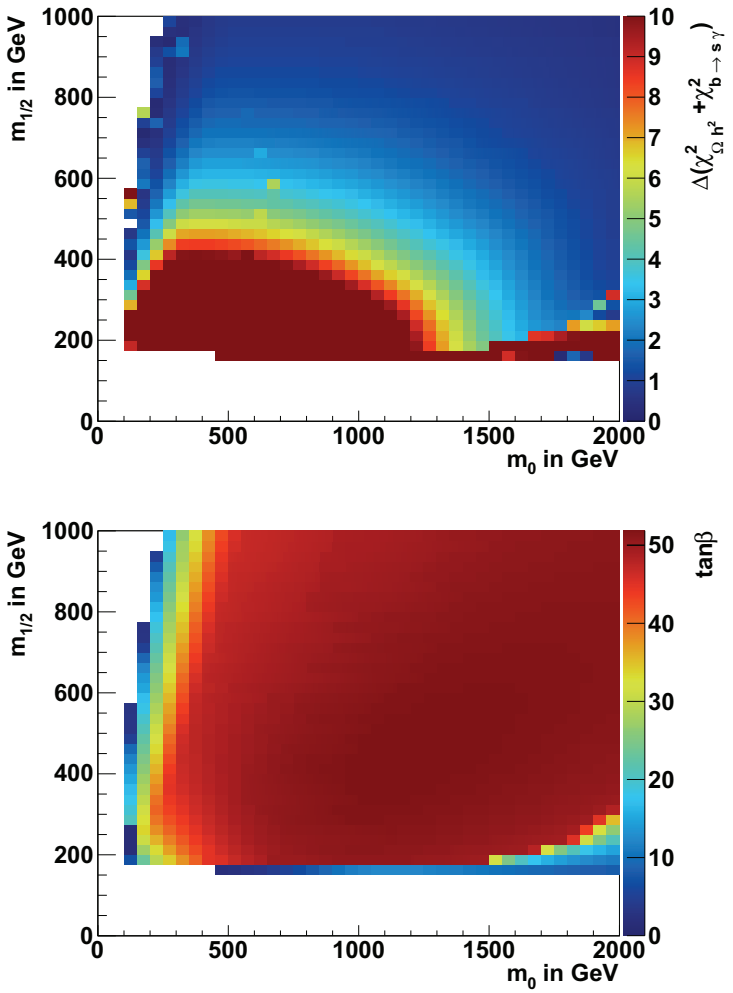

Figure 4.31: Results of the $\tan\beta$ adjustment on a combination of the WMAP and the $b \to s\gamma$ constraint. Top:$\chi^2_{b\to s\gamma} + \chi^2_{\Omega h^2}$. Bottom: Resulting values of $\tan\beta$.

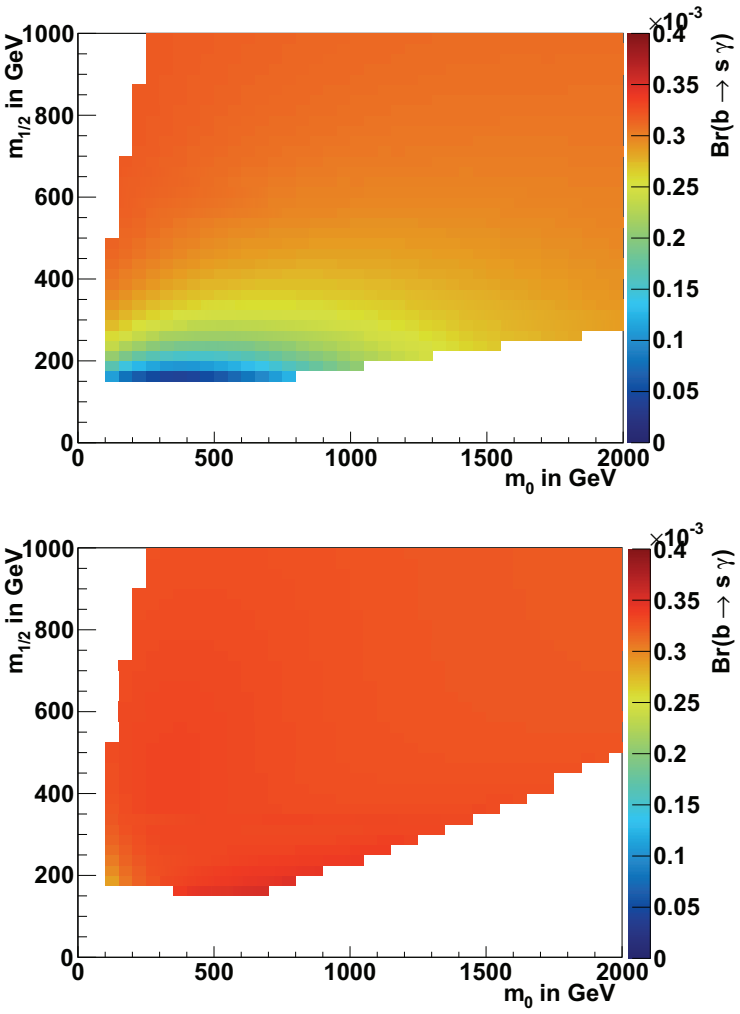

Figure 4.32: $Br(b \to s\gamma)$ for $\tan\beta$ = 10, lowest possible value of $A_0 = -2m_0$ (top) and the highest possible value $A_0 = 3m_0$(bottom). $\tan\beta = 10$ for both plots.

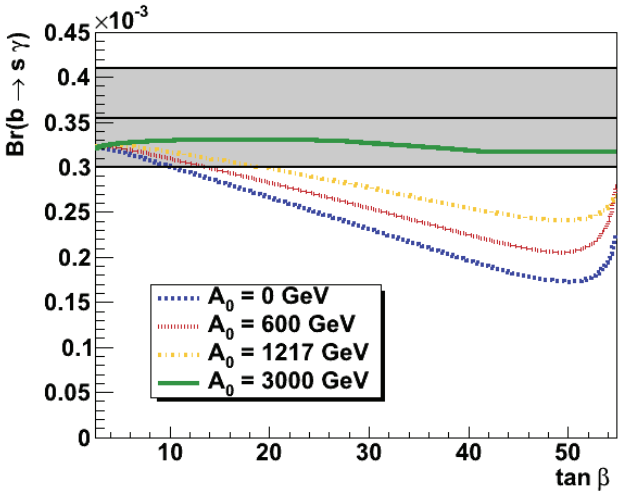

Figure 4.33: $\tan\beta$ dependence of partial $\chi^2_{b\to s\gamma}$ for m_0 = 1000 GeV, $m_{1/2}$ = 400 GeV The four different curves represent vanishing, moderate (600 GeV, 1217 GeV) and high (3000 GeV) values of A_0.

The MSSM can enhance Δa_μ by introducing new particles in the loops. For the magnetic moment of the muon particle combinations to be considered are chargino plus sneutrino and neutralino plus smuon. In Fig. 4.36 the Feynman diagrams of the first order loop corrections of such MSSM diagrams are given.
The change of the magnetic moment caused by SUSY processes can be expressed as:

$$\Delta a_\mu^{\text{SUSY}} \propto \frac{m_\mu^2 \mu M_i \tan\beta}{M^4_{\text{SUSY}}}, \tag{4.18}$$

where M_1 and M_2 are the gaugino masses and M_{SUSY} represents a characteristic sparticle mass from sparticles in the loop.
The experimental limit gives a strong constraint on cMSSM models because the corrections must be neither too small nor too large [64].
In Fig. 4.37 the values of Δa_μ have been plotted for different mass parameters and low (10), moderate (30) and high (50) values of $\tan\beta$. For small mass parameters Δa_μ obtains very high values due to the fact that the particles in the loops become light for these points. The branching ratio is proportional to $\tan\beta$ (Equation 4.18). Therefore it increases linearly with increasing $\tan\beta$. Additionally, for high values of $\tan\beta$ the area fitting the measured value gets expanded which is of great advantage for the scenarios chosen by the Relic Density constraint.
The results of a one-dimensional $\tan\beta$ adjustment to the Relic Density in combination with the anomalous magnetic moment constraint with fixed A_0 = 0 GeV are given in Fig. 4.38. For small mass parameters the χ^2 increases rapidly because of the low loop particle masses. Due to the fact that the low masses correspond to the region where the t-channel annihilation via sfermions contributes $\tan\beta$ can obtain moderate down to low values. This keeps the excluded region small. For moderate values of $\tan\beta$ Δa_μ just gets the right value. The decrease of Δa_μ for high mass parameters happens very slowly due to the

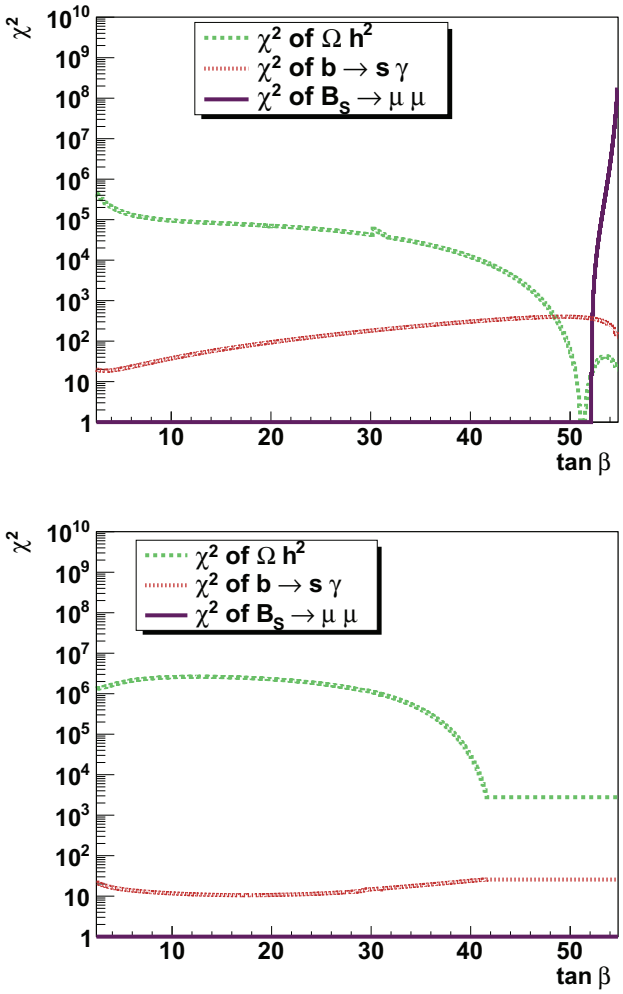

Figure 4.34: χ^2 contributions of Ωh^2, $Br(b \to s\gamma)$ and $Br(B_S \to \mu\mu)$ for m_0 = 600 GeV, $m_{1/2}$ = 400 GeV. Top: A_0 = 906 GeV, Bottom: A_0 = 1670 GeV.

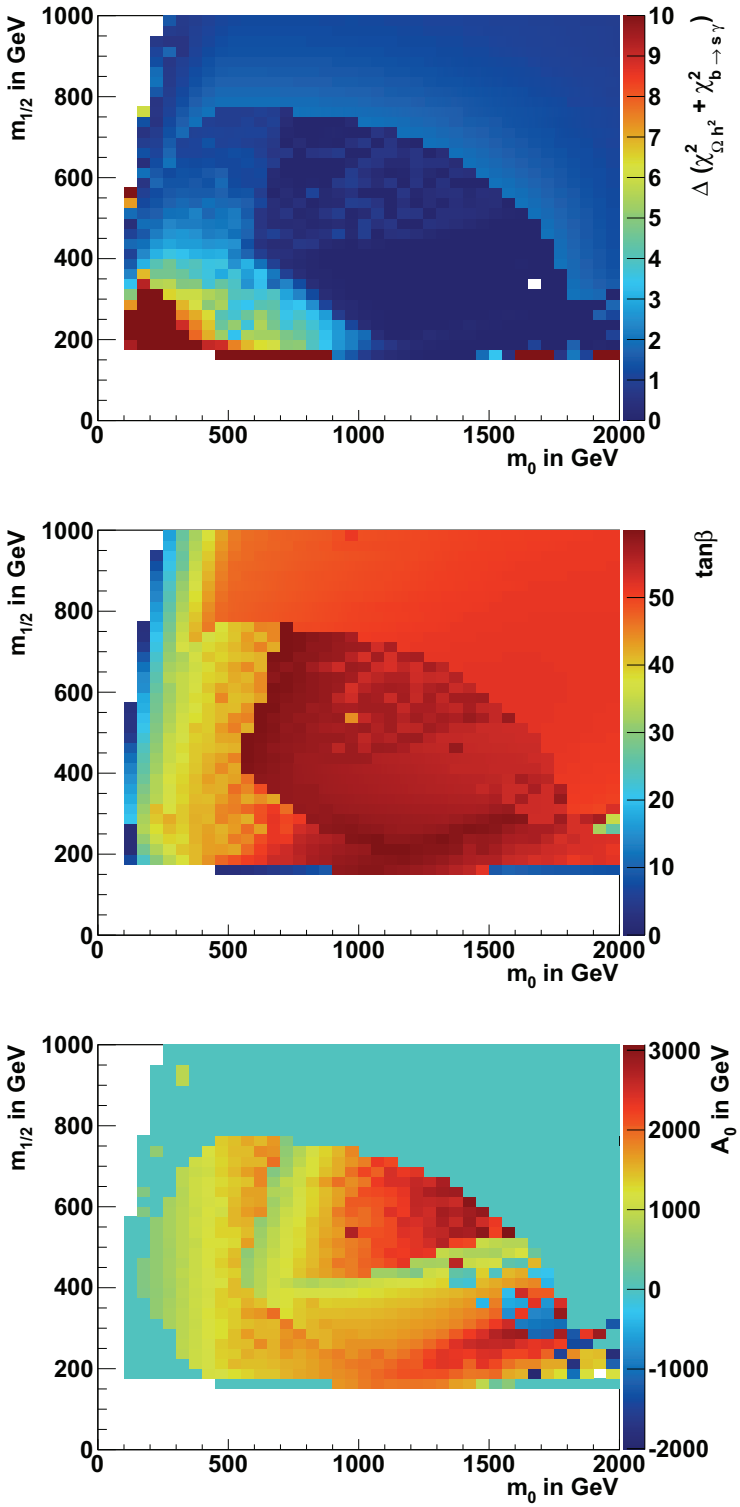

Figure 4.35: Results of two-dimensional $b \to s\gamma$ optimisation: Here $\tan\beta$ and A_0 are adjusted to fit $b \to s\gamma$ and the Relic Density constraint simultaneously. Upper plot: Resulting χ^2 values. Lower plots: resulting parameters $\tan\beta$ (middle) and A_0 (bottom).

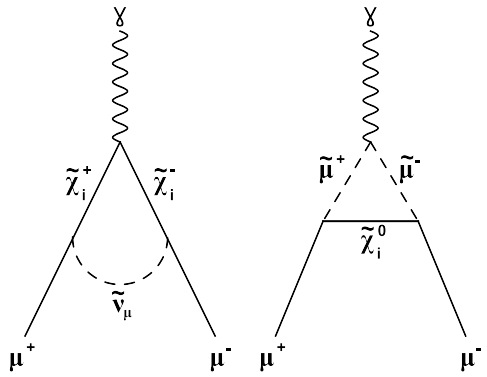

Figure 4.36: SUSY corrections to the anomalous magnetic moment of the muon: The newly introduced particles appear as virtual particles in the loop. First diagram: chargino-sneutrino correction. Second diagram: neutralino-smuon correction. The indices run over all neutralino and chargino generations.

preference of high $\tan\beta$ values in this region and due to the fact that Δa_μ is proportional to $1/M^4_{\text{SUSY}}$.

The question whether an additional adjustment of A_0 helps finding solutions again is answered by Fig. 4.39. Here the $\tan\beta$ and A_0 dependence of $\chi^2_{\Omega h^2} + \chi^2_{\Delta a_\mu}$ at a point, where the $\tan\beta$ adjustment produces moderate χ^2 values has been exemplified. It stands out that Δa_μ is not very sensitive to A_0 and can thus not be improved by an additional adjustment of A_0.

This preconception can be confirmed by the results of a two-dimensional adjustment given in Fig. 4.40. For low values of $m_{1/2}$ jumps in $\tan\beta$ catch the eye of the beholder. These correspond to the two Relic Density solutions around the A^0 resonance. These two solutions are of equal physical significance. Therefore this behaviour does not have to be further examined.

The fact that Δa_μ cannot be further improved implicates that this variable contributes most to the χ^2 function if all constraints get combined especially in the regions of high masses. Thus Δa_μ is the most discriminating constraint in this analysis.

4.2.6 $\mathrm{B}^+ \to \tau^+\nu_\tau$ Constraint

In the SM the branching ratio of the decay channel $B^+ \to \tau^+\nu_\tau$ is calculated from penguin and box diagrams to be

$$Br\left(B_u \to \tau^-\nu_\tau\right)_{\text{SM}} = \frac{G_F^2 m_B m_\tau^2}{8\pi}\left(1 - \frac{m_\tau^2}{m_B^2}\right) f_N^2 \left|V_{ub}\right|^2 \tau_B,$$

where G_F is the Fermi constant, m_B and τ_B the mass and lifetime of the B meson, m_τ the mass of the τ-lepton, V_{ub} the CKM matrix element of the process and f_B the form factor of the B meson [148]. Assuming the CKM element and the form factor as given in [149] the SM branching ratio is calculated as

$$Br\left(B_u \to \tau^-\nu_\tau\right)_{\text{SM}} = (1.17 \pm 0.28) \cdot 10^{-4}$$

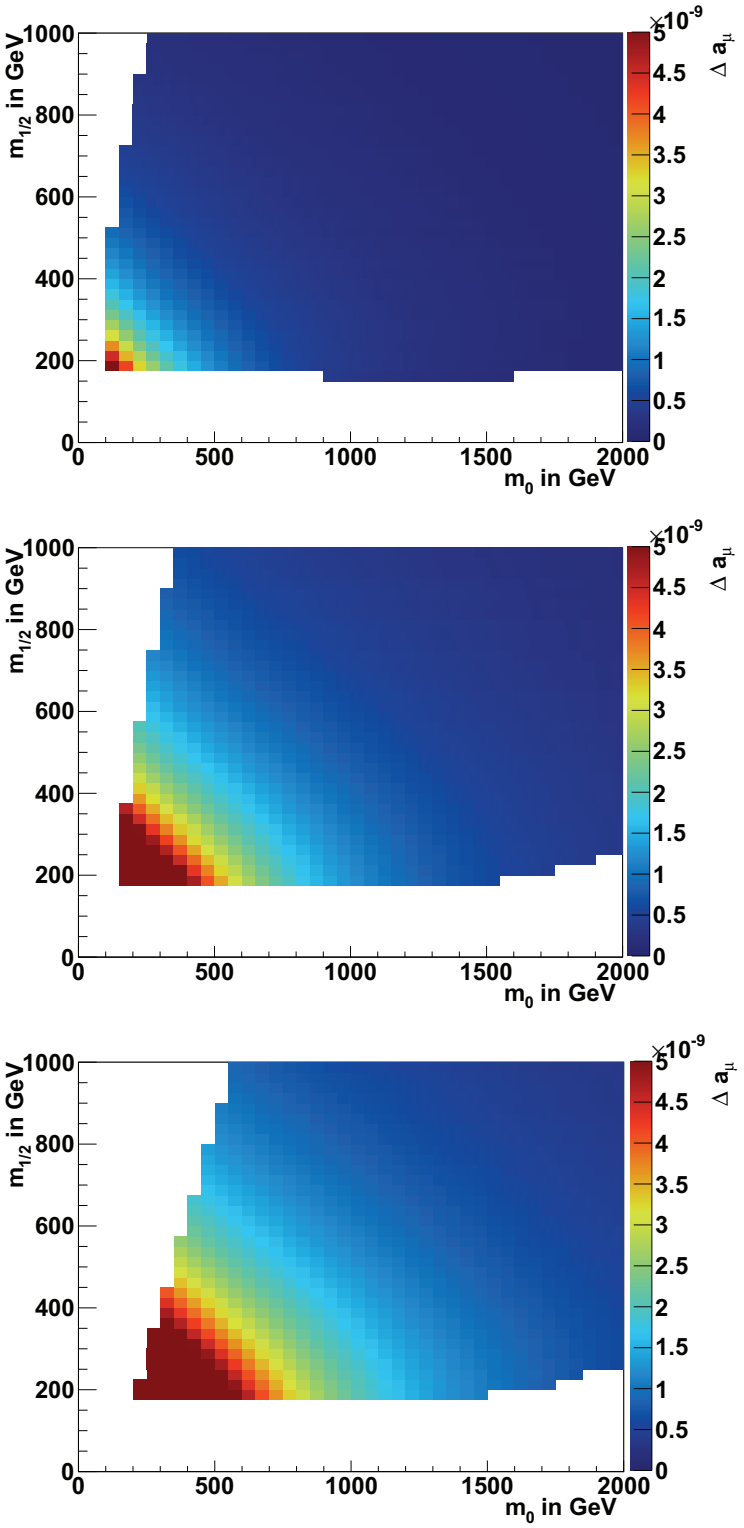

Figure 4.37: Δa_μ for $\tan\beta$ = 10 (top), 30 (middle), 50(bottom).

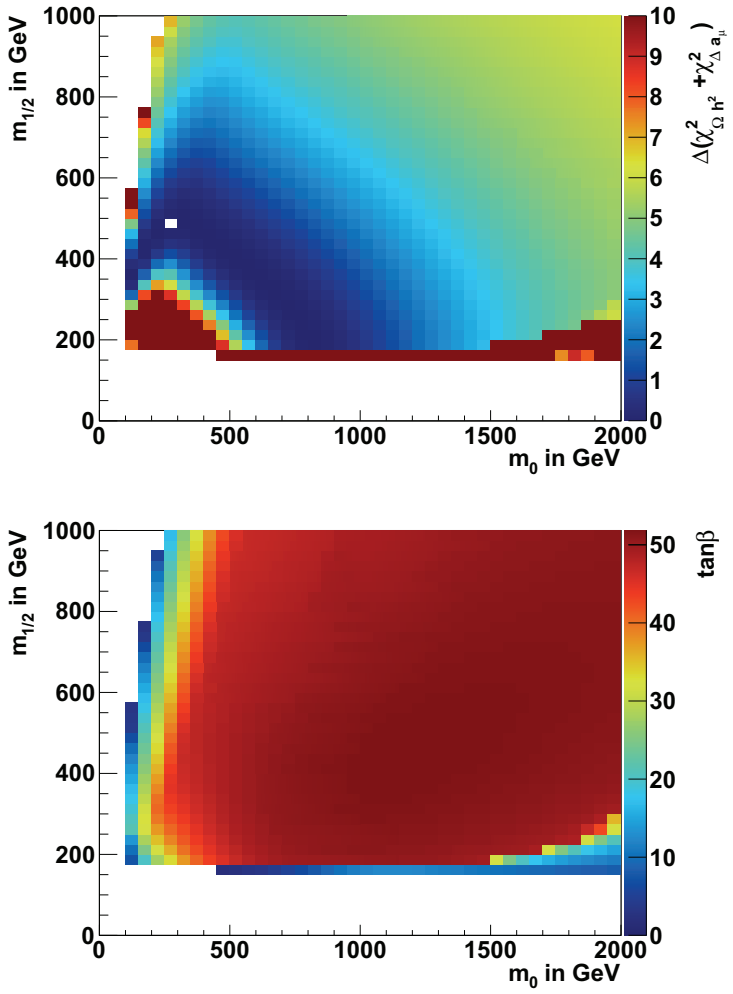

Figure 4.38: Results of the $\tan\beta$ adjustment on a combination of the WMAP and the anomalous magnetic muon constraint. Top: $\chi^2_{\Delta a_\mu} + \chi^2_{\Omega h^2}$. Bottom: Resulting values of $\tan\beta$.

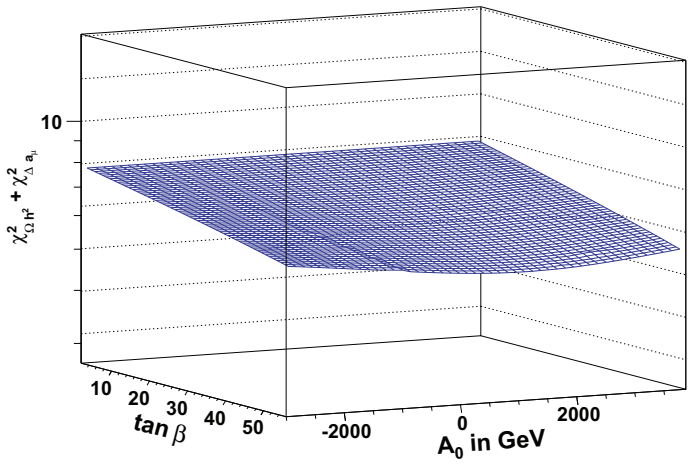

Figure 4.39: $\tan\beta$ and A_0 dependence of partial χ^2: point with too low $g-2$ value (m_0 = 1800 GeV, $m_{1/2}$ = 800 GeV).

for the input values given in A.5. In SUSY additional contributions to the branching ratio come from the charged Higgs boson. The contribution of the weak gauge bosons and the charged Higgs boson interfere destructively. Thus in general SUSY lowers the cross section of this decay. The ratio between the SUSY value and the SM value of the branching ratio can be calculated as:

$$R_{B\tau\nu} = \frac{Br\left(B_u \to \tau^- \nu_\tau\right)_{\text{SUSY}}}{Br\left(B_u \to \tau^- \nu_\tau\right)_{\text{SM}}} = \left(1 - \left(\frac{m_B^2}{m_{H^\pm}^2}\right) \cdot \frac{\tan^2\beta}{1+\epsilon_0 \tan\beta}\right)^2, \tag{4.19}$$

where ϵ_0 is the effective coupling [148]. Experimental measurements show, that this ratio should be[41, 149]:

$$R_{B\tau\nu} = 1.43 \pm 0.44 \tag{4.20}$$

with the inputs given in A.5. The problem with this constraint is that the experiments postulate a value close to or even higher than the SM value, while SUSY contributions lead to a lower value. In Fig. 4.41 the value of $R_{B\tau\nu}$ is plotted for small, moderate and large values of $\tan\beta$. For small values of $\tan\beta$ the ratio is close to the SM ratio. For large values of $\tan\beta$ the ratio drops for small mass parameters.

This conflicts with the Relic Density constraint which postulates a high $\tan\beta$ value, as demonstrated in Fig. 4.38. Here the χ^2 contributions of Ωh^2 and $B^+ \to \tau\nu$ are displayed. It shows that the $\tan\beta$ value preferred by Ωh^2 is nearly the maximum point for the χ^2 contribution of $B^+ \to \tau\nu$. The χ^2 contributions of $B^+ \to \tau\nu$ are not high due to the large theory and measurement uncertainty.

The conflict between Ωh^2 and $B^+ \to \tau^+\nu_\tau$ appears in the one-dimensional optimisation. The results of this $\tan\beta$ adjustment are shown in Fig. 4.43. Here a region for low $m_{1/2}$ is barely excluded. This time the conflict between the constraints cannot be resolved by the choice of high A_0, because $\chi^2_{B^+\to\tau\nu}$ in most cases prefers negative values of A_0. This is shown in Fig. 4.44. Here, $\chi^2_{\Omega h^2} + \chi^2_{B^+\to\tau\nu}$ has been plotted. The two-dimensional optimisation results are shown in Fig. 4.45. In most cases the problem gets circumvented by

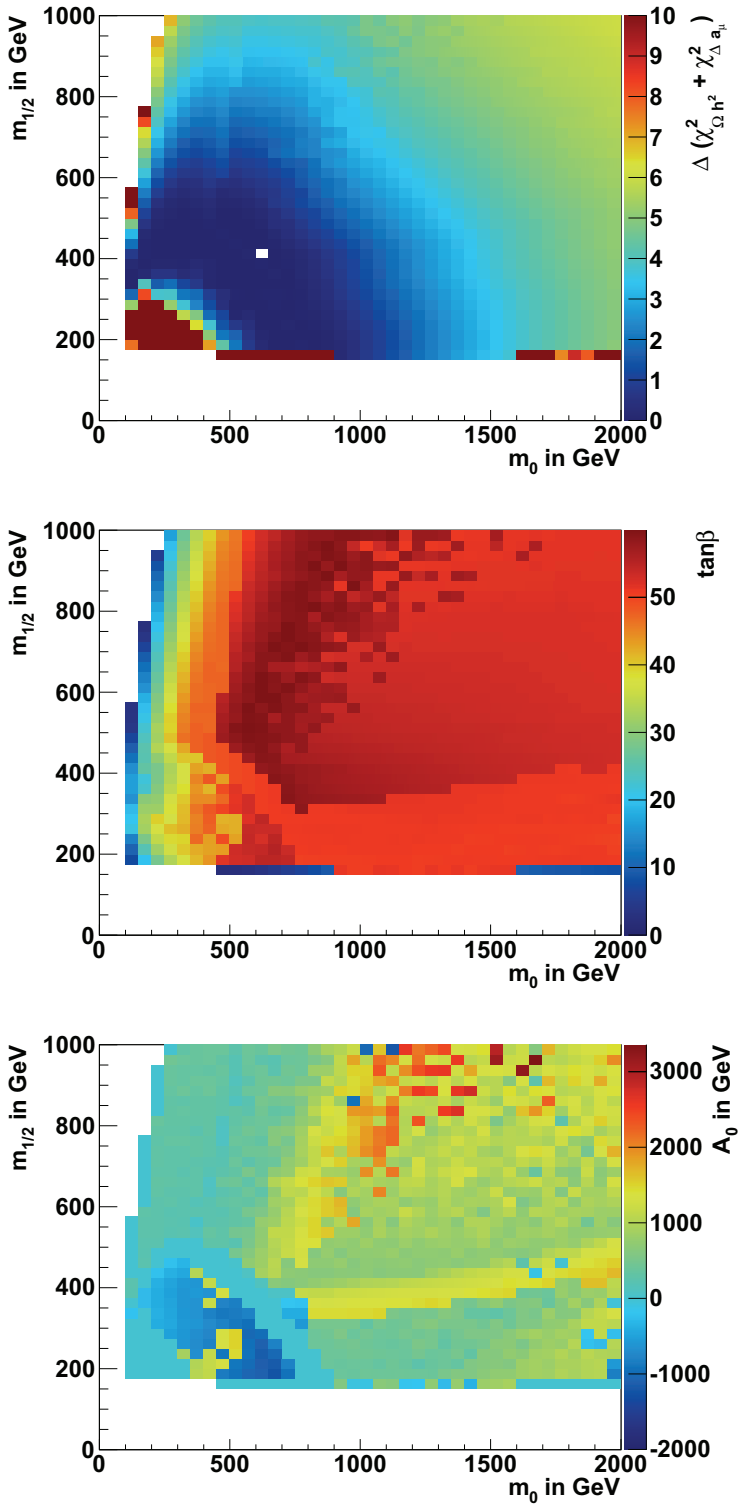

Figure 4.40: Results of two-dimensional Δa_μ optimisation: Here $\tan\beta$ and A_0 are adjusted to fit the anomalous magnetic moment of the muon and the Relic Density constraint simultaneously. Upper plot: Resulting χ^2 values. Lower plots: resulting parameters $\tan\beta$ (middle) and A_0 (bottom)

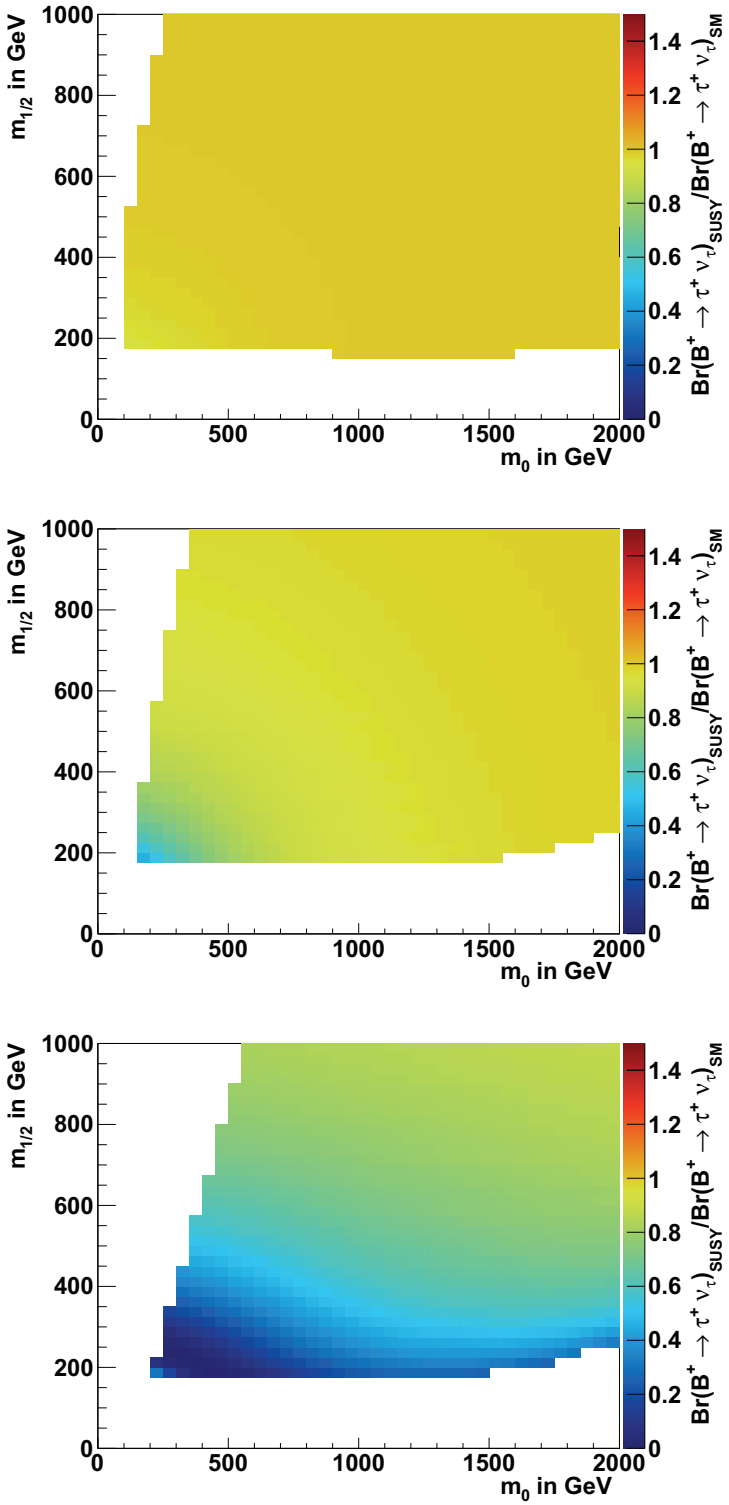

Figure 4.41: $R_{B\tau\nu}$ for $\tan\beta$ = 10 (top), 30 (middle), 50(bottom).

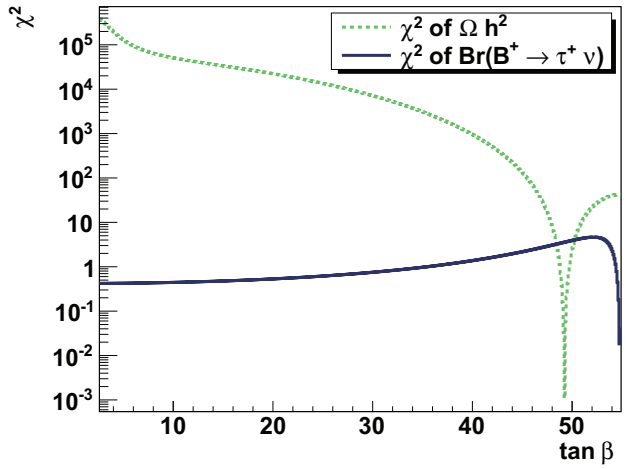

Figure 4.42: $\tan\beta$ dependence of partial $\chi^2_{B^+\to\tau\nu}$ to $\chi^2_{\Omega h^2}$ for m_0 = 600 GeV, $m_{1/2}$ = 200 GeV .

the choice of moderate negative values of A_0, which is in conflict with other constraints. Therefore in a general optimisation the $B^+ \to \tau^+\nu_\tau$ constraint is not expected to become perfectly optimised especially due to the choice of high values of $\tan\beta$ by the Relic Density constraint. However, the uncertainties on the $B^+ \to \tau^+\nu_\tau$ constraint are large and therefore it does not contribute significantly to the total χ^2. Concluding, in the combination of all constraints $B^+ \to \tau^+\nu_\tau$ is expected to add additional small χ^2 contributions for small values of $m_{1/2}$, which is caused by the low Higgs masses due to the Relic Density constraint in this region.

4.2.7 Higgs Mass Constraint

The Higgs boson is the last particle missing in the SM. Thus one of the main goals of the electron-positron collider LEP[1] was the search for the SM Higgs boson. However, it has not be found and therefore an exclusion limit could be determined, which is [89]:

$$m_h > 114.4 \pm 0.9 \pm 1.4 \text{ GeV}. \tag{4.21}$$

Evidently, the uncertainty is dominated by the theoretical error.
In SUSY models the lightest Higgs boson is due to its nature comparable with the SM Higgs boson and the limit obtained at LEP can be applied directly to this particle. Due to the theoretical upper limitation of the lightest SUSY Higgs boson (see Sect. 2.2.4) the Higgs mass limitation around 160 GeV from Tevatron does not have to be accounted in the analysis.
In Fig. 4.46 The results of a two-dimensional parameter adjustment to the relic denisty and Higgs mass constraint. The result is that a region for small up to moderate values of the mass parameters can be excluded by Higgs mass measurements.

[1] Large Electron Positron Collider.

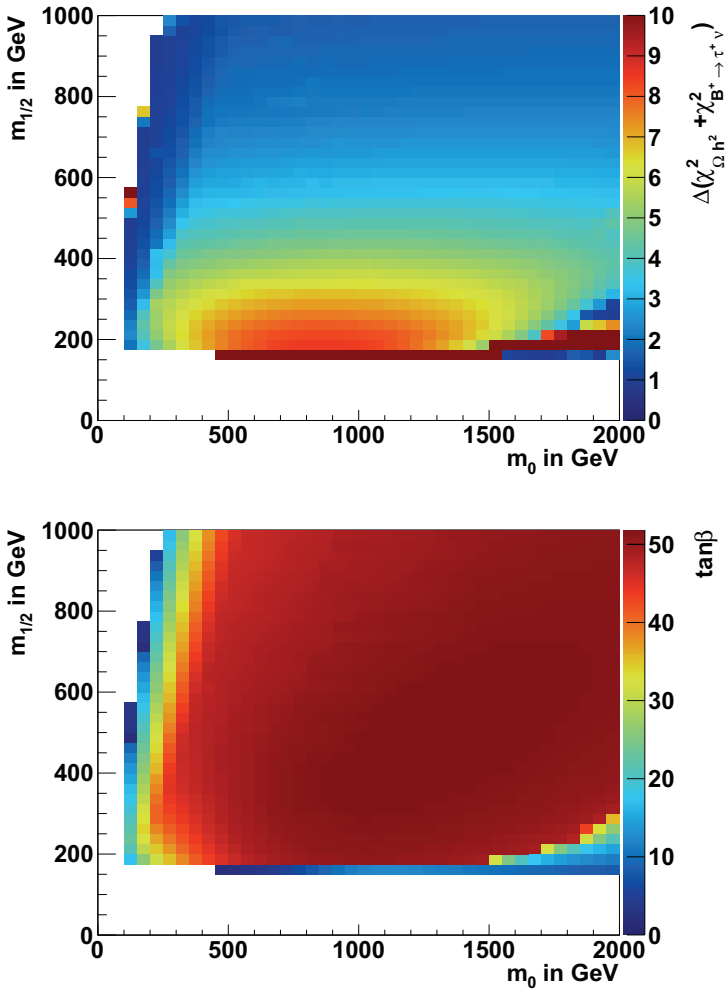

Figure 4.43: Results of one-dimensional partial $\tan\beta$ adjustment. Top: $\chi^2_{B\to\tau\nu} + \chi^2_{\Omega h^2}$. Bottom: Resulting values of $\tan\beta$.

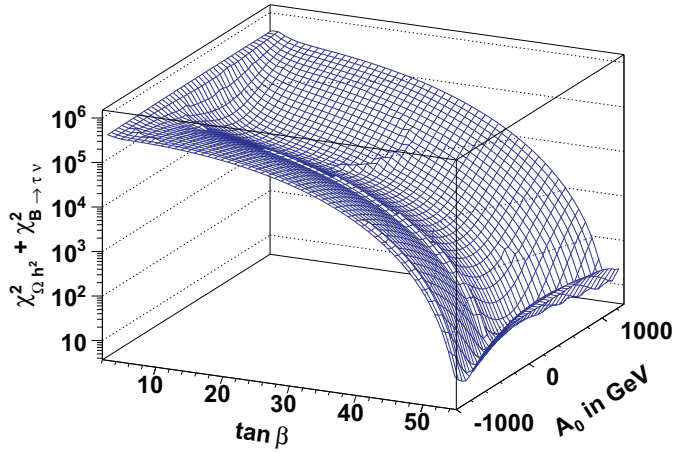

Figure 4.44: $\tan\beta$ and A_0 dependence of partial $\chi^2_{\Omega h^2} + \chi^2_{B^+\to\tau\nu}$ for m_0 = 600 GeV, $m_{1/2}$ = 200 GeV.

Constraint	mean value	linear error	quadratic error
Ωh^2	0.1131	0.0174	0.0144
$Br(b \to s\gamma)$	355·10^{-6}	54·10^{-6}	34·10^{-6}
Δa_μ	30.2·10^{-10}	10.8·10^{-10}	9.0·10^{-10}
$Br(B_s \to \mu\mu)$	$<$4.7·10^{-8}		
m_h in GeV	$>$114.4	2.4	1.7

Table 4.1: Combined errors of the constraints included in the current analysis.

4.2.8 Treatment of the errors

The combination of the theoretical and the experimental error are an important matter in a χ^2 fit because the error effects the different χ^2 terms quadraticly. In general there are two possibilities of combining the errors:

- quadraticly, as $\sigma = \sqrt{\sigma^2_{\text{theory}} + \sigma^2_{\text{experiment}}}$ for Gaussian distributed variables
- linearly, as $\sigma = \sigma_{\text{theory}} + \sigma_{\text{experiment}}$ for other variables.

Tab. 4.1 shows the resulting combined errors. The result is a larger χ^2 term for the quadratic error combination. Especially for $Br(b \to s\gamma)$ the difference between the two error calculations is large.
As shown in Tab. 4.2 the quadratic error combination raises the $\Delta\chi^2$ by a factor of two compared to the linear combination. The largest difference occurs in areas dominated by the $b \to s\gamma$ constraint, which leads to an additional exclusion of points for quadratic error combination as shown in Fig. 4.47. Here the allowed area for linear and quadratic error combination are shown.
To keep the exclusion as conservative as possible the errors are added linearly.

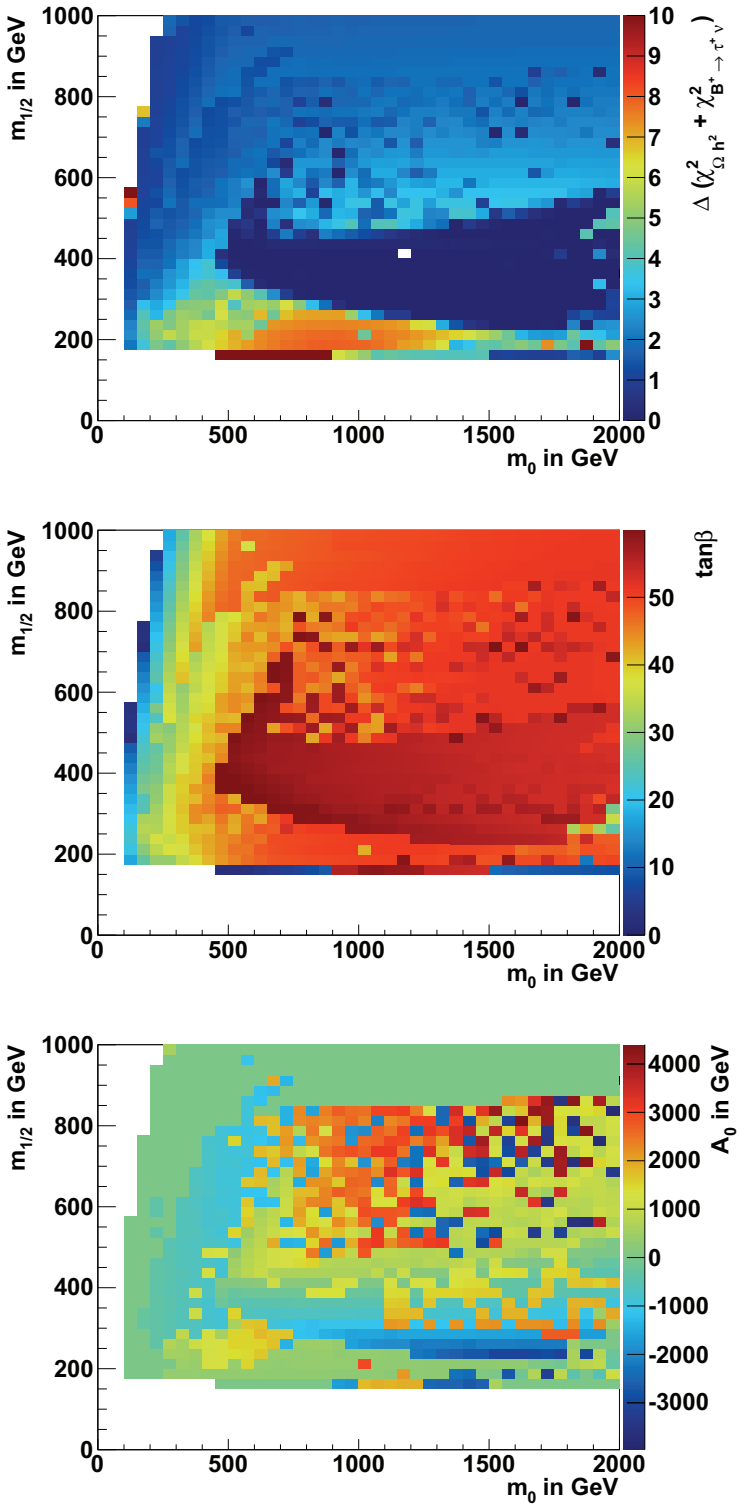

Figure 4.45: Results of two-dimensional $B^+ \to \tau^+\nu_\tau$ optimisation: Here $\tan\beta$ and A_0 are adjusted to fit $B^+ \to \tau^+\nu_\tau$ and the Relic Density constraint simultaneously. Upper plot: Resulting χ^2 values. Lower plots: Resulting parameters of $\tan\beta$ (middle) and A_0 (bottom).

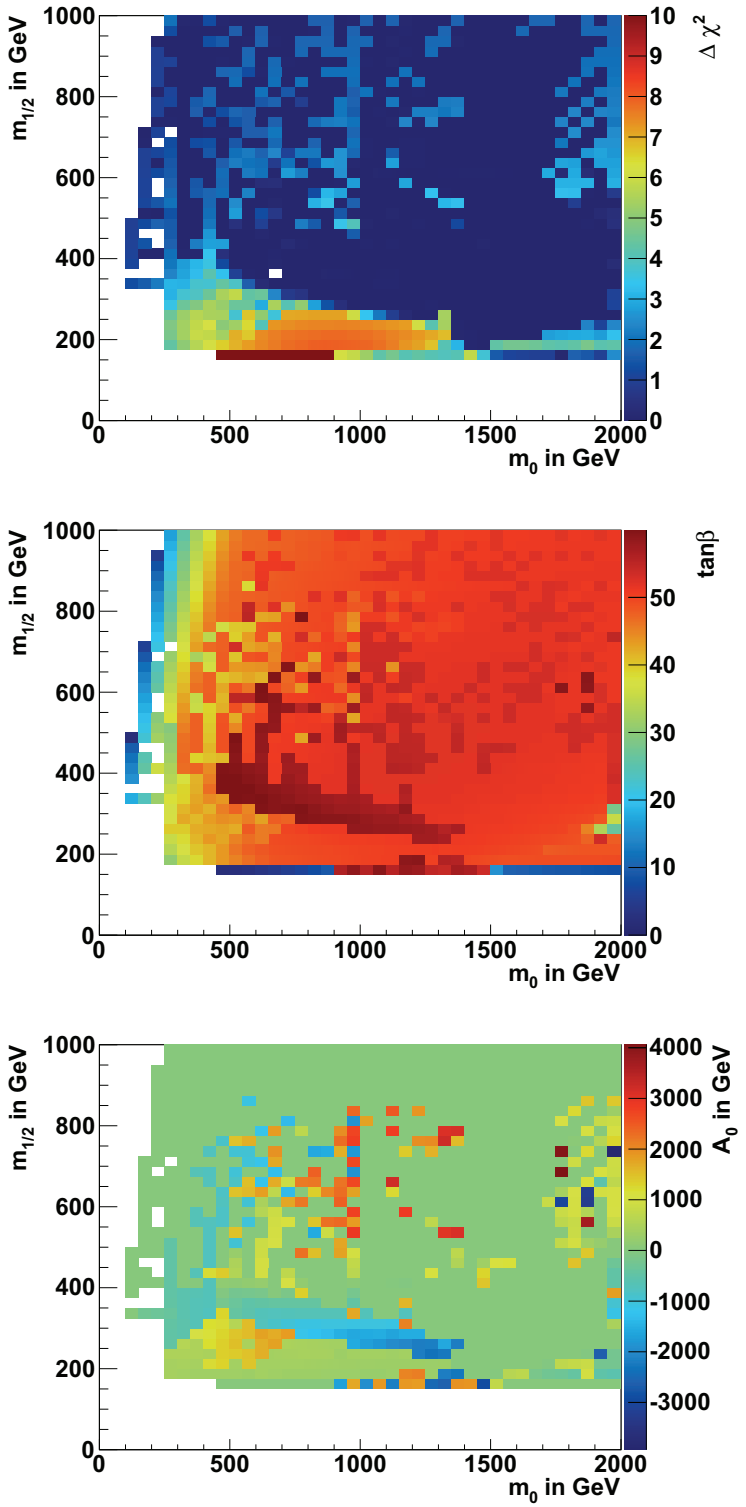

Figure 4.46: Results of two-dimensional m_h optimisation: Here $\tan\beta$ and A_0 are adjusted to fit m_h and the Relic Density constraint simultaneously. Upper plot: Resulting χ^2 values. Lower plots: resulting parameters $\tan\beta$ (middle) and A_0 (bottom).

m_0 in GeV	$m_{1/2}$ in GeV	χ^2, linear	χ^2, quadratic
100	200	23.2	42.7
100	400	3.3	5.5
200	775	6.2	8.2
1000	500	7.3	10.5
1800	350	10.3	14.1
1900	200	9.4	12.8
1900	900	8.4	10.7

Table 4.2: Resulting χ^2 for linear and quadratic error combination.

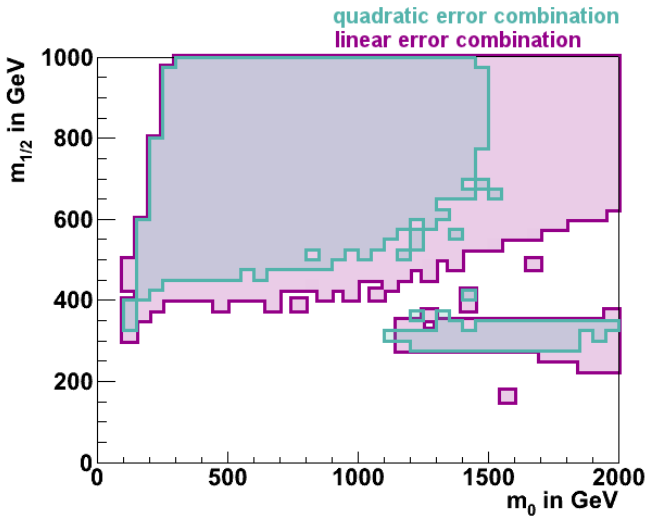

Figure 4.47: Comparison of linearly and quadraticly combined errors: Magenta and cyan area allowed at 95% C.L. Magenta area: Using linear error combination. Cyan area: Using quadratic error combination.

m_0 in GeV	$m_{1/2}$ in GeV	$\tan\beta$	A_0 in GeV	χ^2
100	200	8.4	-195.8	23.2
100	400 (BFP)	14.7	134.2	3.3
200	775	18.7	394.5	6.2
1000	500	44.3	2854.9	7.3
1800	350	50.4	593.7	10.3
1900	200	48.9	889.0	9.4
1900	900	51.9	857.6	8.4

Table 4.3: Resulting χ^2 for whole fit. The resulting $\tan\beta$ and A_0 values are listed in the third and fourth column.

4.2.9 Combination of all constraints

After understanding the dependence of the included constraints on the parameters everything can be combined. The results of such a minimisation are shown in Fig. 4.48.
Tab. 4.3 shows some characteristic points. To identify which constraint is responsible for which exclusion the χ^2 contribution of the different constraints have been used to identify an exclusion region for each individual constraint. The results of this procedure are shown in Fig. 4.49 (different light coloured areas). Furthermore, Tab. 4.4 shows the χ^2 contributions of the different constraints for the same points given in Tab. 4.3. $B_s \to \mu\mu$ does not exclude anything because A_0 can always be adjusted in a way to fit a value below the given upper limit. The left region (white area in upper plot) can be compared to the area left after applying the minimisation on all constraints in combination (magenta area in lower plot).
In general the partial exclusion curves cover the excluded region of the combined fit very well. Close to the partial exclusion areas there is an area which is excluded by the general fit but not by the partial ones. Tab. 4.5 shows the different χ^2 contributions for two neighbour points such that one is located in this region and the other in a partial exclusion region. It can be recognised that all constraints give small contributions, but the sum is large enough to exclude these points.
An eye-catching thing in the results of the scan is the fact that for high values of m_0 the allowed area is divided into two islands. This effect appears because of the high values of $\tan\beta$ favoured all constraints but $B \to \tau\nu$. The high values cause the contribution of $B^+ \to \tau^+\nu_\tau$ to grow very fast with increasing values of $m_{1/2}$. Meanwhile, the χ^2 contribution of the Relic Density grows more moderately. This is because the higher $\tan\beta$ the more sensitive $Br(B^+ \to \tau^+\nu_\tau)$ for mass changings (compare equation 4.19). The Relic Density Ωh^2 dominates the minimisation due to its small uncertainty compared to $B^+ \to \tau^+\nu_\tau$.
The best-fit point of the minimisation is found at m_0 = 100 GeV, $m_{1/2}$ = 400 GeV at $\tan\beta$ = 14.7 and A_0 = 134.2 GeV. The low χ^2 value of 3.2 is caused by the low value of $\tan\beta$ which can be obtained because at this point the leading DM annihilation channel is stau co-annihilation.
Knowing the χ^2 value of the best-fit point the $\Delta\chi^2$ value for each point in the mass plane can be calculated as:

$$\Delta\chi^2 = \chi^2_{\text{tot}} - 3.23. \tag{4.22}$$

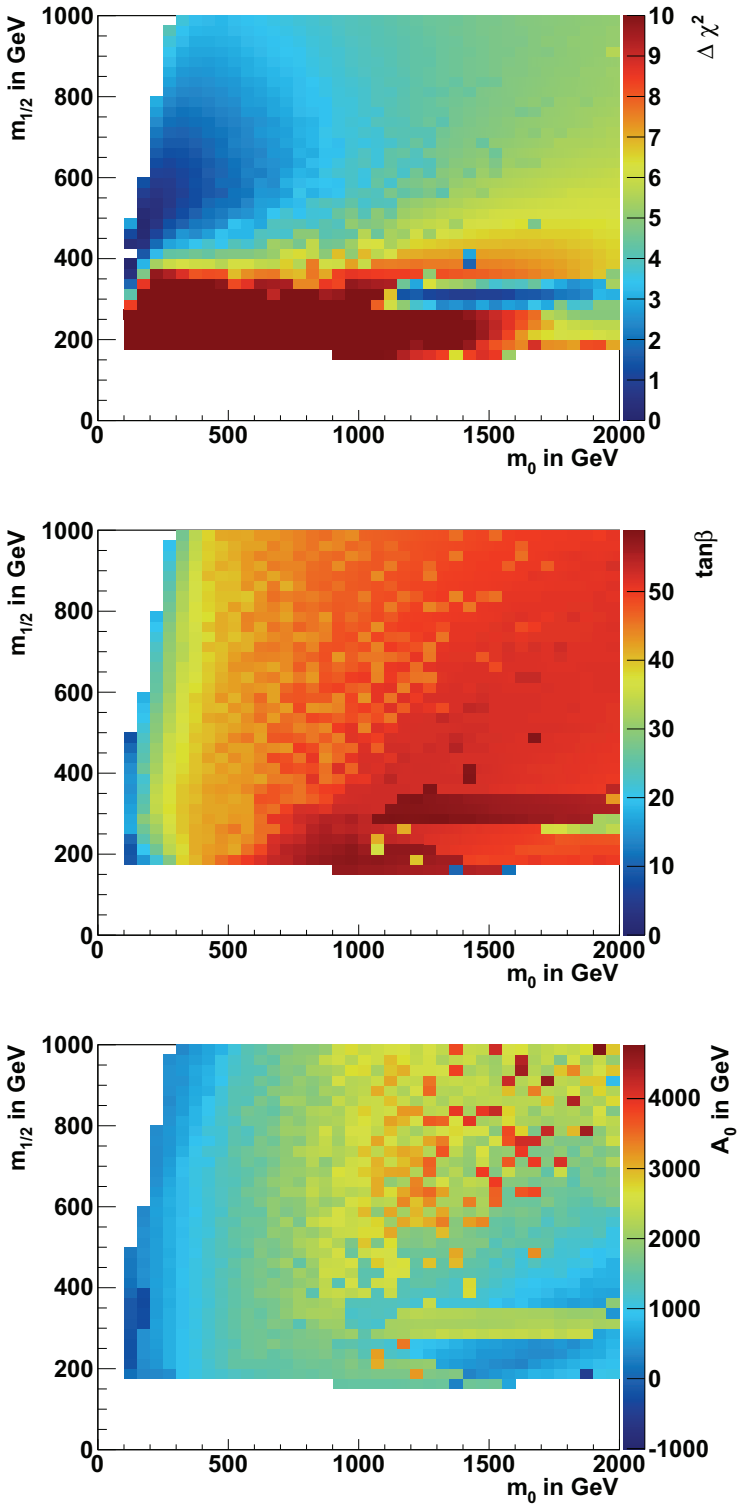

Figure 4.48: Results of two-dimensional optimisation: Here $\tan\beta$ and A_0 are adjusted to fit all constraints simultaneously. Upper plot: Resulting χ^2 values. Lower plots: resulting parameters $\tan\beta$ (middle) and A_0 (bottom).

m_0 in GeV	$m_{1/2}$ in GeV	$\chi^2_{\Omega h^2}$	$\chi^2_{b\to s\gamma}$	$\chi^2_{B^+\to\tau^+\nu_\tau}$	$\chi^2_{\Delta a_\mu}$	$\chi^2_{m_h}$
100	200	10.6 45.5%	4.8 20.8%	1.1 4.7%	0.4 1.9%	6.3 27.0%
100	400 (BFP)	0.02 0.5%	1.0 30.8%	1.1 34.1%	0.8 24.0%	0.3 8.6%
200	775	$7.0{\cdot}10^{-5}$ 0.001%	0.5 8.6%	1.0 16.7%	4.7 74.7%	0
1000	500	0.1 1.9%	0.9 11.8%	1.8 24.3%	3.8 52.3%	0.7 9.8%
1800	350	$2.2{\cdot}10^{-5}$ 0.0002%	1.4 13.6%	4.3 41.8%	4.6 44.6%	0
1900	200	0.07 0.8%	1.2 12.6%	3.3 35.1%	4.9 51.5%	0
1900	900	0.07 0.8%	0.63 7.6%	2.3 27.9%	5.8 69.8%	0

Table 4.4: Resulting χ^2 contributions from different constraints for the points in Tab. 4.3. $\chi^2_{B_S\to\mu\mu}$ is close to zero. The second number in each line is the relative fraction of the total χ^2.

m_0 in GeV	$m_{1/2}$ in GeV	$\chi^2_{\Omega h^2}$	$\chi^2_{b\to s\gamma}$	$\chi^2_{B^+\to\tau^+\nu_\tau}$	$\chi^2_{\Delta a_\mu}$	$\chi^2_{m_h}$
850	325	1.2	1.9	3.3	1.7	3.8
850	350	0.04	3.9	3.7	0.6	3.1

Table 4.5: Resulting partial χ^2 terms. $\chi^2_{B_S\to\mu\mu}$ is zero.

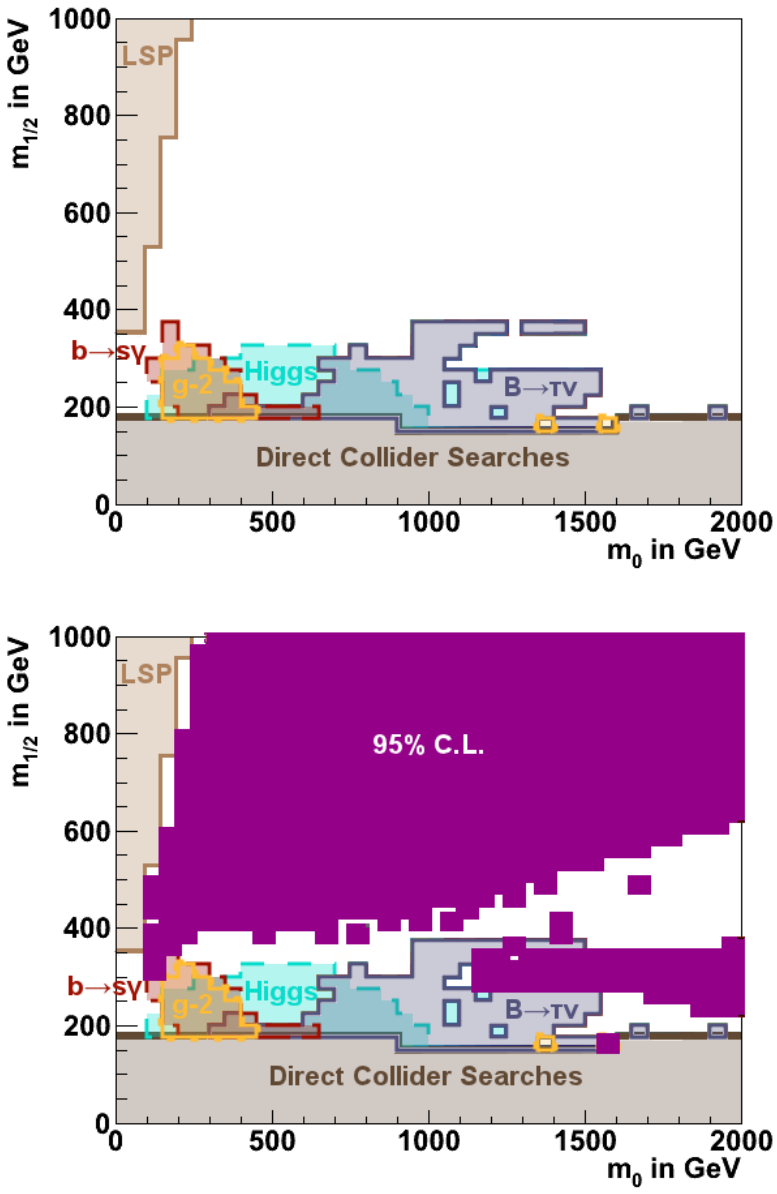

Figure 4.49: Partial exclusion curves (upper plot). Deep red area excluded by $b \to s\gamma$, orange area excluded by anomalous magnetic moment of the muon, cyan area excluded by direct Higgs searches, blue area excluded by $B^+ \to \tau\nu$, dark brown area excluded by direct SUSY searches, ochre shaded area excluded by charged LSP. Lower plot: Magenta area allowed at a 95% confidence level.

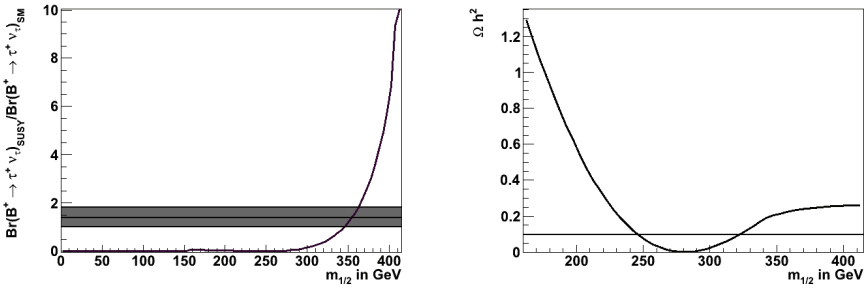

Figure 4.50: Growing of $R_{B^+\to\tau^+\nu_\tau}$ with $m_{1/2}$ (left plot) in comparison with Ωh^2 (right plot).

The exclusion contours of given confidence levels (C.L.) can be drawn by connecting all points with a fixed $\Delta\chi^2$. Tab. A.1 shows the values of the different confidence levels. The resulting exclusion curves are plotted in Fig. 4.51. The difference in the area between the different C.L. is large. This is due to the small difference in χ^2 between two neighbour points.

4.2.10 Comparison with other anayses

There are several other recent analyses, which deal with this topic:

- Ref. [1] uses MCMC techniques to construct the χ^2 function. The cMSSM parameters m_0, $m_{1/2}$, $\tan\beta$ and A_0 are varied simultaneously. The top mass, the mass of the Z boson and the strong coupling constant are treated as constraints.
- Ref. [25] is based on the Bayesian probability definition. It also uses MCMC techniques to construct a sequence of points in parameter space with probability densities proportional to the posterior probability density function. The minimisation was done in an eight dimensional parameter space, with the CMSSM parameters m_0, $m_{1/2}$, $\tan\beta$ and A_0 and the top-quark, bottom-quark mass and the couplings of the strong and electroweak interaction as nuisance parameters.
- Ref. [26] uses a genetic algorithm to run the minimisation with a Frequentist probability interpretation.

Tab. 4.6 shows the included constraints. The two analyses in Ref. [25] and [26] use the same constraints. Additionally, they include cross section limits from direct SUSY searches. The exclusion limits of these two analyses are comparable. In the funnel region they seem to miss points. This can be explained by the fact that the usage of MCMC techniques on parameter spaces with highly correlated variables can miss high probability points. As previously explained, $\tan\beta$ and A_0 are strongly correlated.
In Fig. 4.52 the two 95% CL exclusion curves of Ref. [1] and [25] (orange and blue) are compared to the analysis of this thesis (magenta area). Ref. [1] and [25] seem to obtain contrary results. The analysis of the thesis seems to include solutions of both analyses. It finds solutions between the two areas into which the solution of Ref. [25] is divided. Its

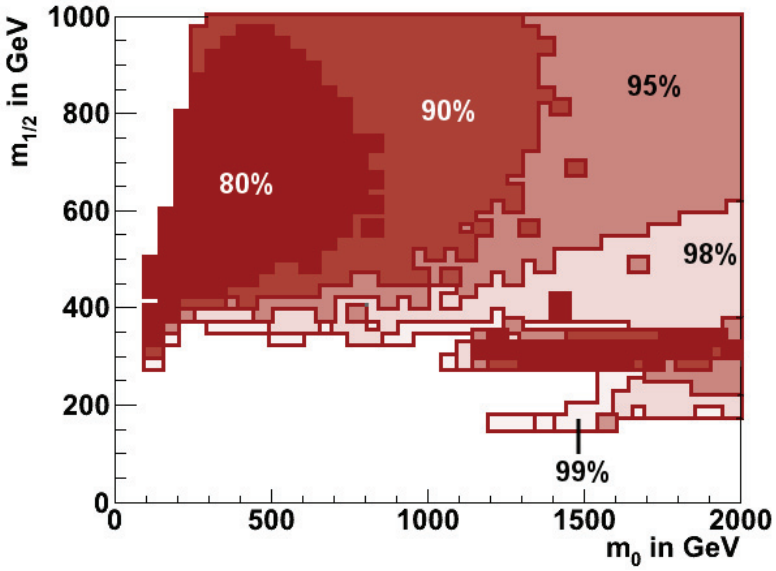

Figure 4.51: Total exclusion curves for different confidence levels.

	[1]	[25], [26]
Δa_μ	(30.2 $\pm$ 0.025 $\pm$ 0.01)· 10^{-10}	(29.5 $\pm$ 8.8 $\pm$ 1)· 10^{-10}
m_h in GeV	$>$ 114.4 $\pm$ 3.0	$>$ 114.4 $\pm$ 3.0
$\frac{Br(b\to s\gamma)_{\text{exp}}}{Br(b\to s\gamma)_{\text{SM}}}$	1.117 $\pm$ 0.05 $\pm$ 0.76 $\pm$ 0.82	
$Br(b \to s\gamma)$		(3.55 $\pm$ 0.26 $\pm$ 0.21) · 10^{-4}
Ωh^2	0.1099 $\pm$ 0.0062 $\pm$ 0.012	0.1099 $\pm$ 0.0062 $\pm$ 0.011
$\frac{Br(B\to\tau\nu)_{\text{exp}}}{Br(B\to\tau\nu)_{\text{SM}}}$	1.15 $\pm$ 0.4	
$Br(B \to \tau\nu)$		(1.32 $\pm$ 0.49 $\pm$ 0.38)· 10^{-4}
$Br(B_d \to \mu\mu)$	$<$ (2.3 $\pm$ 0.01)· 10^{-9}	
$Br(B_s \to \mu\mu)$		$<$ 5.8 · 10^{-8}
$\frac{Br(K\to K_s ll)_{\text{exp}}}{Br(K\to X_s ll)_{\text{SM}}}$	0.99 $\pm$ 0.32	
$\frac{Br(K\to\mu\nu)_{\text{exp}}}{Br(K\to\mu\nu)_{\text{SM}}}$	1.008 $\pm$ 0.014	
$\frac{Br(K\to\pi\nu\bar{\nu})_{\text{exp}}}{Br(K\to\pi\nu\bar{\nu})_{\text{SM}}}$	$<$ 4.5	
$\frac{\Delta M_{B_s}^{\text{exp}}}{\Delta M_{B_s}^{\text{SM}}}$	1.11 $\pm$ 0.01 $\pm$ 0.32	
ΔM_{B_s}		17.77 $\pm$ 0.12 $\pm$ 2.4 ps^{-1}
$\frac{\Delta M_{B_s}^{\text{exp}}/\Delta M_{B_s}^{\text{SM}}}{\Delta M_{B_d}^{\text{exp}}/\Delta M_{B_d}^{\text{SM}}}$	1.09 $\pm$ 0.01 $\pm$ 0.16	
$\frac{\Delta\epsilon_K^{\text{exp}}}{\Delta\epsilon_K^{\text{SM}}}$	0.92 $\pm$ 0.14	

Table 4.6: Constraints used in different analyses.

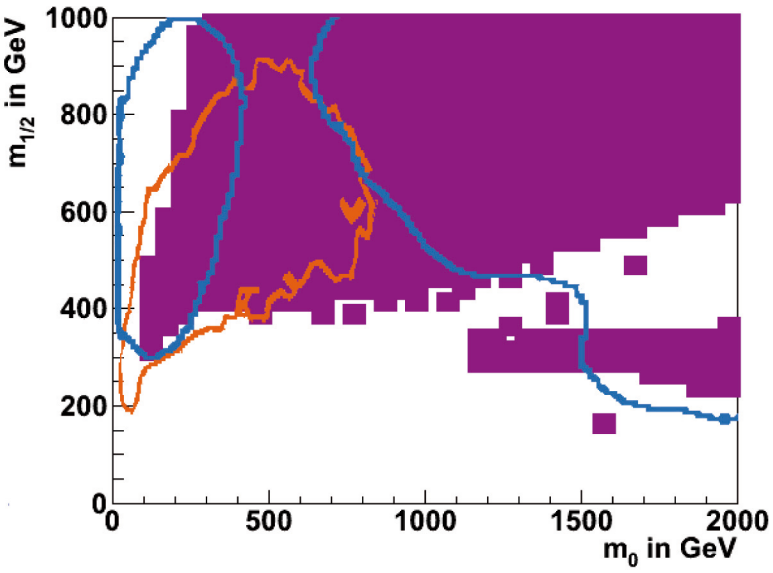

Figure 4.52: Comparison of the analyses (Magenta area: 95% allowed region with linear error combination) with the analysis of [1] (orange) and [25] (blue).

95% CL exclusion semms to be more conservative than the one of Ref. [1].
The difference of the analysis of Ref. [25] is due to the sampling method applied there: A MCMC method varying the mass parameters $\tan\beta$ and A_0 simultaneously has been applied. Because of the correlation of $\tan\beta$ and A_0 this can cause a loss of good solutions in the funnel region (compare Ref. [26]). As previously discussed in the current analysis a multi-step method is applied. This gives the possibility to elude the correlation of $\tan\beta$ and A_0 and therefore find also the points Ref. [25] misses.
The shape of the exclusion curve of Ref. [1] is the same as for the current analysis there is only a difference in the reach. This has two reasons. The first reason is that in the current analysis the linear error combination method is used while Ref. [1] applies the quadratic method. As discussed before the linear combination method allows for a more conservative exclusion. The second issue that makes this discrepancy is the difference in the values of the included constraints. To check the consistency with Ref. [1] the analysis was redone using the same mean values and errors like Ref. [1]. The additional constraints used in Ref. [1] have not been included because they do not contribute much. The results are shown in Fig. 4.53. Evidently, the excluded areas get more comparable. The differences still left could be caused by the different in B-physics calculators applied.
Furthermore, the same analysis was made using Minuit as minimiser by Conny Beskidt [134]. The results are illustrated in Fig. 4.54. The two results look similar. In the low mass area the allowed region is larger with the Minuit analysis.
Additionally, in the area of high m_0 values the region allowed by the current analysis is larger. This is because the MINUIT analysis is more sensitive to the starting point especially in larger parameter spaces. For high values of m_0 the spaces becomes larger in A_0 direction because the Tachyon constraint allows a larger amount of values for A_0.
Concluding, the presented analysis seems to include solutions from Ref. [1] as well as

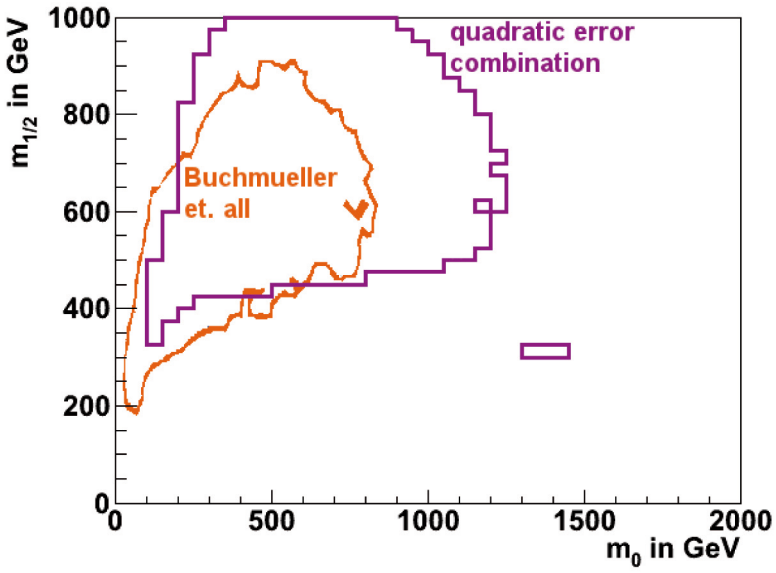

Figure 4.53: Direct Comparison with Ref. [1] (orange). Magenta diagram: Same values for constraints and quadratic error combination method used.

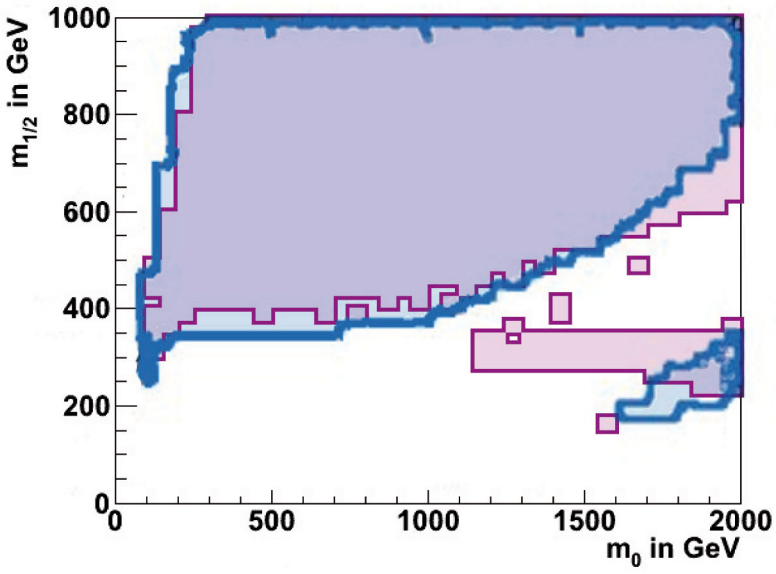

Figure 4.54: Comparison of the current analysis (magenta: 95% C.L.with linear error combination) with the analysis of Conny Beskidt [134] (blue).

solutions from [25]. It is consistent with the analysis done by Conny Beskidt [134] using a completely other method of minimisation.

4.2.11 Inclusion of first LHC Data

The LHC experiments run now for about one year at a centre of mass energy of 7 TeV. This could make a SUSY discovery of low mass cMSSM scenarios possible. However, nothing has been discovered, yet, and thus exclusion curves could be determined.
The CMS[2] experiment for example published its exclusion curve in April 2011 [150]. In the analysis hadronic final states have been used for the exclusion, meaning production of $\tilde{g}\tilde{g}$, $\tilde{g}\tilde{q}$ and $\tilde{q}\tilde{q}$. The integrated luminosity $\mathcal{L}$ was 35 pb^{-1}. Therefore the event number can be calculated by:

$$N = \mathcal{L} \cdot \epsilon \cdot \sigma_{\text{had}}, \tag{4.23}$$

where σ_{had} is the total hadronic cross section from the sum of all combinations of gluinos and squarks of all possible flavours:

$$\sigma_{\text{had}} = \sigma_{\tilde{g}\tilde{g}} + \sum_{\tilde{q}=\tilde{d}}^{\tilde{t}} \sigma_{\tilde{g}\tilde{q}} + \sum_{\tilde{q_1}=\tilde{d}}^{\tilde{t}} \sum_{\tilde{q_2}=\tilde{d}}^{\tilde{q_1}} \sigma_{\tilde{q_1}\tilde{q_2}}. \tag{4.24}$$

The detection efficiency (ϵ) is given by the special configuration of the CMS detector and can be got from [151]. The resulting 95% confidence exclusion curve from CMS for $\tan\beta = 3$ given in Fig. 4.55 corresponds to a number of events of 13.4 including background [150].
The χ^2 is chosen to contribute 5.99 exactly on the CMS exclusion curve which corresponds to a 95% confident exclusion. The number of SUSY events on the exclusion curve is 1.2 and the resulting χ^2 contribution can then be calculated from:

$$\chi^2_{\text{CMS}} = \frac{N^2}{0.47625^2}. \tag{4.25}$$

The exclusion curve is in the area already excluded by $b \to s\gamma$. In Fig. 4.56 the 95% CL. exclusion curve is plotted with and without CMS data. For a few points close to the exclusion limit the χ^2 is raised a bit and therefore the excluded area becomes a bit larger. The distance of the limit to the best-fit point is around 100 GeV. If it would be closer to the best-fit point the minimal χ^2 would raise and therefore the allowed area would get larger. For one point this is already the case for the given exclusion limit. Concluding, the limit calculated by CMS excludes a few points in the low $m_{1/2}$ region but it does not yet effect the best-fit point enough to effect the other points in parameter space.

[2] Compact Muon Solenoid.

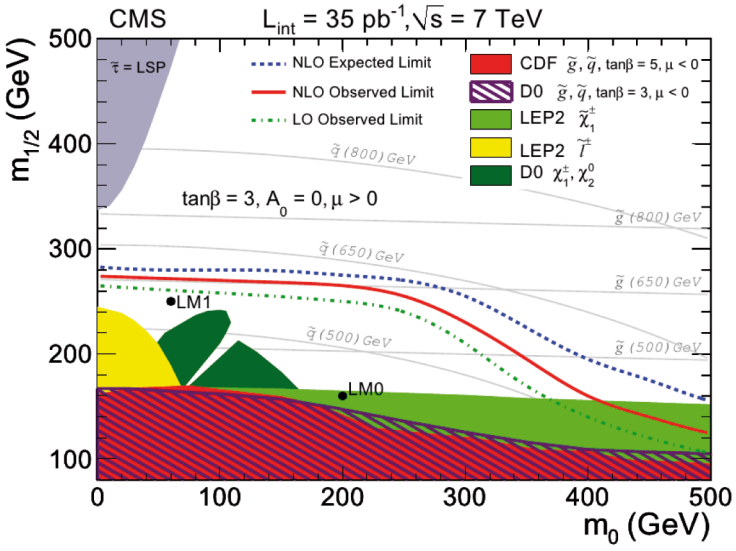

Figure 4.55: 95% C.L. SUSY exclusion curve. Taken from [150].

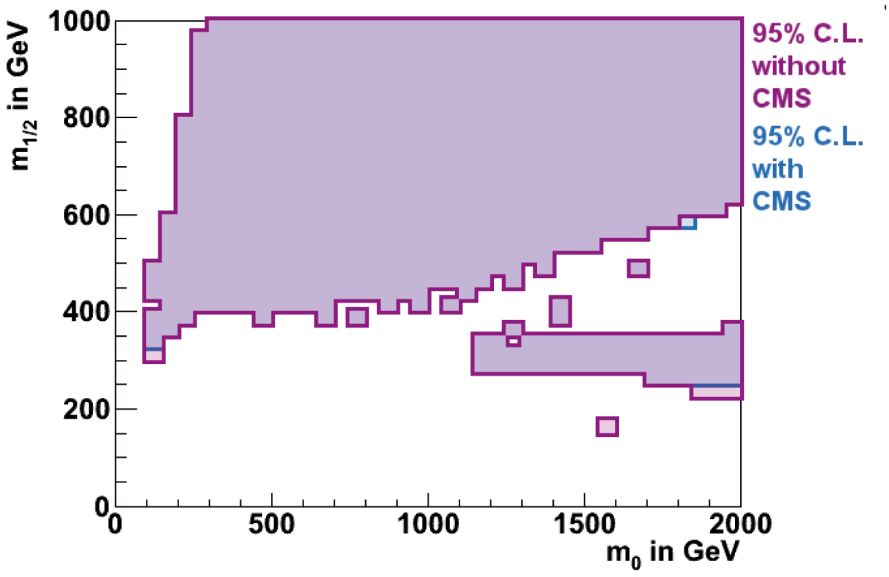

Figure 4.56: 95% exclusion curve including CMS (cyan) and without CMS exclusion curve (magenta).

CHAPTER 5

Conclusion

In this thesis two topics have been discussed: First a case study has been done to answer the question whether the Relic Density can be measured at the Large Hadron Collider (LHC), second a 95% confidence exclusion plot has been calculated from present cosmological and collider data.
The second chapter includes an introduction to the main aspects of SUSY, based on the general knowledge of the SM, and it is argued why the lightest supersymmetric particle (LSP) provides as a perfect Dark Matter (DM) candidate. To reduce the number of free parameters in these models a unification of the SUSY masses and couplings at a grand unified theory scale has been assumed leading to the constrained minimal supersymmetric standard model (cMSSM).
As a first step for solving the two problems a software framework has been developed (see chapter 3).
For relatively heavy SUSY masses the neutralino annihilation cross section is usually too small, i.e. the Relic Density is too high, unless the annihilation via the pseudoscalar Higgs boson A^0 dominates. The value of m_A for the correct Relic Density and correspondingly the Relic Density is a strong fit of $\tan\beta$. The correct Relic Density can be obtained independent of the masses of the superparticles by dealing the correct value of $\tan\beta$. The value of m_A^2 is given by the sum of the two mass terms in the Higgs potential. One mass term obtains negative corrections from the bottom mass, the other from the top mass. To get both terms relatively small one needs the Yukawa couplings of the top and the bottom quark to be similar.The Higgs production cross section is proportional to $\tan^2\beta$ and is therefore enhanced for high values of $\tan\beta$. This allows for an early discovery at the LHC. In this context a method to measure $\tan\beta$ from the cross section of the pseudo-scalar Higgs boson is developed which yields $\tan\beta$ with an uncertainty of 11 - 12%.
From the combination of the expected uncertainties of all parameters used in the Relic Density calculation the uncertainty of the Relic Density could be determined. The result is that up to $m_{1/2}$ = 500 GeV a Relic Density determination with less than 100% uncertainty is possible. This is because for higher masses the cross section of A^0 production becomes too small for precision measurements.
Assuming that DM is completely supersymmetric the neutralino mass can be determined from first pseudoscalar Higgs mass measurements with a precision of 3 - 7%.
For the determination of the exclusion curves using a χ^2 fit it is found that the anomalous magnetic moment of the muon is the most important constraint because it claims a 3σ derivation from the Standard Model value.
The most conservative method is given by linear error combination. This method has been used in the analysis not to risk excluding points wrongly.
The resulting 80, 90, 95, 98 and 99% exclusion curves are determined and shown in Fig. 4.51. The slow increasing of χ^2 leads to large differences in the allowed areas for different confidence levels.
The comparison with other analyses [1, 25, 26] shows that the special multistep fit method

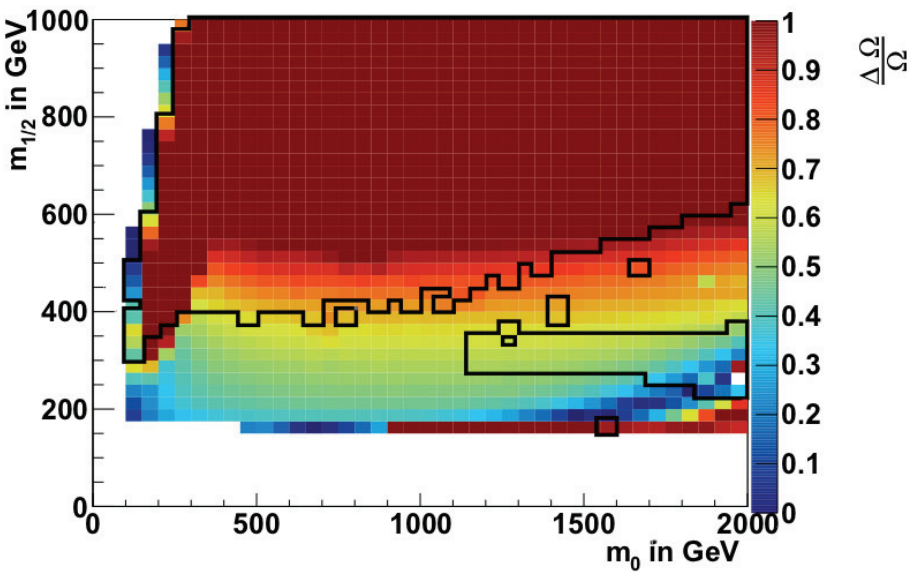

Figure 5.1: The Results from the determination of the relative Relic Density uncertainty (colours) and the 95% C.L. exclusion contour (black line) are shown in the mSUGRA mass parameter plane. The area for $m_{1/2} < 375$ GeV is excluded except a small island for $m_0 > 1050$ GeV.

allows for finding good χ^2 solutions, which cannot be found by analyses. This is because these analyses combine a variation of the cMSSM mass parameters with $\tan\beta$ and A_0 in spite of the strong correlation of the latter two. The current analysis does not exclude any the results of the analysis done so far, but the obtained exclusion curve includes the results of these. The reason for the differences in the analyses [1, 25, 26] could be at the one hand the sampling method which loses points due to the correlation of $\tan\beta$ and A_0 and on the other hand the quadratic combination of the errors.
In Fig. 5.1 the two aspects of Relic Density determination and exclusion curve are combined. Apparently, the major part of the region where a Relic Density determination at the LHC would be possible is already excluded by cosmological and electroweak data.
Concluding, the present constraints exclude only small regions of the simplest cMSSM. High values of $\tan\beta$ are expected in a large region of parameter space. This implies large cross sections for the production cross section of heavy Higgs bosons and could therefore be the first signal of new physics at the LHC. Such scenarios would allow for first estimations of the Relic Density from Higgs searches at the LHC.

APPENDIX A

Important Equations and Methods

A.1 Pauli matrices

- Pauli matrices:

$$\begin{aligned} \sigma_x &= \begin{pmatrix} 0 & 1 \\ 1 & 0 \end{pmatrix} \\ \sigma_y &= \begin{pmatrix} 0 & -i \\ i & 0 \end{pmatrix} \\ \sigma_z &= \begin{pmatrix} 1 & 0 \\ 0 & -1 \end{pmatrix} \end{aligned} \tag{A.1}$$

- Pauli vector:

$$\vec{\sigma} = \sigma_x \cdot \hat{x} + \sigma_y \cdot \hat{y} + \sigma_z \cdot \hat{z} \tag{A.2}$$

- Time component:

$$\sigma_0 = \begin{pmatrix} 1 & 0 \\ 0 & 1 \end{pmatrix} \tag{A.3}$$

A.2 Grassmanian Variables

- Integration

$$\begin{aligned} \int d\theta_\alpha &= 0 \\ \int \theta_\alpha d\theta_\beta &= \delta_{\alpha\beta} \end{aligned} \tag{A.4}$$

A.3 The Gamma Function

The gamma function is defined by

$$\Gamma(x) = \int_0^\infty e^{-t} t^{x-1} dt. \tag{A.5}$$

For integer numbers its value can be calculated as

$$\Gamma(n) = (n-1)! \tag{A.6}$$

Two other important rules:

$$\Gamma(x+1) = x \cdot \Gamma(x)$$

$$\Gamma\left(\frac{1}{2}\right) = \sqrt{\pi}$$

A.4 The Maxiumum Likelihood Method

If a random variable x is distributed according to $f(x;\theta)$ and the value of the pdf f is kown, but θ is unknown the maximum likelihood method gives a possibility to calculate θ given a finite data sample.
Suppose a measurement of the variable x is repeated n times with the result $x_1, ..., x_n$. Under the assumption of a hypothesis $f(x;\theta)$ the probability for the ith measurement to be in $[x_i, x_i + dx_i]$ is $f(x_i;\theta)\, dx_i$.[1].
The so-called likelihood function can be defined by

$$L(\theta) = \prod_{i=1}^{n} f(x_i;\theta)\,. \tag{A.7}$$

One expects the probability to be high for data which was actually measured, thus the data is described best by the model with the highest likelihood function. Thus it has to be maximized. The estimator of the maximum likelihood method is given by

$$\frac{\partial L}{\partial \theta_i} = 0 \quad i = 1, ..., m \tag{A.8}$$

If there are several local minima the highest one has to be taken.

A.5 Input for $Br(B^+ \to \tau^+\nu_\tau)$

The error on SM value of $Br(B^+ \to \tau^+\nu_\tau)$ can be calculated from an error propagation of the SM formula

$$Br(B^+ \to \tau^+\nu_\tau) = \frac{G_F^2 m_B m_\tau^2}{8\pi}\left(1 - \left(\frac{m_\tau}{m_B}\right)^2\right)^2 f_B^2 \left|V_{ub}\right|^2 \tau_B. \tag{A.9}$$

[1] The measurements are assumed to be independent. The values of dx_i do not depend on the parameters

The error propagation is then given as

$$\Delta_{\text{SM}} = \sqrt{\left(\frac{G_F^2 m_\tau^2}{8\pi} f_B^2 |V_{ub}|^2 \tau_B \cdot \left(\left(a - \frac{m_\tau^2}{m_B^2}\right)^2 + 4\left(1 - \frac{m_\tau^2}{m_B^2}\right) \cdot \frac{m_\tau^2}{m_B^2}\right)\right)^2 \Delta_{m_B}^2 + \left(\frac{G_F^2 m_B}{8\pi} f_B^2 |V_{ub}|^2 \tau_B \left(2m_\tau \left(1 - \frac{m_{\tau^2}}{m_B^2}\right)^2 - \left(1 - \frac{m_\tau^2}{m_B^2}\right) \cdot \left(-4\frac{m_\tau^3}{m_B^2}\right)\right)\right)^2 \Delta_{m_\tau}^2 + \left(\frac{G_F^2 m_B m_\tau^2}{8\pi}\left(1 - \frac{m_\tau^2}{m_B^2}\right)^2 \cdot 2 f_B |V_{ub}|^2 \tau_B\right)^2 \Delta f_B + \left(\frac{G_F^2 m_B m_\tau^2}{8\pi}\left(1 - \frac{m_{\tau^2}}{m_B^2}\right)^2 f_B^2 2 |V_{ub}\tau_B|\right)^2 \Delta_{|V_{ub}|}^2 + \frac{G_F^2 m_B m_\tau^2}{8\pi}\left(1 - \frac{m_\tau^2}{m_B^2} f_B^2 |V_{ub}|^2\right)^2 \Delta_{\tau_B}}. \tag{A.10}$$

The values used for the calculation were:

$f_B = 191.067 \pm 2.717 \pm 13.282$ MeV [149]

$|V_{ub}| = 0.00356 + 0.00015 - 0.0020$ [149]

$G_F = 1.16637 \cdot 10^{-5}$ GeV^{-2} [41]

$m_{B^+} = 5279.17 \pm 0.29$ MeV [149]

$\tau_B = (1.638 \pm 0.011) \cdot 10^{-12}$ s [41]

$m_\tau = 1776.82 \pm 0.16$ MeV. [41]

The two error contributions of f_B have been added once linearily and once quadratically after the whole calculation. The error of the ratio between the measured value of [149]

$$Br(B^+ \to \tau^+ \nu_\tau)_{\text{exp}} = (1.68 \pm 0.31) \cdot 10^{-4} \tag{A.11}$$

and the calculated SM value can be calculated again from error propagation:

$$\Delta_R = \sqrt{\left(\frac{\Delta_{\text{exp}}}{Br(B^+ \to \tau^+ \nu_\tau)_{\text{SM}}}\right)^2 + \left(\frac{Br(B^+ \to \tau^+ \nu_\tau)_{\text{exp}}}{Br(B^+ \to \tau^+ \nu_\tau)^2_{\text{SM}}} \cdot \Delta_{\text{SM}}\right)^2}. \tag{A.12}$$

A.6 Confidence levels for two degrees of freedom

$\Delta\chi^2$	Confidence Level
9.210	99%
7.82405	98%
5.99146)	95%
4.60512)	90%
3.21888)	80%

Table A.1: Confidence levels for two degrees of freedom. Taken from [152]

APPENDIX B

Computing Tools

B.1 MicrOMEGAs

The micrOMEGAs code[109] written in Fortran and C calculates properties of cold dark matter for different models of physics beyond the SM. Additionally it contains many routines to calculate other BSM physics constraining values. The ones used in the software package MOPS will be briefly described in this Sec..

- `assignVal(name,val)`

  and

  `findVal(name,&val)`

  can be used to assign and read values of variables. An additional data control function used is

  `pMass(pName).`

  It returns the particle mass of a particle with given name “pName“ [114].

- The validity of the particle spectrum can be checked with

  `sortOddParticles(txt).`

  This function returns a non-zero error for wrong parameter sets. Additionally it stores the name of the lightest odd particle to the passed variable. Therefore it can also be used to check, if the LSP is a potential dark matter candidate[114].

- Another function used to control the validity of the used parameter combination is

  `slhaWarnings(fileName)`

  which writes the warnings from the spectrum calculator into a data file[114].

- In order to check wether the sparticle is beyond any collider limit the function

  `masslimits()`

can be used. It returns a positive value when a direct accelerator limit on sparticle masses from LEP is exceeded[114].

- In micrOMEGAs the mass spectra of the SUSY sparticles can be generated with four different generators: suspect, isajet, spheno, or softSusy. In the present study the function

```
SUGRA(tb,MG1,MG2,MG3,Al,At,Ab,sgn,MHu,MHd,Ml1,Ml3,
      Mr1,Mr3,Mq1,Mq3,Mu1,Mu3,Md1,Md3),
```

  was used to investigate various mSUGRA models. It calculates the MSSM parameters passed to the function based on a set of SUGRA parameters[114].

- There exists also the alternative to pass an already calculated model to micrOMEGAs. This can be done using the function

```
lesHinput(file_name).
```

  This function directly reads les houches accord based files including all particle properties[114].

- For the Relic Density calculation the function

```
darkOmega(&Xf,fast,Beps)
```

  is used. It solves the differential evolution equation using the Runge-Kutta method returning the value of Ωh^2 at current time[114].

- The function

```
nucleonAmplitudes(qBOX,pAsi,pAsd,nAsi,nAsd)
```

  was used to calculate the scattering amplitude for direct dark matter detection. It is able to calculate the spin-dependent and the spin-independent scattering amplitudes for scattering on protons and neutrons. The total cross section for WIMP-nucleon scattering is given by

$$\sigma_{\text{tot}} = \frac{M_\chi^2 M_N^2}{\pi \left(M_\chi + M_N\right)^2} \left(\left| A^{\text{SI}} \right|^2 + 3 \left| A^{\text{SD}} \right|^2 \right), \tag{B.1}$$

  where M_χ is the mass of the WIMP, M_N the mass of the nucleon, A^{SI} the spin-independent and A^{SD} the spin-dependent scattering amplitude[114].

- Additionally to the DM constraints constraints the anomalous magnetic moment of the muon is taken into account. This is done using the function

`gmuon()`.

It returns the contributions from SUSY processes enhancing the value of the anomalous magnetic moment[114].

- The branching ratio of the process $b \to s\gamma$ is calculated using the function

  `bsgnlo()`.

  It includes processes beyond leading order especially important for high values of $\tan\beta$. In the priliminary version used in this thesis a shift is added to the value to simulate NNLO QCD contributions[114].

- The output of

  `bsmumu()`

  is the branching ratio of the process $B_s \to \mu\mu$. The micromegas function includes the loop corrections due to SUSY particles and charged Higgs bosons. It includes corrections effecting high $\tan\beta$ models[114].

- The function

  `btaunu()`

  computes the ratio between the SM value and the SUSY value of the cross section of the process $B^- \to \tau^-\bar{\nu}_\tau$[114].

B.2 ROOT

ROOT is a C++ based interface first developed in the 1960s by Rene Brun and Fons Rademakers. Up to now it grew to a framework including many tools for data analysis. To make the solution of small problems of data analysis easier by shortening program code it includes the C interpreter CINT. In MOPS there are two libraries of this framework included: TFile and TTree[153].
TFile is a root class for file control. In Fig. B.1 the structure of a TFile is adumbrated. It consists of a file header including general file information like the compression level, the number of free data records and the pointers to the first object key and the end of the file. The file header is located in front of all following data objects. After the file header the data objects are located one after the other each with one dedicated logical record header, also called TKey. A TKey includes special informations about the attributive object, like the length of the object date and time when it was written, name and title of the object, pointers to the object and the directory on file [154].

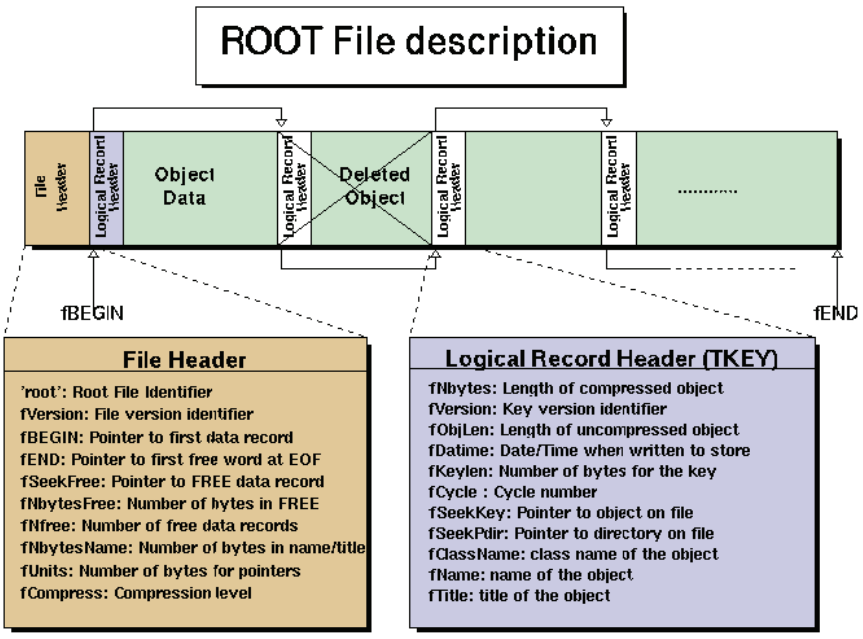

Figure B.1: Structure of a TFile taken from [153].

The structure of a TTree is shown in Fig. B.2. A tree is a tool to store large quantities of same-class objects. It is able to hold all kinds of data. A tree's header consists of its name and title. The body consists of different branches which are independent of each other and whose buffer can be filled with leaf data. Leaf data can be of multiple data types and it can include several elements. If for example three apples and two pears of the data type vegetables has to be stored there can be an branch called apples including the three apples as leaves. The second branch of the tree would be named pears und would include the two pear objects as leaves. A TTree can also include so-called baskets. This technique has not been used in this scope and will therefore not be further discussed[154].

B.3 Minuit

MINUIT[110] was originally written in FORTRAN by Fred James. Since 2002 a C++ version exists.It is a tool to find minima of multiparameter functions and analyse the shape around a minimum. The function to be minimised is caled FCN function. In the C++ version of MINUIT the interface to such kind of function is the FCNBase class. The FCN function has to be implementend as an instance of FCNBase[29].
The input to the FCN function is a list of parameters and has to be stored in an MnUserParaneters object. Each parameter can be chosen to be constant, freely variable or variable within given limits. The limits are put into practise by transformations of the given parameters to a not-limited interval. The transformation for a two sided limited parameter ($[a, b]$) is

$$P_{\text{int}} = \arcsin\left(2 \cdot \frac{P_{\text{ext}} - a}{b - a} - 1\right). \tag{B.2}$$

In our implementation two minimisation methods have been used:

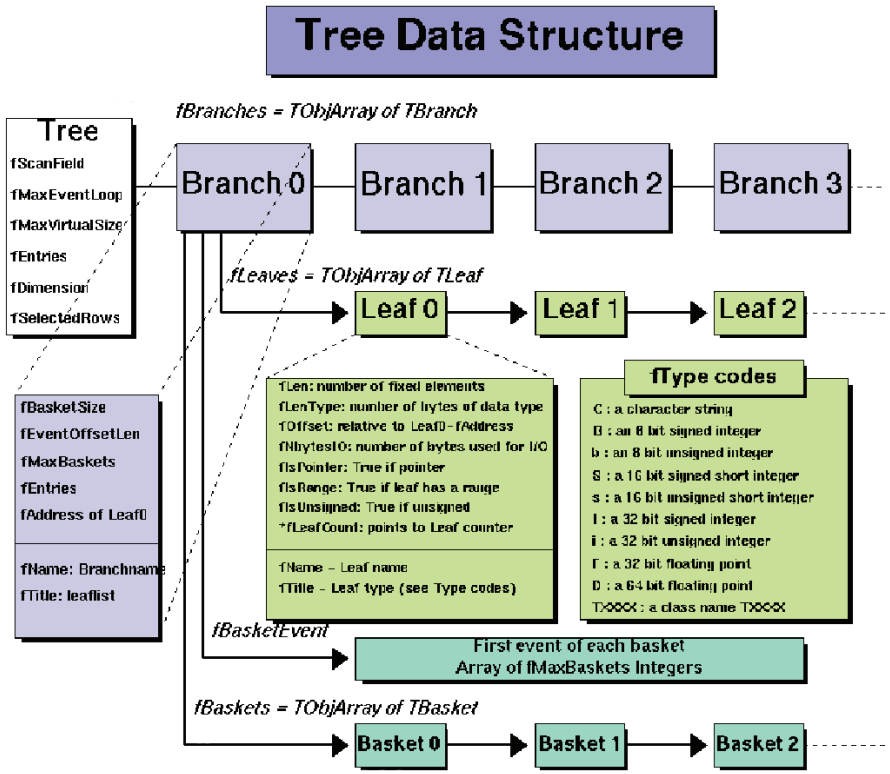

Figure B.2: Structure of a TTree taken from [153].

MIGRAD uses the gradient method for minimisation. It has the advantage to be very accurate. The disadvantage is that it needs the first derivative of the χ^2 function as fit of the parameters.

SIMPLEX is slower than MIGRAD, but it does not use the first derivative. Thus it is not sensitive to uncertainties in the FCN calculation. This makes this method more robust to fluctuations than MIGRAD. Its disadvantage is that it does not always converge and one can not clearly recognize if it converges.

Our solution to use the advantages and minimise the influence of the disadvantages of both methods was a repetition of sequential calls of both methods. This is possible because MINUIT stores the results of a minimisation and is able to take them as starting point for a new minimisation[29].

Danksagungen

Zum erfolgreichen Abschluss meiner Dissertation haben sehr viele Menschen im privaten und im beruflichen Bereich beigetragen. Darum vielen Dank an alle, die mich immer wieder aufgebaut und zum Durchhalten motiviert haben.

Viel Dank gilt hierbei meinem Doktorvater Prof. Dr. Wim de Boer, der mir ermöglicht hat diese Arbeit fertigzustellen und natürlich auch Prof. Dr. Thomas Müller, der sich zur Übernahme des Korreferats bereiterklärt hat.
Im Speziellen möchte ich Prof. Dr. Dmitri Kazakov danken, der mir durch zahlreiche Diskussionen und einen Aufenthalt in Moskau auf theoretischer Ebene auf den richtigen Weg geholfen hat.
Des Weiteren danke ich Tim Küstner und Conny Beskidt für die schöne und sehr erfolgreiche Zusammenarbeit. Ihr beide habt die letzten zwei Jahre meiner Dissertation stark bereichert!
Sehr dankbar bin ich auch meinen Korrektoren, die diesen Text tapfer in seiner Rohfassung gelesen haben: Dr. Markus Weber, Anna Owen, Dr. Markus Schwarz und Sebastian Vöcking.

Für ein gutes Arbeitsklima und zahlreiche physikalische Diskussionen danke ich: Markus Bonsch, Dr. Altan Cakir, Felix Frensch, Simon Lemaire, Dr. Martin Niegel, Thorsten Serr, Christian Skole, Daniel Tröndle, Stefan Wayand, Simon Kunz und Dr. Markus Weber. Hierbei gilt mein Dank auch dem gesamten EKP, insbesondere dem Admin-Team, das immer sehr zuverlässig für eine funktionierende IT-Infrastruktur gesorgt hat.
Dem „Graduiertenkolleg für Hochenergie- und Teilchenastrophysik“ danke ich für die finanzielle Unterstützung.

Bei meiner Danksagung möchte ich auch nicht vergessen die Frau zu erwähnen, die mich dazu motiviert hat, mich in Richtung Teilchenpyhsik zu spezialisieren und die mir immer ein Vorbild war: Prof. Dr. Anna Lipniacka, meine Summer Student-Betreuerin am CERN.
Ohne ein ausgewogenes Privatleben ist eine erfolgreiche Dissertation nicht möglich. Darum möchte ich mich an dieser Stelle ganze herzlich bei meinen Freunden und meiner Familie für die emotionale Unterstützung danken und dass sie mir Abenlenkung geboten haben, wenn es notwendig war. Bei meiner Familie möchte ich mich zudem auch für die finanzielle Unterstützung während des Studiums bedanken.

Zuletzt möchte ich mich noch bei Sebastian Vöcking bedanken, der mir nicht von der Seite gewichen ist, auch wenn es sehr, sehr stressig wurde und mir immer den Rücken freigehalten hat. Danke!

Bibliography

[1] O. Buchmueller, R. Cavanaugh, A. De Roeck, J.R. Ellis, H. Flacher, et al. Predictions for Supersymmetric Particle Masses using Indirect Experimental and Cosmological Constraints. JHEP, 0809:117, 2008.

[2] Murray Gell-Mann. A Schematic Model of Baryons and Mesons. Phys.Lett., 8:214–215, 1964.

[3] S.L. Glashow, J. Iliopoulos, and L. Maiani. Weak Interactions with Lepton-Hadron Symmetry. Phys.Rev., D2:1285–1292, 1970.

[4] S. L. Glashow. Partial Symmetries of Weak Interactions. Nucl. Phys., 22:579–588, 1961.

[5] Gerard 't Hooft. Renormalizable Lagrangians for Massive Yang-Mills Fields. Nucl.Phys., B35:167–188, 1971.

[6] Gerard 't Hooft and M.J.G. Veltman. Regularization and Renormalization of Gauge Fields. Nucl.Phys., B44:189–213, 1972.

[7] Gerard 't Hooft and M.J.G. Veltman. Combinatorics of gauge fields. Nucl.Phys., B50:318–353, 1972.

[8] D.J. Gross and Frank Wilczek. Asymptotically Free Gauge Theories. 1. Phys.Rev., D8:3633–3652, 1973.

[9] D.J. Gross and Frank Wilczek. Ultraviolet Behavior of Nonabelian Gauge Theories. Phys.Rev.Lett., 30:1343–1346, 1973.

[10] H.David Politzer. Reliable Perturbative Results for Strong Interactions? Phys.Rev.Lett., 30:1346–1349, 1973.

[11] H.David Politzer. Asymptotic Freedom: An Approach to Strong Interactions. Phys.Rept., 14:129–180, 1974.

[12] L.D. Faddeev and V.N. Popov. Feynman Diagrams for the Yang-Mills Field. Phys.Lett., B25:29–30, 1967.

[13] Howard Georgi and Sheldon L. Glashow. Unified weak and electromagnetic interactions without neutral currents. Phys.Rev.Lett., 28:1494, 1972.

[14] Abdus Salam and John Clive Ward. Electromagnetic and weak interactions. Phys.Lett., 13:168–171, 1964.

[15] Steven Weinberg. A Model of Leptons. Phys.Rev.Lett., 19:1264–1266, 1967.

[16] F. Zwicky. Spectral displacement of extra galactic nebulae. Helv. Phys. Acta, 6:110–127, 1933.

[17] E. Komatsu et al. Five-Year Wilkinson Microwave Anisotropy Probe (WMAP) Observations:Cosmological Interpretation. Astrophys. J. Suppl., 180:330–376, 2009.

[18] E. W. Kolb and M.S. Turner. The early Universe. Westview Press, 1990.

[19] Yu.A. Golfand and E.P. Likhtman. Extension of the Algebra of Poincare Group Generators and Violation of p Invariance. JETP Lett., 13:323–326, 1971.

[20] D.V. Volkov and V.P. Akulov. Possible universal neutrino interaction. JETP Lett., 16:438–440, 1972.

[21] J. Wess and B. Zumino. A Lagrangian Model Invariant Under Supergauge Transformations. Phys.Lett., B49:52, 1974.

[22] J. Wess and B. Zumino. Supergauge Invariant Extension of Quantum Electrodynamics. Nucl.Phys., B78:1, 1974.

[23] S. Ferrara, J. Wess, and B. Zumino. Supergauge Multiplets and Superfields. Phys.Lett., B51:239, 1974.

[24] J. Iliopoulos and B. Zumino. Broken Supergauge Symmetry and Renormalization. Nucl.Phys., B76:310, 1974.

[25] Roberto Trotta, Farhan Feroz, Mike P. Hobson, Leszek Roszkowski, and Roberto Ruiz de Austri. The Impact of priors and observables on parameter inferences in the Constrained MSSM. JHEP, 0812:024, 2008.

[26] Yashar Akrami, Pat Scott, Joakim Edsjo, Jan Conrad, and Lars Bergstrom. A Profile Likelihood Analysis of the Constrained MSSM with Genetic Algorithms. JHEP, 1004:057, 2010.

[27] Luke Tierney. Markov chains for exploring posterior distributions. Annals of Statistics, 22:1701–1762, 1994.

[28] S. Richardson W. R. Gilks and D. J. Spiegelhalter. Markov Chain Monte Carlo in Practice. Chapman& Hall/CRC, 1996.

[29] Fred James and Matthias Winkler. Minuit users guide. seal.cern.ch/documents/minuit/, June 2004.

[30] D.J. Griffiths. Introduction to Elementary Particles. Wiley-VCH, 2008.

[31] F. Englert and R. Brout. Broken Symmetry and the Mass of Gauge Vector Mesons. Phys.Rev.Lett., 13:321–322, 1964.

[32] G.S. Guralnik, C.R. Hagen, and T.W.B. Kibble. Global Conservation Laws and Massless Particles. Phys.Rev.Lett., 13:585–587, 1964.

[33] Peter W. Higgs. Broken symmetries, massless particles and gauge fields. Phys.Lett., 12:132–133, 1964.

[34] Peter W. Higgs. Broken Symmetries and the Masses of Gauge Bosons. Phys.Rev.Lett., 13:508–509, 1964.

[35] Peter W. Higgs. Spontaneous Symmetry Breakdown without Massless Bosons. Phys.Rev., 145:1156–1163, 1966.

[36] Jeffrey Goldstone, Abdus Salam, and Steven Weinberg. Broken Symmetries. Phys.Rev., 127:965–970, 1962.

[37] J.A. Thomas. Neutrino oscillations - present status and future plans. World Scientific, 2008.

[38] O.W. Greenberg. Spin and Unitary Spin Independence in a Paraquark Model of Baryons and Mesons. Phys.Rev.Lett., 13:598–602, 1964. Introduces the symmetry that was to become color.

[39] M.Y. Han and Yoichiro Nambu. Three Triplet Model with Double SU(3) Symmetry. Phys.Rev., 139:B1006–B1010, 1965.

[40] H. Fritzsch, Murray Gell-Mann, and H. Leutwyler. Advantages of the Color Octet Gluon Picture. Phys.Lett., B47:365–368, 1973. Introduces the term 'color'.

[41] K. Nakamura et. al. J.Phys G, 37(075021), 2010.

[42] M.E. Peskin and D.V. Schroeder. An Introduction to Quantum Field Theory. Westview Press, 1995.

[43] S. Tomonaga. On a relativistically invariant formulation of the quantum theory of wave fields. Prog.Theor.Phys., 1:27–42, 1946.

[44] Julian S. Schwinger. Quantum electrodynamics. I A covariant formulation. Phys.Rev., 74:1439, 1948.

[45] Julian S. Schwinger. Quantum electrodynamics. 2. Vacuum polarization and selfenergy. Phys.Rev., 75:651, 1948.

[46] Julian S. Schwinger. Quantum electrodynamics. III: The electromagnetic properties of the electron: Radiative corrections to scattering. Phys.Rev., 76:790–817, 1949.

[47] R.P. Feynman. The Theory of positrons. Phys.Rev., 76:749–759, 1949.

[48] R.P. Feynman. Space - time approach to quantum electrodynamics. Phys.Rev., 76:769–789, 1949.

[49] R.P. Feynman. Mathematical formulation of the quantum theory of electromagnetic interaction. Phys.Rev., 80:440–457, 1950.

[50] Julian S. Schwinger. Renormalization Theory of Quantum Electrodynamics: An Individual View. 1980.

[51] Abdelhak Djouadi. The Anatomy of electro-weak symmetry breaking. I: The Higgs boson in the standard model. Phys.Rept., 457:1–216, 2008.

[52] CERN Summer Student Lectures 2006.

[53] W. de Boer. Grand unified theories and supersymmetry in particle physics and cosmology. Prog.Part.Nucl.Phys., 33:201–302, 1994.

[54] Dmitri Kazakov. Beyond the standard model(on the search for supersymmetry). arXiv:hep-ph/0012288v2, January 2001.

[55] Sidney R. Coleman and J. Mandula. ALL POSSIBLE SYMMETRIES OF THE S MATRIX. Phys.Rev., 159:1251–1256, 1967.

[56] Stephen P. Martin. A Supersymmetry primer. 1997.

[57] Ugo Amaldi, Wim de Boer, Paul H. Frampton, Hermann Furstenau, and James T. Liu. Consistency checks of grand unified theories. Phys.Lett., B281:374–383, 1992.

[58] Ian Aitchison. Supersymmetry in Particle Physics. Cambridge, 2007.

[59] L. O'Raifeartaigh. Spontaneous Symmetry Breaking for Chiral Scalar Superfields. Nucl.Phys., B96:331, 1975.

[60] Pierre Fayet. Supersymmetry and Weak, Electromagnetic and Strong Interactions. Phys.Lett., B64:159, 1976.

[61] Pierre Fayet. Spontaneously Broken Supersymmetric Theories of Weak, Electromagnetic and Strong Interactions. Phys.Lett., B69:489, 1977.

[62] Pierre Fayet. Relations Between the Masses of the Superpartners of Leptons and Quarks, the Goldstino Couplings and the Neutral Currents. Phys.Lett., B84:416, 1979.

[63] Glennys R. Farrar and Pierre Fayet. Phenomenology of the Production, Decay, and Detection of New Hadronic States Associated with Supersymmetry. Phys.Lett., B76:575–579, 1978.

[64] Howard Baer and Xerxes Tata. Weak Scale Supersymmetry. Cambridge, 2006.

[65] Savas Dimopoulos, Stuart Raby, and Frank Wilczek. Proton Decay in Supersymmetric Models. Phys.Lett., B112:133, 1982.

[66] Steven Weinberg. Supersymmetry at Ordinary Energies. 1. Masses and Conservation Laws. Phys.Rev., D26:287, 1982.

[67] N. Sakai and Tsutomu Yanagida. Proton Decay in a Class of Supersymmetric Grand Unified Models. Nucl.Phys., B197:533, 1982.

[68] Savas Dimopoulos and Howard Georgi. Softly Broken Supersymmetry and SU(5). Nucl.Phys., B193:150, 1981.

[69] Pran Nath and Richard L. Arnowitt. Generalized Supergauge Symmetry as a New Framework for Unified Gauge Theories. Phys.Lett., B56:177, 1975.

[70] Richard L. Arnowitt, Pran Nath, and B. Zumino. Superfield Densities and Action Principle in Curved Superspace. Phys.Lett., B56:81, 1975.

[71] Daniel Z. Freedman, P. van Nieuwenhuizen, and S. Ferrara. Progress Toward a Theory of Supergravity. Phys.Rev., D13:3214–3218, 1976.

[72] Stanley Deser and B. Zumino. A Complete Action for the Spinning String. Phys.Lett., B65:369–373, 1976.

[73] Daniel Z. Freedman and P. van Nieuwenhuizen. Properties of Supergravity Theory. Phys.Rev., D14:912, 1976.

[74] E. Cremmer, B. Julia, Joel Scherk, S. Ferrara, L. Girardello, et al. Spontaneous Symmetry Breaking and Higgs Effect in Supergravity Without Cosmological Constant. Nucl.Phys., B147:105, 1979.

[75] Jonathan A. Bagger. Coupling the Gauge Invariant Supersymmetric Nonlinear Sigma Model to Supergravity. Nucl.Phys., B211:302, 1983.

[76] E. Cremmer, S. Ferrara, L. Girardello, and Antoine Van Proeyen. Yang-Mills Theories with Local Supersymmetry: Lagrangian, Transformation Laws and SuperHiggs Effect. Nucl.Phys., B212:413, 1983.

[77] Michael Dine and Willy Fischler. A Phenomenological Model of Particle Physics Based on Supersymmetry. Phys.Lett., B110:227, 1982.

[78] Chiara R. Nappi and Burt A. Ovrut. Supersymmetric Extension of the SU(3) x SU(2) x U(1) Model. Phys.Lett., B113:175, 1982.

[79] Luis Alvarez-Gaume, Mark Claudson, and Mark B. Wise. Low-Energy Supersymmetry. Nucl.Phys., B207:96, 1982.

[80] Michael Dine and Ann E. Nelson. Dynamical supersymmetry breaking at low-energies. Phys.Rev., D48:1277–1287, 1993.

[81] Michael Dine, Ann E. Nelson, and Yuri Shirman. Low-energy dynamical supersymmetry breaking simplified. Phys.Rev., D51:1362–1370, 1995.

[82] Michael Dine, Ann E. Nelson, Yosef Nir, and Yuri Shirman. New tools for low-energy dynamical supersymmetry breaking. Phys.Rev., D53:2658–2669, 1996.

[83] Lisa Randall and Raman Sundrum. Out of this world supersymmetry breaking. Nucl.Phys., B557:79–118, 1999.

[84] Gian F. Giudice, Markus A. Luty, Hitoshi Murayama, and Riccardo Rattazzi. Gaugino mass without singlets. JHEP, 9812:027, 1998.

[85] Luis E. Ibanez and Graham G. Ross. SU(2)-L x U(1) Symmetry Breaking as a Radiative Effect of Supersymmetry Breaking in Guts. Phys.Lett., B110:215–220, 1982.

[86] John R. Ellis, Dimitri V. Nanopoulos, and K. Tamvakis. Grand Unification in Simple Supergravity. Phys.Lett., B121:123, 1983.

[87] Luis Alvarez-Gaume, J. Polchinski, and Mark B. Wise. Minimal Low-Energy Supergravity. Nucl.Phys., B221:495, 1983. Revised version.

[88] Abdelhak Djouadi. The Anatomy of electro-weak symmetry breaking. II. The Higgs bosons in the minimal supersymmetric model. Phys.Rept., 459:1–241, 2008.

[89] R. Barate et al. Search for the standard model Higgs boson at LEP. Phys. Lett., B565:61–75, 2003.

[90] P. Peebles J. Ostriker and A. Yahil. The size and mass of galaxies, and the mass of the universe. Astrophysical Journal, 193(L1-L4), 1974.

[91] A. Kaasik J. Einasto and E. Saar. Dynamical evidence for massive coronas of galaxies. Nature, 250:309–310, 1974.

[92] M. Weber. Reconstruction of the galactic dark matter density from astronomical observations and diffuse galactic gamma rays. IEKP-KA/2010-3, February 2010.

[93] Gianfranco Bertone, Dan Hooper, and Joseph Silk. Particle dark matter: Evidence, candidates and constraints. Phys.Rept., 405:279–390, 2005.

[94] J. Bekenstein and Mordehai Milgrom. Does the missing mass problem signal the breakdown of Newtonian gravity? Astrophys. J., 286:7–14, 1984.

[95] O. Bienayme, B. Famaey, X. Wu, H. S. Zhao, and D. Aubert. Galactic kinematics with modified Newtonian dynamics. 2009.

[96] Anthony Aguirre, Joop Schaye, and Eliot Quataert. Problems for MOND in clusters and the Ly-alpha forest. Astrophys.J., 561:550, 2001.

[97] B. Paczynski. Gravitational microlensing by the galactic halo. Astrophys. J., 304:L1–L5, 1986.

[98] Theodor Kaluza. On the Problem of Unity in Physics. Sitzungsber. Preuss. Akad. Wiss. Berlin (Math. Phys.), 1921:966–972, 1921.

[99] Marco Regis, Marco Serone, and Piero Ullio. A Dark Matter Candidate from an Extra (Non-Universal) Dimension. JHEP, 0703:084, 2007.

[100] Christian Weinheimer. The Neutrino mass direct measurements. pages 335–344, 2003.

[101] Y. Suzuki. Kamiokande solar neutrino results. Nucl. Phys. Proc. Suppl., 38:54–59, 1995.

[102] Q. R. Ahmad et al. Direct evidence for neutrino flavor transformation from neutral-current interactions in the Sudbury Neutrino Observatory. Phys. Rev. Lett., 89:011301, 2002.

[103] M. H. Ahn et al. Measurement of Neutrino Oscillation by the K2K Experiment. Phys. Rev., D74:072003, 2006.

[104] G. Drexlin. Final neutrino oscillation results from LSND and KARMEN. Nucl. Phys. Proc. Suppl., 118:146–153, 2003.

[105] Kim Griest and Marc Kamionkowski. Unitarity Limits on the Mass and Radius of Dark Matter Particles. Phys.Rev.Lett., 64:615, 1990.

[106] Edward W. Kolb, Daniel J.H. Chung, and Antonio Riotto. WIMPzillas! pages 91–105, 1998.

[107] Lars Bergstrom. Non-baryonic dark matter: Observational evidence and detection methods. Rept. Prog. Phys., 63:793, 2000.

[108] R.D. Peccei and Helen R. Quinn. CP Conservation in the Presence of Instantons. Phys.Rev.Lett., 38:1440–1443, 1977.

[109] G. Belanger et al. Indirect search for dark matter with micrOMEGAs2.4. Comput. Phys. Commun., 182:842–856, 2011.

[110] http://lcgapp.cern.ch/project/cls/work-packages/mathlibs/minuit/.

[111] G. Cowen. Statistical Data Analysis. Oxford Science Publications, 1998.

[112] W.K. Hastings. Monte Carlo Sampling Methods Using Markov Chains and Their Applications. Biometrika, 57:97109, 1970.

[113] N. Metropolis, A.W. Rosenbluth, M.N. Rosenbluth, A.H. Teller, and E. Teller. Equation of state calculations by fast computing machines. J.Chem.Phys., 21:1087–1092, 1953.

[114] A. Pukhov G. Belanger, F. Boudjema and A. Semenov. The micromegas users manual, version 2.4. http://lapth.in2p3.fr/micromegas/, May 2010.

[115] H. Balzert. UML 2 in 5 Tagen. W3L, 2005.

[116] C. Sander. Interpretation of the Excess in Diffuse Galactic Gamma Rays above 1 GeV as Dark Matter Annihilation Signal. Dissertation, Universitaet Karlsruhe, July 2005. IEKP-KA/2005-12.

[117] Jonathan L. Feng, Konstantin T. Matchev, and Takeo Moroi. Multi - TeV scalars are natural in minimal supergravity. Phys.Rev.Lett., 84:2322–2325, 2000.

[118] Jonathan L. Feng, Konstantin T. Matchev, and Takeo Moroi. Focus points and naturalness in supersymmetry. Phys.Rev., D61:075005, 2000.

[119] John R. Ellis, Toby Falk, and Keith A. Olive. Neutralino - Stau coannihilation and the cosmological upper limit on the mass of the lightest supersymmetric particle. Phys.Lett., B444:367–372, 1998.

[120] John R. Ellis, Toby Falk, Keith A. Olive, and Mark Srednicki. Calculations of neutralino-stau coannihilation channels and the cosmologically relevant region of MSSM parameter space. Astropart.Phys., 13:181–213, 2000.

[121] A.B. Lahanas, Dimitri V. Nanopoulos, and V.C. Spanos. Neutralino relic density in a universe with nonvanishing cosmological constant. Phys.Rev., D62:023515, 2000.

[122] Richard L. Arnowitt, Bhaskar Dutta, and Y. Santoso. Coannihilation effects in supergravity and D-brane models. Nucl.Phys., B606:59–83, 2001.

[123] Takeshi Nihei, Leszek Roszkowski, and Roberto Ruiz de Austri. Exact cross-sections for the neutralino slepton coannihilation. JHEP, 0207:024, 2002.

[124] Conny Beskidt, Wim de Boer, Tim Hanisch, Eva Ziebarth, Valery Zhukov, et al. Constraints on Supersymmetry from Relic Density compared with future Higgs Searches at the LHC. Phys.Lett., B695:143–148, 2011.

[125] Richard L. Arnowitt, Bhaskar Dutta, Alfredo Gurrola, Teruki Kamon, Abram Krislock, et al. Determining the Dark Matter Relic Density in the mSUGRA (X0(1))- tau Co-Annhiliation Region at the LHC. Phys.Rev.Lett., 100:231802, 2008.

[126] CMS Collaboration. Discovery potential and measurement of a dilepton mass edge in susy events at $\sqrt{s}$= 10 tev. CMS PAS SUS-09-002, July 2009.

[127] G.L. Bayatian et al. CMS technical design report, volume II: Physics performance. J.Phys.G, G34:995–1579, 2007.

[128] R. Kinnunen and S. Lehti. Search for the heavy neutral MSSM Higgs bosons with the H/A —> tau+ tau- —> electron + jet decay mode. 2006. CERN-CMS-NOTE-2006-075.

[129] S. Gennai, A. Nikitenko, and L. Wendland. Search for MSSM heavy neutral Higgs boson in tau tau —> two jet decay mode. 2006. CMS-NOTE-2006-126.

[130] D. Kotlinski A. Kalinowski, M. Konecki. Search for MSSM Heavy Neutral Higgs Boson in tau tau $\rightarrow$ mu + jet decay mode. 2006. CERN-CMS-NOTE-2006-105.

[131] S. Lehti. Study of $H/A \rightarrow \tau\tau \rightarrow e\mu + X$ in CMS. 2006. CMS-NOTE-2006-101.

[132] A. Pukhov, E. Boos, M. Dubinin, V. Edneral, V. Ilyin, et al. CompHEP: A Package for evaluation of Feynman diagrams and integration over multiparticle phase space. 1999. User's manual for version 33.

[133] T. Hanisch. Relic density determination at the lhc. Diplomarbeit, Karlsruher Institut fuer Technologie, August 2010. IEKP-KA/2010-19.

[134] C. Beskidt. Massengrenzen auf sypersymmetrische teilchen aus kosmologischen und elektroschwachen praezissionsdaten im vergleich zu den erwartungen am lhc. Diplomarbeit, Karlsruher Institut fuer Technologie, May 2011.

[135] A. Pukhov, private communication.

[136] A. J. Buras. Flavour dynamics: Cp violation and rare decays. TUM-HEP-402/01, January 2001.

[137] C. Bobeth, T. Ewerth, F. Kruger, and J. Urban. Analysis of neutral Higgs boson contributions to the decays $\bar{B}(\ s) \rightarrow \ell^+\ell^-$ and $\bar{B} \rightarrow K\ell^+\ell^-$. Phys.Rev., D64:074014, 2001.

[138] Richard L. Arnowitt, Bhaskar Dutta, T. Kamon, and M. Tanaka. Detection of $B_s \rightarrow \mu^+\mu^-$ at the Tevatron run II and constraints on the SUSY parameter space. Phys.Lett., B538:121–129, 2002.

[139] Z. Liu N. Chen, D. Feldman and P. Nath. Susy and higgs signatures implied by cancellations in $b \rightarrow s\gamma$. Phys.Lett.B, 685:174–181, 2009.

[140] E. Barberio et al. Averages of $b-$hadron properties at the end of 2005. 2006.

[141] Takeo Moroi. The Muon anomalous magnetic dipole moment in the minimal supersymmetric standard model. Phys.Rev., D53:6565–6575, 1996.

[142] G. Degrassi and G.F. Giudice. QED logarithms in the electroweak corrections to the muon anomalous magnetic moment. Phys.Rev., D58:053007, 1998.

[143] S. Heinemeyer, D. Stockinger, and G. Weiglein. Two loop SUSY corrections to the anomalous magnetic moment of the muon. Nucl.Phys., B690:62–80, 2004.

[144] Sven Heinemeyer, Dominik Stockinger, and Georg Weiglein. Electroweak and supersymmetric two-loop corrections to (g-2)(mu). Nucl.Phys., B699:103–123, 2004.

[145] G.W. Bennett et al. Final Report of the Muon E821 Anomalous Magnetic Moment Measurement at BNL. Phys.Rev., D73:072003, 2006. Summary of E821 Collaboration measurements of the muon anomalous magnetic moment, each reported earlier in Letters or Brief Reports. Revised version submitted to Phys.Rev.D.

[146] Michel Davier. The Hadronic contribution to (g-2)(mu). Nucl.Phys.Proc.Suppl., 169:288–296, 2007.

[147] David W. Hertzog, James P. Miller, Eduardo de Rafael, B. Lee Roberts, and Dominik Stockinger. The Physics case for the new muon (g-2) experiment. 2007.

[148] Gino Isidori and Paride Paradisi. Hints of large tan(beta) in flavour physics. Phys.Lett., B639:499–507, 2006.

[149] A. Lenz, U. Nierste, J. Charles, S. Descotes-Genon, A. Jantsch, et al. Anatomy of New Physics in $B - \bar{B}$ mixing. Phys.Rev., D83:036004, 2011.

[150] Vardan Khachatryan et al. Search for Supersymmetry in pp Collisions at 7 TeV in Events with Jets and Missing Transverse Energy. Phys.Lett., B698:196–218, 2011.

[151] https://twiki.cern.ch/twiki/bin/view/CMSPublic/PhysicsResultsSUS11001.

[152] http://www.hostsrv.com/webmaa/app1/MSP/webm1010/chi2.

[153] http://root.cern.ch/drupal/.

[154] The ROOT team. Root user's guide 5.26. http://root.cern.ch/drupal/content/users-guide, May 2009.